universität wien

MASTERARBEIT

Titel der Masterarbeit

Physical Constraints on the Evolution of Hotspot Swells on Earth and Venus

Verfasser

Elisabeth Fahrngruber Bakk. rer. nat.

angestrebter akademischer Grad

Master of Science (MSc)

Vienna, 2015

Abstract

Since the planets Earth and Venus are very similar regarding their sizes and bulk densities, comparable heat budgets are assumed as well. However, whereas plate tectonics is a dominant mechanism of heat transport through the lithosphere on Earth, it is not observed on Venus. Hotspot volcanism may be the dominant heat transfer mechanism on Venus. Nine regions on Venus have been identified that resemble hotspots on Earth: they are characterized by positive geoid anomalies, topographic swells, and abundant volcanism. The majority of these topographic rises comprise some of the largest volcanoes found on Venus. These volcanic constructs are among the youngest features of the planet. They formed during the resurfacing event which is a preferred theory describing the heat budget of Venus. Resurfacing is characterized by vigorous volcanism. It may be a periodic event in the course of which the entire surface of Venus is renewed. The length of such a resurfacing event is not known. In two different ways the durations of growth of the large volcanoes were calculated: by making assumptions about the mantle plumes which are the cause of hotspots, and by making use of the observable topography. It was established that each single volcano grew within less than a million years, which is consistent with the resurfacing theory. It also became apparent that the calculation that assumes plate tectonics is not applicable to Venus.

Zusammenfassung

Erde und Venus sind sich hinsichtlich ihrer Größe und ihrer Zusammensetzung sehr ähnlich. Deshalb werden auch ähnliche Energiehaushalte für die beiden Planeten angenommen. Auf der Erde wird der Wärmetransport durch die Lithosphäre in Form von Plattentektonik sichtbar. Auf der Venus wird allerdings keine Plattentektonik beobachtet. Eine andere Art von Wärmetransport durch die Lithosphäre ist der Hotspot-Vulkanismus, der auf der Venus eine entscheidende Rolle spielt. Es wurden insgesamt neun Regionen auf dem Planeten gefunden, die Hotspots auf der Erde ähneln. Das heißt, sie sind gekennzeichnet durch Schwereanomalien, topographische Erhebungen und reichlich Vulkanismus. Auf den meisten dieser Anhöhen befinden sich einige der größten Vulkane des gesamten Planeten. Die Vulkane zählen zu den jüngsten Gebilden des Planeten. Sie entstanden in einer Periode des sogenannten Resurfacing. Dies ist eine beliebte Theorie, die beschreibt, wie Venus ihre innere Wärme verlieren könnte. Resurfacing ist von starkem Vulkanismus gekennzeichnet. Es könnte sich dabei um ein periodisches Ereignis handeln im Laufe dessen die gesamte Oberfläche der Venus erneuert wird. Die Dauer des Ereignisses ist unbekannt und kann nur abgeschätzt werden. Auf zwei Rechnungsweisen wurde die Entstehungsdauer der einzelnen Vulkane berechnet. Einerseits wird eine Rechnungsart angewendet, die sich für die Erde als brauchbar erwiesen hat. Diese Herangehensweise basiert auf dem Vorhandensein von Plattentektonik. Andererseits werden Annahmen über die Plumes, die die topographischen Erhebungen verursachen, getroffen, indem von der beobachtbaren Topographie ausgegangen wird. Es zeigt sich, dass die erste Rechnungsart nicht für die Venus gilt. Die zweite liefert Ergebnisse, nämlich Entstehungsdauern der Vulkane von weniger als einer Million Jahre, die mit der Theorie des Resurfacing vereinbar sind.

Acknowledgments

My thanks go to my supervisor Univ.-Prof. Dr. Maria G. Firneis for her support and guidance. Moreover, I would like to thank Johannes Leitner for his useful input and encouragement through the learning process of this master's thesis.

Special thanks go to my parents for their unconditional love. Without their patience and care, this paper would not have been possible.

I want to express my gratitude to my friends for standing by me throughout the years, and to Patricia Trinkl, Matthias Kühtreiber, and Devan Smith, who kept me sane and never stopped believing in me.

Contents

List of Figures

List of Tables

Chapter 1

Introduction

An important issue concerning planets is their heat budget. How do they lose their internal heat? Which of the present mechanisms of heat transport dominates? The answers to these questions give clues about the activity of planets, their geology, and their possible future. Little is known about our neighboring planet Venus. It is veiled by a thick layer of clouds, and a hostile environment is created by extreme surface temperatures of more than 700 K and a bone-breaking atmospheric pressure of about 90 bar (Faure and Mensing, 2007). This makes it hard to investigate the planet.

Multitudes of scientists generated countless papers developing many theories and applying numerous numerical studies in order to understand the dynamics on Venus and its present state which is often seen as the future of Earth. Our planet gets rid of internal heat predominantly by plate tectonics. Due to the random distribution of mostly pristine impact craters, the surface of Venus is believed to be comparatively young. Moreover, the entire surface is thought to be approximately of the same age (Strom et al., 1994). Therefore, the theory of resurfacing was introduced by Turcotte (1993).

Resurfacing may be a recurring event which is characterized by vigorous volcanism. Due to the lack of plate tectonics, volcanism is seen as the consequence of mantle plumes. These plumes are accumulations of hot rock material that rise through the mantle. Their surface manifestations are called hotspots. Nine such hotspot regions are located on Venus, believed to be possibly active at present (Smrekar et al., 2010). They are among other features characterized by volcanic constructs such as coronae and large volcanoes.

This study is concerned with those nine regions and, in particular, their large volcanoes in the framework of resurfacing. In the first section, Earth and its heat budget will be presented in detail in order to be able to notice similarities as well

as differences to Venus better. Moreover, mantle plumes and hotspots as well as their characteristics will be explained in this section. The second section addresses Venus in comparison to Earth. Section three is devoted to the nine hotspot regions located on Venus. In section four and five, I will present my computations as well as the results, respectively. Finally, the results are discussed in section six.

Chapter 2

Structure of Earth

Earth, with a diameter of about 12,742 km and a mean density of 5.52 g cm^{-3} (Fowler, 2005), consists of three main layers in terms of each layer's physical and chemical properties: the core, the mantle and the crust. The core has a radius of about 3,500 km and, consisting mostly of metallic iron and nickel, sulfur and silicium, a mean density of 10.6 g cm^{-3}. It is divided into two parts. Whereas the inner core is solid but near the melting point, the outer core is molten. The middle layer is the mantle, with a thickness of about 2,840 km and a mean density of 4.6 g cm^{-3}. The mantle is divided into two parts as well: the lower mantle, also known as the mesosphere, and the upper mantle. The outermost layer, the crust, is the thinnest and with a mean density of 2.67 g cm^{-3} the lightest layer. At some ocean ridges the crust is only about 5 km thick, but it can extend to a depth of about 70-80 km in collisional orogens, such as the Himalayas (Cattermole, 1994; Condie, 2001; Bahlburg and Breitkreuz, 2004; Schmincke, 2004).

This knowledge is based on the spreading of compressional and shear waves, also called P- and S-waves, respectively. Seismic waves form during earthquakes and artificial explosions. Their velocities are dependent on physical (such as pressure, density, and temperature) and chemical properties. Shear waves, for example, can propagate in solids, but not in liquids (Davies, 2001; Schmincke, 2004). Thus they give information about the interior of Earth. At the crust-mantle boundary as well as at the core-mantle boundary, the wave velocities change (Condie, 2001). The base of the mantle is defined by the so-called D"-layer with a width of about 100-200 km (Farnetani and Hofmann, 2011). The seismic wave velocities show a large decrease here. At the crust-mantle boundary, there is an abrupt increase in the seismic wave velocities. This discontinuity layer at the base of the crust is called Mohorovičić discontinuity, in short: Moho (Condie, 2001).

The upper and the lower mantle are divided by the 660-km discontinuity. It is

marked by large increases in seismic-wave velocity and density. Its thickness is on average only about 5 km, but it has an extension of up to 20 km. The discontinuity is probably caused by a phase change in Mg_2SiO_4 (forsterite). Phase change may be responsible for another discontinuity in the Earth's mantle, the 410-km discontinuity with a thickness of about 10 km. Magnesium-rich olivine breaks down to the high-pressure Mg-silicate phase wadsleyite. The area between these two continuities is called transition zone. There is yet another zone in the mantle that is characterized by the behavior of seismic waves (Condie, 2001). As the name of the Low-Velocity Zone (LVZ) implies, seismic wave velocities are characterized by a decrease of up to 2% in this area (Schmincke, 2004). Furthermore, the electrical conductivity in this area is high. The LVZ lies in the upper mantle and extends from the base of the crust to depths of 180-220 km with a thickness of 100-200 km (Condie, 2001).

The LVZ lies right beneath the lithosphere. This term is used when describing the structure of the Earth regarding the dynamic behavior of its interior. The lithosphere is the cold and rigid outer layer of Earth. It comprises the crust and the uppermost mantle which are mechanically coupled. Because of the low temperature of its rocks, they hardly deform and the lithosphere stays rigid for long periods of geologic time. The rest of the upper mantle consists of rocks that are sufficiently hot and thus allow solid-state creep. This region beneath the lithosphere is called asthenosphere. The asthenosphere is a solid, but weaker and more mobile layer. In response to applied forces it shows a fluid-like behavior on geologic timescales. The lithosphere-asthenosphere boundary is defined by an isotherm with a value of about $1,300°C$. The rocks above this isotherm show rigid behavior because their temperature is below $1,300°C$, the rocks below the isotherm can deform since they are sufficiently hot (Burke and Wilson, 1976; Turcotte and Schubert, 2002; Schmincke, 2004).

Because of the lower density of the lithosphere, it practically slides over the asthenosphere. The lithosphere consists of separate plates (about 16 large and many smaller ones) that move in relation to one another. This motion of the plates, called plate tectonics, is thought to be driven by convection currents in the mantle (Bahlburg and Breitkreuz, 2004; Schmincke, 2004). At ocean ridges, hot mantle material ascends, cools, and creates new oceanic lithosphere, pushing the adjacent plates away. This process is known as seafloor spreading. Due to the rigidity of the plates, their interior does not deform significantly. Diverging convection currents from the mantle can also put stress on the overlying continental lithosphere. If this stress continues for a long time, it can rift the rigid lithosphere apart into two new plates, and new oceanic lithosphere will be created in between the diverging
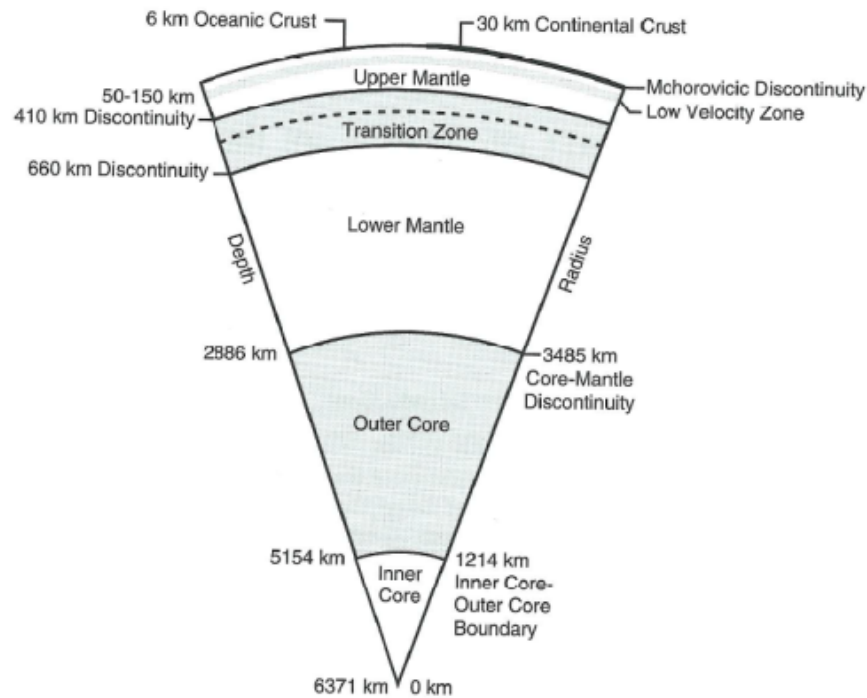
Figure 2.1: The structure of Earth, from Schubert et al. (2001)

plates. This process is called continental rifting (Turcotte and Schubert, 2002; Bahlburg and Breitkreuz, 2004).

Since the surface of Earth is rather constant and new plate area is constantly created, there must be a process destructing the plates. When two plates converge, one descends beneath the other one and is reabsorbed into the underlying mantle. This process that takes place at ocean trenches is called subduction. Just as new oceans can be created by continental rifting, existing oceans can be swallowed and disappear from the surface of Earth on a geologic timescale (Turcotte and Schubert, 2002; Bahlburg and Breitkreuz, 2004).

An important term in order to describe the interaction between the lithosphere and the asthenosphere is isostasy. This word describes the ideal state of rest of the lighter crust on the dense underlying mantle in the absence of disturbing forces. However, permanent dynamic processes, such as erosion, sedimentation, waxing and waning of ice sheets, and extrusive volcanism, disturb isostasy (Watts, 2001). In order to maintain isostatic equilibrium, the asthenosphere responds to the motion of the lithosphere with a fluid-like behavior on a geologic timescale (Bahlburg and Breitkreuz, 2004).

It was observed that mountain ranges have smaller gravitational attractions than

was previously expected from their topographical features (Davies, 2001). In order to explain this discrepancy, a mass deficiency beneath the mountain ranges of about equal mass as the mountains themselves was assumed, similar to Archimedes' principle. This states that a body in water is buoyed up by a force equal to the weight of the fluid that is displaced by the body (Turcotte and Schubert, 2002; Fowler, 2005).

A couple of models aim to explain isostasy. One of the principal models was suggested by George B. Airy. He assumed a dense, fluid interior of the Earth overlaid by a lighter, rigid outer layer (Davies, 2001; Watts, 2001). The continents that are anchored in the lithosphere can be compared to blocks of wood or icebergs floating on water (Burke and Wilson, 1976). It is well known that an iceberg, whose peak is higher than another's, is larger and extends deeper into the water than its counterpart. According to the Airy-model, continents behave in the same way. The higher the topography rises, the deeper its roots reach into the interior of the Earth (Davies, 2001; Turcotte and Schubert, 2002). Following this, the thickness of the lithosphere varies. The oceanic lithosphere in general is thinner than the continental one, a fact which research has confirmed (Bahlburg and Breitkreuz, 2004). The density of the lithosphere, however, is constant (Fowler, 2005).

Another principal isostasy-model was established by John H. Pratt. Following the Pratt-model, differential thermal expansion and, hence, differing lateral densities within the crust cause the depressions and elevations on the surface of the Earth. Low-density rocks lie below high-standing topography and high-density rocks are below low-lying regions. This means that the mass in all vertical columns with the same cross-sectional area is of the same amount (Davies, 2001; Watts, 2001). In both models, geological features are compensated locally. The third isostasy-model which considers regional rather than local compensation was introduced by Felix A. Vening Meinesz. In this model, topography weighs on the surface of the crust. As a consequence of this weight, the crust bends below it like an elastic plate and may even reach into the underlying denser substratum. This scheme resembles the Airy model but with a broader root due to a rigid crust (Watts, 2001).

In all three models, at or below a specific depth, pressures are equal and the weight of the mass of one imaginary column is equal to the weight of any other column all around the Earth. This is the compensation depth. However, the depths of compensation of the different models do not agree with each other (Watts, 2001). Isostasy can be tested by using the gravity field of the Earth. The gravity field is dependent on the shape of the planet as well as the masses distributed within it. Discrepancies between the measured gravity field and that which would be

expected based on the topography and its compensation should point out where isostatic equilibrium by compensation is achieved and to which degree. First, the measured values of the gravity field have to be corrected. The first correction is made in regard of the flattened shape of the Earth and its rotation. Correcting for the height at which the gravity measurement was made rather than at sea level yields the free-air gravity anomaly. In this correction, no mass is assumed between mean sea level and the height of measurement (Watts, 2001; Fowler, 2005).

If the effect of gravity of the mass between sea level and the measurement point is also considered in the correction, the Bouguer anomaly is obtained (Watts, 2001; Fowler, 2005). In general, Bouguer anomalies are negative above topography of high elevation, reflecting the mass deficiency at depth, and positive above the floor of the deep ocean. Whereas in the Bouguer anomaly, only the gravitational attraction of the mass above sea level is considered, the isostatic anomaly additionally includes the gravitational attraction of the mass below sea level and, hence, the mass deficiency by which the topography is supported (Kearey and Vine, 1996). Isostatic anomalies can be compared to free-air anomalies: if the anomalies are small, the region is compensated (Fowler, 2005). Although gravity anomalies reveal whether topography is in isostatic equilibrium, they do not disclose the form of compensation (Kearey and Vine, 1996).

2.1   Heat Budget

It is common knowledge that the interior of Earth is hot. Volcanic eruptions discharge hot magma from the Earth's interior, and geysers eject hot water. Measurements of the temperature in mines and boreholes show that the temperature increases with depth (Davies, 2001). At the center of Earth, the temperature is estimated to be 5,700 $\pm$ 500 °C, whereas on the surface, Earth has an average temperature of a few degrees Celsius. The rate of the increasing temperature with increasing depth is described by the geothermal gradient (Fowler, 2005).

Since the time of its formation, Earth loses heat by transporting it from the hot, deep interior to the surface. Part of this heat originates from the core, the so-called primordial heat. More heat is generated by the decay of the radioactive elements uranium, thorium, and potassium in the rocks of the mantle. In fact, about 80% of the heat lost from the surface of Earth is attributed to radiogenic heat production (Turcotte and Schubert, 2002).

There exist three mechanisms of how heat is transported: conduction, convection, and radiation. The latter is negligible in the Earth's interior. Conduction is the

transfer of heat through a medium by interactions of atoms or molecules within the material. By colliding with each other, the kinetic energy of the particles is transmitted. Convection means that the medium itself moves and transports heat. This mechanism is more effective than conduction (Turcotte and Schubert, 2002; Fowler, 2005). Convection is driven by internal buoyancy, which is caused by horizontal density gradients. Density gradients arise due to thermal boundary layers (TBL) or compositional differences. A TBL is a zone that acts as the boundary of two distinct layers of matter which possess significant differences in temperature. A TBL also serves as the energy distribution layer in which heat is passed from one layer to another (Farnetani and Hofmann, 2011). Buoyancy will cause instability within the thermal boundary layer. This will lead to a fluid from a particular boundary layer leaving its boundaries and, therefore, driving convection (Davies, 2001).

Because of the high pressure and temperature in the interior of Earth, the solid mantle rocks behave like a fluid on a geologic timescale (Schubert et al., 2001). In this context, the so-called Rayleigh number is of importance. It compares the heat that is transported by convection to the heat that is transferred by conduction (Fowler, 2005). The dimensionless number is written as:

$$Ra = \frac{\alpha g \Delta T d^3}{\nu \kappa} \ . \tag{2.1}$$

The coefficient of thermal expansion is denoted by α. The more a fluid expands, the more its density will decrease and, subsequently, its buoyancy will increase, driving convection. The gravitational acceleration is g, ΔT is the difference in temperature across the boundary layer, and d is the thickness of the layer. The quantities in the denominator, kinematic viscosity, ν, and thermal diffusivity, κ, oppose convection. The more viscous a fluid is, the less likely it is to move, and the more a fluid diffuses heat, the less likely it is to convect. Thermal diffusivity, in fact, describes the efficiency of conduction (Fowler, 2005).

A critical value of the dimensionless Rayleigh number describes the onset of convection. Determining an exact value of the critical Rayleigh number Ra_c is difficult, since the number depends on the details of heating, the given boundary conditions as well as the form of the fluid. Nonetheless, it can be said that Ra_c is of the order of 10^3. For the upper mantle of Earth, an estimated value of Ra is about 10^6, for the entire mantle the value lies in the range 10^7 and 10^9. In either case, the estimated value is well above the critical value (Turcotte and Schubert, 2002; Fowler, 2005).

Convection, thus, is the main mechanism of heat transport in the mantle of Earth,

manifesting itself in the form of plate tectonics on the surface. Knowing how Earth controls its heat budget does not allow drawing similar conclusions about other terrestrial planets or moons. Mars, Mercury, and the Earth's Moon all have globally continuous lithospheric shells. The dominating heat transfer mechanism of these bodies is conduction (Solomon and Head, 1982; Cattermole, 1994). On Jupiter's moon Io, however, hotspot volcanism appears as the dominant mechanism (Solomon and Head, 1982; Williams et al., 2011). On Earth, conduction plays a minor role in the mantle, but it dominates in the crust, because the crust material is rigid and cannot flow (Fowler, 2005). Hotspot volcanism occurs on Earth as well, but it contributes less than 10% to the terrestrial heat loss (Hill et al., 1992; Malamud and Turcotte, 1999; Schmincke, 2004).
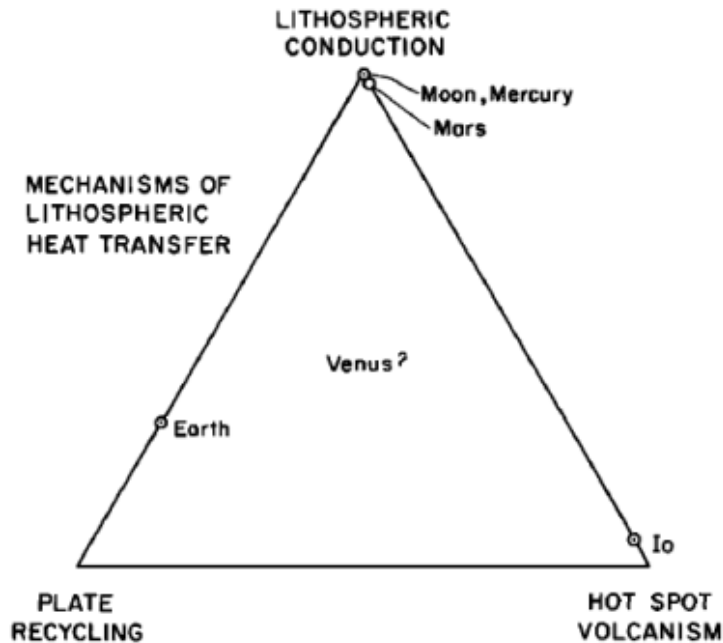
Figure 2.2: Mechanisms of heat transport: A schematic diagram showing the importance of the various mechanisms of heat transport on the terrestrial planets and a couple of satellites, from Solomon and Head (1982)

2.2 Hotspots

Most volcanoes form along plate boundaries: island arc volcanoes are a result of subduction, at mid-ocean ridges hot magma rises due to seafloor spreading, and rifting of continental plates is another source of volcanism (Cattermole, 1994;

Bahlburg and Breitkreuz, 2004). Hotspots are isolated centers of volcanic activity that are found within the interiors of plates and which therefore are not direct consequences of the plate tectonic processes. The Hawaiian Islands are the most prominent example. However, hotspots are not uncommon at a spreading ridge. According to Farnetani and Hofmann (2011), at least 21 hotspots are located near an ocean ridge, including Iceland, Galapagos, and the Azores. Iceland counts as a hotspot because of an anomalous thick oceanic crust that has been elevated above sea level (Burke and Wilson, 1976; Turcotte and Schubert, 2002). The oceanic crust with a normal thickness of 8-10 km has thickened below Iceland to about 40 km. Moreover, the Mid-Atlantic Ridge near Iceland is unusually shallow (Farnetani and Hofmann, 2011).

Another reason, why Iceland counts as a hotspot, is that the volume of lava that the Iceland hotspot has ejected exceeds the one at mid-ocean ridges (Burke and Wilson, 1976). About 30% of the globally ejected lava on Earth within the past 500 years is attributable to the Iceland hotspot (Waugh, 2002).

Furthermore, hotspot volcanoes can be distinguished from volcanoes at plate boundaries by the composition of lava and hence the style of eruption. The lavas of hotspot volcanoes are like those of ocean ridges basalts, but they are richer in alkali metals, such as lithium, sodium, and potassium. Moreover, they have a lower viscosity and they lack volatiles (Burke and Wilson, 1976; Cattermole, 1994; Bahlburg and Breitkreuz, 2004). The viscosity of lava flows is dependent on their temperature as well as the concentration of silica (SiO_2). The more silica lava contains, the more viscous it is. Rhyolite lava with 70 wt% SiO_2 is much more viscous than basalt lava with about 50 wt% SiO_2 (Faure and Mensing, 2007).

The effusion at hotspot volcanoes is rather quiescent in contrast to the violently explosive eruptions of volcanoes associated with plate boundaries. This is a consequence of the different tectonic settings. The lava that rises at plate boundaries may be infused with subducted oceanic crust, ocean floor sediments, and silica-rich continental crust, material that contains volatiles and tends to erupt explosively. The magma at hotspots with low silica and volatile contents rises from the mantle without being mixed up (Burke and Wilson, 1976; Cattermole, 1994; Bahlburg and Breitkreuz, 2004).

The composition of lava of the Hawaiian hotspot differs from the hotspot lava described above. Whereas most hotspot lavas have a lack of tholeiites, at the Hawaiian hotspot tholeiites dominate at the growing stage of the volcanoes. However, the hotspots have in common that intermediate and felsic lavas, both with high silica contents, are very uncommon (Cattermole, 1994; Condie, 2001).

The two most common appearances of basaltic lava are the pahoehoe and aa lavas.

The former is of very low viscosity and therefore can flow for many kilometers through lava tubes. Once solidified on the Earth's surface, the pahoehoe lava shows a very smooth surface. If pahoehoe lava cools rather slowly, it can change to aa lava due to increasing crystallinity. This type of lava is of higher viscosity than pahoehoe and forms at a lower temperature, but it is still very fluid. Whereas pahoehoe lava is very characteristic for Hawaii, aa lava is also typical of many other hotspots. Its surface is less smooth but rather consists of loose, broken up and sharp blocks and ridges. The transition of pahoehoe to aa lava cannot be reversed (Schmincke, 2004).

As the composition of the lavas is different, so are the volcanic edifices that are built up. Shield volcanoes are built up by fluid lava as found at hotspots. Therefore they are of low height and large diameter. In addition to shield volcanoes, subsidence calderas along with shield- and fissure-related flows that form volcanic plains are generated. These volcanic edifices are not restricted to hotspots but are also formed along mid-ocean ridges and continental rifts. Similarly, strato-volcanoes primarily form at subduction zones, but are also possible at hotspots. They are accompanied by viscous flows, endogenous domes, and pyroclastic flow deposits (Cattermole, 1994).

Hotspots are seen as the surface manifestations of mantle plumes. A mantle plume is thought to be an accumulation of hot, buoyant material in the mantle that rises because of its relatively lower density. While ascending through the mantle, the mantle plume is believed to take the shape of a mushroom, with a head on top and a trailing tail. As the plume reaches the base of the denser lithosphere, it spreads horizontally beneath it. Morgan (1971) was a pioneer in developing the idea of the correlation between hotspots and mantle plumes.

The total number of hotspots on Earth is unclear, largely due to the uncertain criteria which define a hotspot. Morgan (1972b) estimated there to be about 20 hotspots, while Burke and Wilson (1976) mentioned 122 hotspots, which could be an underestimation by their own account. A hotspot could be seen as any amount of mid-plate volcanism that is independent of the global mid-ocean ridge as well as of the island arc system which are consequences of seafloor spreading and subduction, respectively. With this loose definition the total number is high. If a hotspot is a volcanic center that is also persistent in time, the total number decreases. The St. Helena hotspot in the Southern Atlantic Ocean, for example, is one of the oldest known hotspots on Earth. It began to produce basaltic lava about 145 m.y. ago (Crough, 1983; Schubert et al., 2001).

The distribution of hotspots is neither random nor uniform (Turcotte and Oxburgh, 1978; Stefanick and Jurdy, 1984; Richards et al., 1988; Sleep, 1990). Numerous

hotspots can be found in Africa, but there are comparatively few on the rest of the globe (Turcotte and Oxburgh, 1978). Stefanick and Jurdy (1984) performed three statistical analyses on two different hotspot data sets, one comprising 42 hotspots (Crough and Jurdy, 1980) and one 117 (Burke and Wilson, 1976). They performed the chi-square test on boxes of equal areas, reviewed the cumulative distribution, and constructed a density function. All three methods yield a non-uniform distribution, although there appears to be a concentration of hotspots on half of Earth's surface with a rather uniform distribution. Hotspots can be isolated (such as Hawaii and Iceland), in closely spaced families or loosely grouped (Sleep, 1990).

Moreover, hotspots can be found in both oceanic and continental areas. Hawaii and Iceland are both oceanic examples, while Yellowstone in the Western United States is a continental one (Turcotte and Schubert, 2002). However, most hotspots seem to be located in the ocean. Morgan (1972a) as well as Burke and Wilson (1976) explained this inequality as follows: if a plate comes to rest on a hotspot, a dome will swell up. It continues growing until deep fissures will develop and the plate may rupture as a consequence and create a new ocean. Another explanation for this discrepancy may be that the continental lithosphere is up to 150 km thicker than the oceanic one. Considering decompression melting, the conditions beneath the oceanic lithosphere are ideal for the melting of plumes. One last reason for this discrepancy is that continents that have a lack of hotspots accumulate over downwellings. Plumes hardly ascend there (Farnetani and Hofmann, 2011).

One characteristic of hotspots is that often they represent the end of a well-defined chain of volcanoes; the so-called hotspot track. The age of the volcanoes increase almost linearly with increasing distance from the hotspot. Wilson (1963) was the first to suggest that these tracks are generated as the Earth's crust moves over a hotspot that is relatively fixed, although he suggested convection currents as the cause of hotspots, rather than mantle plumes. As the volcano moves with the crust past the hotspot, the volcano is cut off from the magma source. While one or more new volcanic centers form above the hotspot, the old volcano flattens by erosion (Condie, 2001). It will become denser as it cools and, hence, finally subside isostatically (Schmincke, 2004). The depth of these underwater volcanoes, known as guyots, increases with advancing age (Condie, 2001).

Again, the most prominent example of a hotspot track is the Hawaiian-Emperor chain that includes more than 100 shield volcanoes. The majority of these are seamounts. There is a significant bend between the Emperor chain and the Hawaiian chain which implies that the underlying Pacific plate changed its motion from north to north-west about 43 m.y. ago. The Hawaiian-Emperor chain reaches

from today's youngest member of that chain, Lō'ihi Seamount, an active submarine volcano, over almost 6,000 km of active volcanoes, eroded volcanic edifices, atolls, and guyots to the Meiji Seamount near the Aleutian Islands. It spans a period of time of about 80 m.y. (Condie, 2001; Schubert et al., 2001).

Such hotspot tracks can also be found on the continents, but they are less well defined than in ocean basins. The thicker continental lithosphere makes it more difficult to form a clear hotspot track. The most prominent example of a continental hotspot track is the Yellowstone track in North America (Condie, 2001).

As indicated above, many hotspots are marked by active or recently active volcanism. Nonetheless, not all hotspots possess such an extensive volcanic history. Bermuda, for example, has been quiescent for about 30 m.y. Since it lies on top of a seafloor swell, it can be seen as a hotspot. According to Schubert et al. (2001), hotspots without extensive volcanism that lie on top of seafloor swells or broad topographic rises, qualify as such.

One important characteristic of hotspots is that many of them are overlain by topographic swells. These swells are often elongated parallel to the direction of motion of the underlying plate and therefore have the same orientation as hotspot tracks. They start with a steep uplift at the active hotspot, and then gradually decrease (Crough, 1983). They typically have a relief of 500-1,000 m (up to $3,000$ m) and widths of 1,000-2,000 km and occur in both the oceanic and the continental lithosphere (Herzen et al., 1982; Malamud and Turcotte, 1999). The cross-sectional shape of swells appears to be quite simple: they are rather flat with gently sloping sides (Crough, 1983). The hotspot volcanoes and the underlying swell form simultaneously as the plate moves over the hotspot. As the plate moves on and the volcanoes age, the swell subsides abnormally fast - faster than normal oceanic crust (Condie, 2001). What distinguishes the continental swells from their oceanic counterparts is that continental swells do not have a noticeable elongate shape. It might be that erosion covers their tracks (Crough, 1983).

The origin and the support of swells have not been completely understood yet. Several hypotheses on how hotspot swells are formed have been suggested. However, most of these hypotheses have weaknesses and, hence, could be ruled out (Crough, 1983; Vogt and Jung, 2007). Today, dynamic support by the mantle plume itself is favored. Whenever the plume head, which is estimated to be up to 250°C hotter than the surrounding mantle material, impinges on the rigid lithosphere, it spreads laterally (Schmincke, 2004; Farnetani and Hofmann, 2011). The mushroom-like head causes uplift of the overlying lithosphere by applying stresses to the base of it (Cadio et al., 2012). However, the "dynamic uplift" model may be supported by the "thermal rejuvenation" model as is believed in the case of
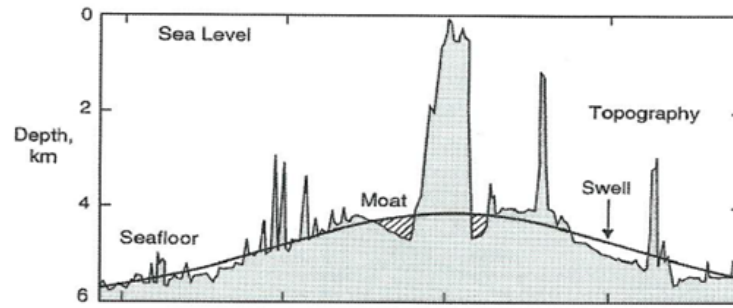
Figure 2.3: Hotspot swell: Topographic profile of the Hawaiian ridge showing the topographic swell, from Turcotte and Schubert (2002)

Hawaii (e.g. Li et al., 2004). The thermal rejuvenation model combines reheating and thinning of the lithosphere. The base of the lithosphere is heated and gradually replaced by less dense asthenospheric material (Farnetani and Hofmann, 2011; Cadio et al., 2012).

The hotspot swells are associated with positive geoid anomalies. The geoid is the Earth's gravitational equipotential surface. It roughly coincides with sea level. The upward motion of the mantle plume raises the surface of Earth. Air or water on the surface of Earth is replaced by denser rock material, which is compensated by the lighter mantle material at depth. This contribution to the geoid is called a positive geoid anomaly (Condie, 2001).

The geoid anomalies at the hotspots are rather small. However, there are two instances of unusual anomalies situated in the South-Central Pacific and in Africa known as "superswells" caused by superplumes, or large-scale mantle upwellings. These are believed to be regions of the convective mantle that are warm (and therefore buoyant) due to the absence of subduction zones, where cool lithosphere is reintegrated into the mantle. In other words, these upward flows constitute the counterpart of the downward motion of subducted material. The two superswells, thousands of kilometers in diameter and one kilometer or more in height, are underlain by zones in the lower mantle of low seismic velocity (Condie, 2001; Farnetani and Hofmann, 2011). Moreover, there is evidence that these massive upwellings are chemically distinct (Ishii and Tromp, 1999; Masters et al., 2000). Most hotspots and, hence, mantle plumes, occur within these large mantle upwellings, indicating that plumes are more probable to form in regions of upwelling (Condie, 2001). It has been suggested that the mantle upwellings feed the majority of hotspots, as the superplumes impinge on the lithosphere and spread laterally (Schmincke, 2004; Vogt and Jung, 2007).

In general, there is a poor correlation between gravity and topography on Earth

(Cattermole, 1994). The largest gravity anomalies overlie subduction zones as well as convergence zones. However, the two superswells are characterized by gravity highs as well (Davies, 2001). At higher spatial resolution, also hotspots show gravity highs (Condie, 2001; Davies, 2001). These gravity highs reflect the denser mantle material which rises in the mantle plumes. Although the rising material is less dense than the material of the surrounding mantle, it is still denser than the crustal material (Condie, 2005).

Hotspots are often associated with so-called Large Igneous Provinces (LIPs). These are large accumulations of voluminous, mostly mafic (rich in magnesium and iron) rock emplacements whose occurrence is not solely restricted to hotspots (Coffin and Eldholm, 1994). They are believed to mark the initiation of magmatism caused by a mantle plume. Richards et al. (1989) suggested in their mantle plume initiation model that the voluminous emplacement of a Large Igneous Province (LIP) can be attributed to the head of the mantle plume, whereas the magma which effuses during the succeeding hotspot activity originates from the plume tail. Even though LIPs include large volumes of magma, their emplacement occurs within a rather short amount of time, namely a few million years.

One other characteristic of hotspots is high heat flow, reflecting a mantle plume source (Condie, 2001). On Earth, the total heat loss is about (42-44) x 10^{12} W, which makes an average heat flow of about 82-86 mW m^{-2}. The oceans account for approximately 70% of the total heat loss. The major part of the heat loss originates at mid-ocean ridges, where new oceanic lithosphere is created and cools (Fowler, 2005). The values of heat flow here lie in the range of 100 up to 200 mW m^{-2}, and even more. Thus, it is significantly higher than the average value (Condie, 2005). The younger the underlying oceanic crust and, accordingly, the more recent tectonic activity regarding continental regions, the higher the measured heat flow (Fowler, 2005). The lowest heat flow values are found above old and stable regions, such as deep ocean basins and trenches as well as shield areas and platforms, respectively. These values lie in a range of $40 - 50$ mW m^{-2}. Hotspots (following Condie (2005) including volcanic islands and oceanic plateaus) show heat flows with values between 50 and 80 mW m^{-2}.

As mentioned before, hotspots seem to be relatively fixed with respect to the mantle. Morgan (1972b) studied three island chains in the Pacific plate: the Hawaiian-Emperor seamount chain, the Tuamotu-Line, and the Austral-Gilbert-Marshall island chains. These chains show some similarities that cannot be ignored. All three island chains are rather parallel, they grow older toward the northwest, and they show recent volcanic activity at the southeastern end (Burke and Wilson, 1976). These similarities indicate that they have been generated by

the same cause, namely the rigid Pacific plate moving over three fixed hotspots: Hawaii, Easter, and the MacDonald Seamount, respectively. However, the exact location of the hotspot that is responsible for the Tuamotu-Line island chain is controversial (Condie, 2001; Schubert et al., 2001). Nonetheless, Morgan (1972b) measured that whereas the Hawaiian-Emperor seamount and the Tuamotu-Line island chains trace the same motion fairly exactly, the hotspot responsible for the Austral-Gilbert-Marshall chain moved at a rate of about 1 cm yr^{-1} with respect to the others, which is a lot less than the velocities of plates (Farnetani and Hofmann, 2011). Therefore, it is safe to say that hotspots are relatively fixed in the mantle forming a reference frame. This so-called hotspot reference frame can be used to reconstruct the past motion of the plates (Condie, 2001).

Also the relative motions of the hotspots in the Atlantic Ocean on the one hand and the Indian Ocean on the other hand have been studied (Burke et al., 1973; Molnar and Francheteau, 1975). The discrepancies between these two groups are even bigger, that is to say in the range of plate velocities (Condie, 2001; Courtillot et al., 2003). Comparisons between the groups have to be made with caution.

Nonetheless, it should be noted that not all hotspots are characterized by the mentioned features. Many hotspots are variable. They produce either segmented tracks or show short pulses of activity. For those, the relative stationarity is a less accurate description (Malamud and Turcotte, 1999). Some hotspots lack a Large Igneous Province (Farnetani and Hofmann, 2011). Bermuda has been mentioned before as an example of a hotspot that lacks an extensive volcanic history. Vogt and Jung (2007) point out more features which are characteristic for hotspots that Bermuda does not show. The Bermuda rise, for example, runs perpendicular to the direction of the motion of the plate. Further, there is no age-progressive chain as clear as Hawaii, but rather a cluster of four volcanic edifices. The orientation of this cluster is in a right angle to the direction of the motion of the plate, as well (Vogt and Jung, 2007).

2.3   Mantle Plumes

As has been mentioned before, the reason for hotspots is believed to be a mantle plume, an accumulation of mantle material (solid rocks) that is hotter than the material of the surrounding mantle, thus, less dense and therefore rises upwards (Condie, 2001; Farnetani and Hofmann, 2011). A mantle plume consists of two distinct parts: a leading, symmetrical and almost spherical head at the top and a trailing, rather narrow conduit or tail which connects the plume head to the

source region (Condie, 2001). The morphology of the mantle plume is dependent on the viscosity contrast between the hot plume material and the rock material of the mantle above the rising plume. If this viscosity contrast is low, then the radius of the plume head will be insignificantly bigger than the trailing tail. However, if the contrast is big, the mantle plume assumes a more mushroom-like shape with a large head and a narrow tail. This plume shape is favored as it is expected that the mantle plume is a few hundred degrees hotter than the surrounding mantle and therefore significantly less viscous (Farnetani and Hofmann, 2011). Moreover, the less viscous the plume material is, the thinner the tail will be. This relation is based on the fact that for a similar flow rate a thin tail is sufficient for less viscous material. Buoyancy flux and temperature differences show almost no effect onto the structure of the plume (Condie, 2001).

As the mantle plume rises through the mantle, the head entrains material of the surrounding mantle (Condie, 2001). After reaching the base of the lithosphere, plume heads will spread horizontally in the comparatively weaker asthenosphere and partial melting due to decompression occurs (Condie, 2001; Smrekar and Stofan, 2006). Heads can be between 500 and 3000 km in diameter, whereas the tails are expected to have diameters between 100 and 300 km, as based on fluid dynamics. However, diameters of plume tails estimated by tomographic imaging (Montelli et al., 2004) reach values of 400 km. Plume heads with diameters of more than 1500 km are referred to as superplumes (Hill et al., 1992; Condie, 2001; Farnetani and Hofmann, 2011). Experiments by Olson and Nam (1986) showed that, as the mantle plume head impinges upon the base of the lithosphere, the surface will be uplifted rapidly while the crust is compressed as well as extended (Faure and Mensing, 2007). As the plume head stagnates and flattens, the surface will slowly subside. According to models by Farnetani and Richards (1994), uplift of the surface is always followed by significant flood volcanism. Once the plume head has stopped its upwards motion, the tail will provide the head with hot mantle material from the source region (Condie, 2001).

The source regions of mantle plumes are thermal boundary layers (TBL). Rayleigh-Taylor instabilities generate plumes as indicated by fluid dynamical considerations (Loper and Stacey, 1983; Farnetani and Hofmann, 2011). However, the plume only separates from the TBL and starts rising after it has reached a sufficiently large volume. The size of the plume head before separation is determined by the mantle viscosity. The viscosity of today's mantle of the Earth has a value of 1022 Pa s. Thus, a plume head only starts to rise after it has reached a diameter of about 400-600 km. Owing to the fact that Earth's mantle used to be hotter with a lower viscosity, mantle plumes that cause hotspots nowadays were comparatively
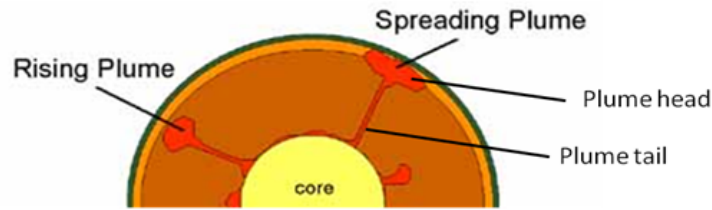
Figure 2.4: Sketch of mantle plumes rising from the core-mantle boundary. Head and tail are clearly discernible. As the mantle plume reaches the lithosphere, the head spreads out laterally, (`http://faculty.weber.edu/bdattilo/shknbk/notes/htsptplm.htm`, retrieved: 2014-10-27)

smaller whenever they separated from the thermal boundary layer and started ascending (Condie, 2001).

How long does it take a mantle plume to rise up to the base of the lithosphere? According to Griffiths and Campbell (1990), the rate of rise of the mantle plume head is determined by the viscosity of the surrounding material. Moreover, the larger the volume flux of the mantle plume and the larger the temperature difference between the plume material and the surrounding rocks, the faster the mantle plume rises. Mantle plumes with these parameters will also accumulate the greatest volume. Furthermore, they are hardly affected by entrainment of the surrounding mantle material. In today's Earth mantle it takes such a plume about 50 m.y. to rise (Condie, 2001).

Since the plume tail is much smaller than the head, the buoyancy contrast there will be considerably weaker. Therefore, it is subject to distortion by mantle flow. A strong distortion may cause the plume head to be separated from the tail, which may split up. The disconnected segments may be incorporated into the surrounding mantle. Plumes with high buoyancy fluxes are more resistant to distortion. From the fact that hotspot locations do not change in relation to one another, it can be concluded that there is little distortion. This indicates that plumes rise with a high velocity owing to an upper mantle that is much less viscous than the lower mantle (Condie, 2001).

The origin of mantle plumes is unclear, especially because they cannot be easily observed. Mantle plumes arise due to instabilities in thermal boundary layers. The D"-layer at the core-mantle-boundary is such a thermal boundary layer and therefore Morgan (1972b) suggested the lower mantle as the source of mantle plumes. A deep source would explain that hotspots are relatively fixed compared to the plates that drift over them (Courtillot et al., 2003). Moreover, mid-ocean ridges migrating over hotspots leave the hotspot track unaltered (DePaolo and Manga, 2003). In addition, the enriched magma compositions support the idea of

deep mantle sources rather than shallow ones (Condie, 2001).

In recent years professional opinions shifted toward shallow sources of mantle plumes due to a lack of evidence of deep plumes as well as fundamental features of hotspots that could not be explained by a deep source region (e.g. McNutt et al., 1997; Christiansen et al., 2002; Anderson, 2005). The mantle transition zone between the 410-km and the 660-km discontinuities may be another thermal boundary layer that could be the origin of plumes (Courtillot et al., 2003; Fowler, 2005). However, Farnetani and Hofmann (2011) doubt that this second thermal boundary layer exists arguing that phase change would not stop the mantle from convecting. Moreover, if a mantle plume originates from the 660-km discontinuity, it will not be able to entrain a lot of material before it reaches the lithosphere. Therefore, a shallow mantle plume will only have a diameter of about 300 km as it stagnates (Griffiths and Campbell, 1990; Condie, 2001). Furthermore, such a small plume would hardly be able to produce a large igneous province as are observed at the onset of hotspots (Courtillot et al., 2003).

The following observations have been identified as evidence in support of mantle plumes. First of all, the Rayleigh number of the Earth's mantle with a value between 10^6 and 10^8 is high enough in order to allow convection and to ensure that thermal boundary layers, such as the D"-layer, become unstable from time to time and enable mantle plumes to arise (Farnetani and Hofmann, 2011). Moreover, the magma erupted at hotspots shows a distinct geochemical composition with isotopic signatures that clearly distinguishes it from magma erupted at mid-ocean ridges (Hofmann, 1997). Furthermore, Burke and Torsvik (2004) reconstructed the eruption sites of 25 LIPs of the last 200 m.y. by using a paleomagnetic reference model. This model makes use of the magnetism that remains in the rocks that they have acquired in the varying magnetic field of the planet (Condie, 2001). Burke and Torsvik (2004) found out that at the time of eruption, 90% of the LIPs were located above zones of low S-wave velocities indicating regions of hotter material (Farnetani and Hofmann, 2011). Last but not least, although the seismic detection of the narrow mantle plume tails in the deep is challenging, a few thorough studies have yielded promising results. On the one hand, Romanovicz and Gung (2002) imaged two mantle plumes by seismic elastic tomography deep in the mantle, namely the two superplumes beneath the South-Central Pacific and Africa. The two superplumes could also be an accumulation of several smaller mantle plumes instead (Schubert et al., 2004). Montelli et al. (2004), on the other hand, show tomographic evidence for at least six deep plumes that originate from the lowermost mantle. Additionally, other plumes seem to occur only in the upper mantle.

However, a distinct chemical composition of hotspot lava on its own is not a proof of the existence of an underlying (deep) mantle plume. At first, scientists believed that the composition of hotspot lava differs from that at mid-ocean ridges, whose source is the upper mantle, because it was derived from the lowermost mantle. This led to a layered mantle model with a depleted upper mantle and a primitive lower mantle (Farnetani and Hofmann, 2011). However, subduction slabs were imaged (e.g. der Hilst et al., 1997) that extended down into the lowermost mantle, destroying the chemical separation between the layers. Moreover, at several hotspots, magma was found that showed crustal-like components that were derived from subducted oceanic crust as suggested by Hofmann (1997). This recycled crust material seems to be more common in mantle plumes than in mid-ocean ridges. Christensen and Hofmann (1994) showed with numerical models that the denser recycled material may sink to the base of the mantle and be stored there before it may be reintegrated into mantle plumes. Therefore, it is nearly impossible to glean sufficient geochemical evidence to prove if an object is, in fact, a mantle plume (Farnetani and Hofmann, 2011).

Morgan (1978) introduced the idea of more than just one type of hotspot. Courtillot et al. (2003) distinguished between three different types of hotspots. For hotspots caused by deep mantle plumes, they listed five criteria: the presence of a hotspot track and of flood basalt at its origin, a large buoyancy flux (in excess of 10^3 kg s^{-1}), a low shear wave velocity in the mantle beneath the hotspot showing the presence of less dense and probably hotter material, as well as high Helium or Neon ratios. This last criterion was still based on the layered-mantle model. It was believed that mantle plume-derived basalts were characterized by a high ^{3}He/^{4}He ratio as opposed to basalts at mid-ocean ridges. The non-radiogenic ^{3}He isotope, one of the primordial noble gases, was thought to be primarily located in the primitive lower mantle. The ^{4}He isotope is the result of uranium and thorium decay (Farley and Neroda, 1998; Farnetani and Hofmann, 2011). They applied these criteria to a list of 49 hotspots and, as a result, obtained only seven hotspots that fulfill most of the criteria. Hawaii and Iceland are two of those primary plumes (Courtillot et al., 2003).

According to Courtillot et al. (2003), the secondary plumes arise from the two superplumes beneath Africa and the South Pacific. The superplumes themselves originate from the lower mantle like the primary mantle plumes. In a chemically heterogeneous mantle, the formation of both deep mantle plumes and superplumes arises naturally. According to Davaille (1999), the local buoyancy ratio makes the difference, namely the ratio between the chemical density anomaly and the thermal density anomaly. If this ratio is low, a superplume is formed, whereas if the

ratio is high, a primary plume is generated. Courtillot et al. (2003) suggest that the South Pacific superplume is stuck at the transition zone in the upper mantle. Due to a thermal boundary layer between the superplume and the surrounding mantle, secondary plumes could be generated. The secondary plumes distinguish themselves from the primary plumes in being rather short lived and therefore forming short hotspot tracks that lack flood basalts at their onset. Possible examples for hotspots caused by secondary mantle plumes are Tahiti and Pitcairn. The third type of hotspot as according to Courtillot et al. (2003) is not due to a mantle plume. Condie (2001) mentions, in addition to the mantle plume model, three basic models that try to explain the age-progressive hotspot tracks. One of these models is the propagating fracture model. It is assumed here that the lithosphere breaks up due to stresses. The fracture of the lithosphere migrates through the moving lithosphere into its direction of motion but is slightly offset due to transform faults. Volcanism arises originating from the asthenosphere. Magma penetrates the lithosphere where new fractures were formed. As the fracture moves on, a chain of volcanoes is created (Green, 1971). Another model by Wilson (1963) propagates a system of convection currents in the mantle of Earth. While mid-ocean ridges lie on top of such rising currents, volcanic chains such as Hawaii are formed offside. Lava rises from the stable core of a convection cell to the surface which is carried by a jet stream. The third model was introduced by Shaw (1973). It describes shearing between the lithosphere and asthenosphere. The terms "lithosphere" and "asthenosphere" here are based on kinematic concepts and not on seismic criteria. The counterflow that is regulated by thermal feedback causes melting in the asthenosphere by dynamic effects. The shear melting is fixed relative to the deep mantle (Shaw, 1973).

However, none of these alternative models can explain all the observed features of hotspots, such as the hotspot swell and the enrichment of magma compositions suggestive of the deep mantle as the source region. The mantle plume model can explain various relationships between melting, the lithosphere, temperature and such, and due to this, it is the only model which has persisted throughout time (Condie, 2001). It has to be mentioned that there is little direct (geological, geophysical, geochemical, petrological) evidence for the existence of plumes and there are still some observations that the mantle plume model cannot adequately explain. Nevertheless, although there are a few skeptics (look, for example, at `www.mantleplumes.org`), the concept has, in general, steadily gained acceptance since it is consistent with the present understanding of the dynamics in the mantle (Schubert et al., 2001).

Chapter 3

Venus compared to Earth

Venus is said to be the sister planet of Earth due to their similar sizes, bulk densities and gravities. With a diameter of 12,104 km, Venus is only slightly smaller than Earth. The densities are 5,515 kg m^{-3} (Turcotte and Schubert, 2002) and 5,243 kg m^{-3} for Earth and Venus, respectively, and their gravities 9.81 m s^{-2} and 8.87 m s^{-2}. Owing to similarities in size and density, Venus is expected to have an internal structure analogous to Earth: a core with a radius of about 3,450 km that is expected to be partly molten resembling the core of Earth, a mantle with a resulting thickness of about 2,600 km, and a crust (Cattermole, 1994; Faure and Mensing, 2007).

A number of investigations, however, showed that these two planets are, in fact, quite different. The surface temperature of Venus of about 470°C combined with the atmospheric pressure of 90 bar lead to a very inhospitable environment. The high temperature on Venus is a result of the high amount of carbon dioxide in the atmosphere. Whereas on Earth carbon dioxide accounts for only about 0.031% of the atmosphere, on Venus it accounts for more than 90%. Sunlight that reaches the surface of Venus heats up the rocky surface of Venus. The rocks emit infrared

Table 3.1: Selected physical properties of Earth and Venus. The values designated with an asterisk are from Turcotte and Schubert (2002), the rest from `http://nssdc.gsfc.nasa.gov/planetary/factsheet/venusfact.html`, retrieved: 2014-10-27.

	Earth	Venus
Radius [km]	6,371	6,051.8
Mass [10^{24} kg]	5.9726	4.8676
Mean density [kg m^{-3}]	5,515*	5,243
Surface gravity [m s^{-2}]	9.81*	8.87
Surface temperature [K]	288*	730*
Surface pressure [bar]	1.014	92

radiation which is absorbed by carbon dioxide in the atmosphere. The energy of the radiation is converted into heat resulting in the greenhouse effect. It should be mentioned that, although Venus is closer to the Sun than Earth, its surface receives less sunlight than Earth because Venus is covered by a thick layer of clouds at a height of about 50 km consisting of droplets of almost pure sulfuric acid. The surface of the planet receives only about 20% of the sunlight reaching Venus. The rest is reflected back into space by the clouds (Cattermole, 1994; Faure and Mensing, 2007).

The striking lack of water is no surprise considering the extreme temperatures on Venus. It is not known, however, why the water disappeared in the first place. Like Earth, Venus received water from comets and icy planetesimals. Due to the high velocities of the impacting bodies, water and other volatiles vaporized and remained in the atmosphere. It is still unknown, if the water vapor condensed forming an ocean on Venus similar to Earth and then re-evaporated. A possible explanation for the disappearance of water is that, once evaporated, the molecules were dissociated by ultraviolet radiation of the Sun. Due to their small mass, the hydrogen molecules escaped from the atmosphere into space when the gravitational attraction of the planet could not retain them. However, this model does not explain the fate of the oxygen gas, which would not be expected to leave the atmosphere of Venus (Cattermole, 1994; Faure and Mensing, 2007).

Due to the lack of water, it is believed that Venus does not have an asthenosphere and thus, no plate tectonics. The water in the Earth's lithosphere is believed to make it sufficiently weak in order to break into plates that then slide over the asthenosphere (Smrekar and Stofan, 2006). The global oceanic rift system and the arcuate oceanic trenches are direct consequences of plate tectonics. Such features can hardly be found on Venus (Cattermole, 1994; Turcotte and Schubert, 2002).

Besides the absence of water, Venus also lacks an intrinsic magnetic field (Faure and Mensing, 2007). The reason for this is unknown, considering that the way in which the terrestrial magnetic field is generated is still not fully understood. The theory currently employed to describe magnetism maintained by planets and stars is known as Dynamo action. Using Earth as an example, this theory states that as electric currents pass through the electrically conductive liquid outer core surrounding Earths solid iron inner core, an existing magnetic field is maintained which is prone to decay (Turcotte and Schubert, 2002; Fowler, 2005).

However, a few hypotheses attempt to explain the absence of a magnetic field of Venus. One explanation is the slow rotation of Venus. Stevenson et al. (1983), however, argue that the rate of the rotation is sufficiently high so that the Coriolis effect plays an important role in large-scale motions in the core. If there is an ad-

equate energy source, then Venus should have a dynamo. Another explanation is that the core of Venus is either completely solidified or liquid, which precludes the generation of a magnetic field by dynamo action (Schubert et al., 2001). Nimmo (2002) suggests that the lack of plate tectonics may be the reason for the missing magnetic field. Without plate tectonics, the mantle of Venus cannot cool fast enough in order to generate core convection and subsequently a geodynamo.

3.1 Observing Venus

The layer of clouds that enshrouds Venus makes it difficult to observe and investigate the planet. Not even the most powerful optical telescope can penetrate these clouds. In the 1940s, an invention of a new technique made it finally possible: radio detection and ranging, better known as radar. This technique works with electromagnetic waves at wavelengths that are much longer (0.8-70.0 cm) than those of the visual part of the spectrum (0.4-0.7 μm). Neither clouds nor darkness were a hindrance any longer (Cattermole, 1994).

The tricky part with this technique, however, is interpreting the images. This is much more complicated than interpreting visual images. With radar, an antenna sends pulses of electromagnetic energy towards an object that reflects the energy back to the antenna. Therefore, on the one hand, the received images show the reflectivity of the surface. On visual images, highly reflective areas appear bright. On radar images, however, they may appear dark. This is because the incoming pulses of electromagnetic energy are not being reflected directly back to the antenna, but rather away from it as according to the well-known law of reflection which states that the angle of the incident ray is equal to the angle of the reflected ray. Therefore, a highly reflective surface, such as a smooth metallic region, will appear black on a radar image (Cattermole, 1994).

On the other hand, radar images are also a function of present terrain properties. The surface with which the electromagnetic energy pulse comes in contact with interacts with this pulse and sends it modified back to the antenna. The modifications give information about the material of the surface and its electrical properties as well as its texture. Furthermore, information about the types of rocks, the slope and the roughness of the ground on a centimeter scale can be gained. Rough surface materials appear radar-bright, whereas radar-dark areas represent smooth areas. Coupling all this information with altimetric data, a lot about the properties of the surface of the planet and its geological history can be learned (Cattermole, 1994).

Being now able to investigate the surface of Venus, one property of Venus unique among the other terrestrial planets in the Solar System became apparent: the distribution and condition of impact craters. There exist nearly one thousand impact craters on Venus, but small craters with diameters of only a few kilometers are rare. The smallest ones found have diameters of 1.5 km. The absence of smaller craters is due to the thick layer of clouds that destroys small objects when passing through, keeping them from reaching the surface of the planet. The objects that passed the layer of clouds left impact craters on the surface of Venus that show a uniform distribution. This indicates that the entire surface of the planet has the same age (Cattermole, 1994; Strom et al., 1994; Faure and Mensing, 2007).

Another important feature of the impact craters on Venus is their pristine condition. Only about 10% of the craters are fractured, and even fewer are embayed by lava, although Venus is known for intense volcanism in its history (Strom et al., 1994). The pristine condition implies that the lithosphere of Venus must have been rigid enough so that the profiles of the craters are retained. Some craters are surrounded by a halo, probably consisting of ejecta deposits. Craters that have been modified in some way make it possible to draw conclusions about volcanic, tectonic, and aeolian processes. Their basically undegraded form implies, for example, that little major erosion occurs on Venus (Cattermole, 1994).

At first sight, the distribution of the impact craters on Venus seems entirely random regarding their sizes, locations and conditions. A closer look reveals that the distribution of the craters regarding modifications is not spatially random. Specifically, some of the hotspot regions stand out here, such as Beta, Atla and Themis Regiones. They not only lack pristine craters, but are even abundant in tectonically or volcanically modified craters, hinting at recent geologic activity (Cattermole, 1994; Strom et al., 1994).

One last conclusion can be drawn from the impact craters: there are much less numerous large craters, which implies that the surface of Venus is geologically very young (Faure and Mensing, 2007). The mean surface age of Venus is suggested to be about 750 m.y., but estimates range between 300 m.y. and 1 b.y. (McKinnon et al., 1997; Stofan and Brian, 2012).

Basilevsky and Head (2002a) estimated the age of craters at least 30 km in diameter and their adjacent units by analyzing the craters radar-dark deposits. Those are thought to be either fine-grained ejecta, or zones that have been smoothed by the atmospheric shock wave associated with an impact (Phillips et al., 1991a; Herrick and Phillips, 1994). They base their analysis on the assumption that the deposits forming a radar-dark halo vanish with time due to aeolian processes and therefore are a sign of the age of the crater. Depending on the degree of

degradation, Basilevsky and Head (2002a) set the ages as follows: A crater with a dark parabola has a lifetime of about 0.1 - 0.15 T. The next stage of degradation is a clear dark halo, which has a lifetime of 0.3 T. T is the global mean age of the planet's surface. Craters with no discernible haloes are believed to be older (Cattermole, 1994).

In addition to the mean absolute surface age of Venus, relative age differences can be estimated by analyzing their relations such as crosscutting, embayment, and superposition. Stratigraphic methods are a reliable way to determine the mean ages of a few geologic units (Strom et al., 1994; Basilevsky and Head, 2000). These units are characterized by their radar brightness, the smoothness of their surfaces, patterns, and specific features, such as fractures, ridges, and shields. Younger units usually embay or superpose older ones. This is not true for every boundary zone between two geologic units, but for the majority it is. Therefore, a time sequence of the geologic units can be established. However, the emplacements of the different units overlap in time. Basilevsky and Head (2000) summarized the geologic mapping work of several authors and thereby established a relative time sequence that seems to be valid on the entire surface of Venus.

The mean surface age of Venus as estimated by means of the crater distribution is basically equal to the estimated mean age of the most widespread plains on the planet, the so-called regional plains (Basilevsky and Head, 2000; Stofan and Brian, 2012). They cover about 75% of the planet's surface (Buczkowski, 2006). The regional plains comprise two different units. The generally older shield plains and the younger wrinkle ridged plains. The shield plains are characterized by clusters of volcanic shields with diameters between 3 and 15 km. The wrinkle ridges are up to 2 km wide and they have lengths of several tens of km (Basilevsky and Head, 2000; Stofan and Brian, 2012).

There exist several other plains units, but I want to mention only the significant ones. The stratigraphically oldest unit is tessera material. It was formed by tectonic deformation and is characterized by a minimum of two sets of ridges and grooves crosscutting each other. The youngest units are smooth plains and lobate plains. The plains units are generally thought to be of volcanic origin. Whereas the two youngest units are associated with prominent volcanic constructs, the sources of other plains are not always discernible (Basilevsky and Head, 2000; Stofan and Brian, 2012).

The emplacement of those plains occurs contemporaneously or alternates with episodes of tectonic deformation. Depending on the appearance of the fractures, different tectonic units can be distinguished (Basilevsky, 2008).

3.2   The heat budget of Venus

Earth and Venus are very similar regarding their sizes and bulk densities. It is assumed that the heat budgets of both planets are similar and, hence, the concentration of heat-producing elements (Turcotte, 1993, 1995; Cattermole, 1994). The majority of the heat (about 70%) lost on Earth can be attributed to plate tectonics, whereas hotspots are responsible for less than 10% (*fig.* 2.2). Venus, however, has no plate tectonics (Smrekar and Stofan, 2006). Recalling the Rayleigh number, a possible explanation for this lack can be found. Hence, the temperature difference between the surface of Venus and its core-mantle-boundary is about 80% of that on Earth. Moreover, the gravitational acceleration is smaller as well. This results in a Rayleigh number which is about half as big as the terrestrial one (Aitta, 2012).

Besides a lack of plate tectonics, hotspots contribute only a small fraction to the heat loss as well, because there are simply not enough hotspot features to account for a larger portion of the heat budget. Some heat may also be lost by conduction through the lithosphere. With decreasing thickness of the lithosphere, heat is lost more rapidly. However, the thickness of the Venusian lithosphere is a matter of debate (Smrekar and Stofan, 2006).

Several hypotheses have been presented (e.g. Turcotte, 1995) of which the theory of resurfacing seems most likely. The young age of the Venusian surface and the random distribution of craters as well as their pristine condition are explained by this process (Strom et al., 1994).

On Earth, ongoing geological processes obliterate old impact craters, eventually rejuvenating the entire surface. In other words, these geological processes affect only small areas at a time. On Venus, however, rejuvenation is a violent process in the course of which the global surface is completely resurfaced on a recurring basis (Faure and Mensing, 2007). The resurfacing event comprises the formation of tesserae and regional plains (Basilevsky et al., 1997). In the process of resurfacing, all previously formed impact craters as well as other topographic features are eliminated (Faure and Mensing, 2007).

The manner in which resurfacing takes place is unknown. The models proposed so far fall into two categories: equilibrium resurfacing and global resurfacing. The former model, also called gradual resurfacing, first presented by Phillips et al. (1992), proposes that resurfacing occurs at a more-or-less constant rate up to the present in the form of volcanism. Therefore, the rate at which areas are resurfaced and, hence, craters destroyed, balances the rate at which new craters are formed. This theory, however, does not satisfactorily explain the observed density, distri-

bution and condition of the impact craters (Strom et al., 1994).

More probable, thus, is the so-called global resurfacing, also termed catastrophic resurfacing, introduced by Schaber et al. (1992a,b). In this model it is assumed that the global surface is completely resurfaced on a recurring basis. An episode of global violent volcanism combined with tectonism is followed by an episode of quiescence during which volcanic and tectonic activities are highly limited. The single rigid lithosphere thickens due to conductive cooling and the interior heats up until decompression leads to the formation of magma on a global scale. The lithosphere becomes unstable and a new episode of volcanism and tectonism begins. These activities, however, are not synchronous all over the planet as is proved by stratigraphic relations of differently aged terrains. The latest global resurfacing event must have ceased abruptly in order to explain the constraints given by the impact craters (Turcotte, 1993; Strom et al., 1994).

How long the last episode of global resurfacing lasted, is not known. Strom et al. (1994) estimated a length of tens of millions of years. They further assumed that the resurfacing event ended within 10 m.y, if not less. Since then, only little volcanism has occurred (Smrekar and Stofan, 2006).
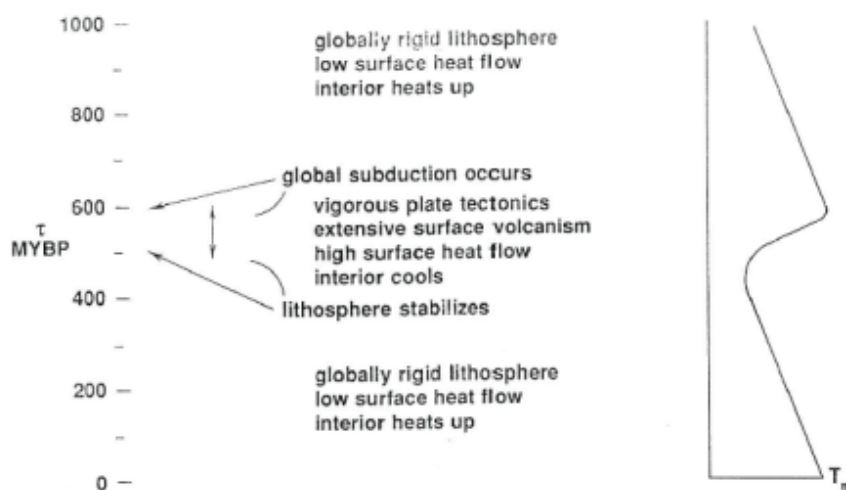

Figure 3.1: Illustration of global resurfacing, from Turcotte (1993)

3.3 Volcanism on Venus

All volcanoes on Venus seem to be currently dormant. However, some of them, for example Sapas and Maat Montes in western Eistla Regio, appear to have been

active until geologically recently because associated lava flows are radar bright
meaning that their surface is rather rough and young. As on Earth, there seem
to be at least two different kinds of lavas on Venus, apparent from differences in
their viscosities (Faure and Mensing, 2007).

The chemical composition of rocks found at the landing sites on Venus is com-
parable to average tholeiitic and alkali basalt as found on Earth (Francis and
Oppenheimer, 2004). Moreover, the pictures that the Venera landers took show
either a slabby landscape or isolated rocks surrounded by fine-grained material
reminiscent of terrestrial regions like the Snake River Plains in the USA (Cat-
termole, 1994). Also in radar images, lava flows resemble terrestrial low-viscosity
pahoehoe flows with smooth surfaces rather than aa lava. This contrasts with the-
oretical considerations that predict that on Venus, pahoehoe lava changes more
rapidly to aa lava than on Earth (Head and Wilson, 1986; Cattermole, 1994).

Like Venus, neither Mars nor the Moon shows evidence that plate tectonics ever
occurred there. On the Moon, extensive floods of basaltic magma were effused,
covering the floors of impact craters and building up along fractures. Low shield
volcanoes and a few steep-sided domes can be found as well as deposits of explosive
eruptions, long lobate flows and sinuous lava channels. On Mars, similar landforms
as on the Moon can be found. However, volcanism on Mars was more centralized
resulting in huge shield volcanoes suggesting long-lived underlying mantle plumes
and a crust that hardly moved. Some of the volcanoes have traces of phreatomag-
matic activity indicating that on Mars there used to be more volatiles than there
are now (Cattermole, 1994).

Therefore, on Venus similar evidence of volcanism as on other planets might be
expected. However, the extreme surface temperature and atmospheric pressure
may influence volcanic processes (Cattermole, 1994). Theoretical considerations
(e.g. Head and Wilson, 1986; Hess and Head, 1990) come to the conclusion that,
due to the high pressure that inhibits the exsolution of volatiles close to the sur-
face, up to ten times the wt% of water or carbon dioxide as on Earth would have
to be dissolved on Venus (Cattermole, 1994; Frankel, 2005). Considering the dry
environment on Venus, pyroclastic deposits seem less likely. However, in the event
of pyroclastic activity, eruption clouds only rise as far as one-third of the height
as on Earth, and even only one-fifteenth as on Mars, provided that the same mass
eruption rate is involved (Cattermole, 1994; Francis and Oppenheimer, 2004).
On the radar images, some materials are interpreted as pyroclastic deposits (e.g.
McGill, 2000).

Nevertheless, Venusian lava flows and volcanic edifices are much like their terres-
trial counterparts (Cattermole, 1994). Compared to lava flow fields on Earth, a

few of the ones on Venus are huge. They reach lengths of several hundred kilometers, which indicates major outpourings of lava. One would expect that such enormous sizes are possible due to the high surface temperature on Venus which keeps lavas hot and mobile for longer than on Earth (Francis and Oppenheimer, 2004). However, models indicate that the dense CO_2-rich atmosphere acts as a medium through which a lot of the lava's heat is convected away. Hence, lava even cools faster on Venus than on Earth (Frankel, 2005). Comparing the volumes of the Venusian flow fields and the flood basalts on Earth shows that the Venusian ones are still ten to a hundred times larger (Cattermole, 1994). It is suggested that due to the dense atmosphere a crust forms rapidly on the surface of the lava which isolates the hot lava from the atmosphere. Therefore, below this crust lava could flow without hindrance and form large lava flows (Slyuta and Nikolayeva, 1992; Frankel, 2005).

The major flow fields are not randomly distributed but are, among others, concentrated on Atla and Beta Regiones. The flow direction of some of the lava flows could be determined. It strengthens the assumption that large lava eruptions played a major role in the resurfacing event, especially in topographically low regions (Cattermole, 1994).

Stofan et al. (2001) divided the flow fields of a few volcanoes into groups according to their morphology. Digitate flows, therefore, are significantly longer than they are wide. They are interpreted to originate from eruptions of a rather short duration with a high effusion rate. Fan-shaped flows consist of compound flows that originate from a discernible vent. They have the appearance of a fan in planform. Sheet-like flows consist of individual broad flows overlapping each other. The individual flows are not always identifiable.

A large number of small volcanic structures are distributed over the Venusian surface. They preferably form in the lowland plains. The constructs are divided into three groups: shield volcanoes, volcanic cones and domes (Guest et al., 1992). The majority of these structures have diameters in the range of 2 and 8 km. Shield volcanoes are the most common of the three types. In general they are less than 200 m in height, but they can be up to 20 km across. Most of them cover a circular base area. A single pit is located on the summit. They often occur in groups, which are called shield fields. Moreover, they often are associated with other major volcanic edifices, such as coronae and arachnoids. Venusian cones are believed to form in a similar way as terrestrial cinder cones. The Venusian ones generally have a diameter of less than 15 km. Volcanic domes are larger than their terrestrial counterparts with diameters in the range of 20 to 30 km and a height of 1 km. The domes occur isolated or, like the shield volcanoes, form

groups. Most of them are rather circular with steep, clear margins that often are heavily fractured, and have a summit pit (Cattermole, 1994).

Regarding intermediate edifices (with diameters between 20 and 100 km), most abundant are constructs with diameters in the range of 20 to 40 km. According to Crumpler et al. (1997), the Magellan volcano catalog lists 289 intermediate volcanoes. A subclass of these volcanoes, a type of volcano surrounded by radiating lava flows with lobate margins, is called the anemone type. Sometimes the lava flows are not discernible. In these cases, a volcanic origin is implied by either the presence of a central pit or a conical peak or by other nearby volcanic edifices. Some of these anemone-type volcanoes have a summit caldera, whereas others are associated with elongate or fissure-like depressions. Again, their distribution is not entirely random, but they rather concentrate in the region between Beta, Atla, Themis and Imdr Regiones as well as on the flanks of the equatorial highlands (Cattermole, 1994).

According to Crumpler et al. (1997), there are 167 large volcanoes on Venus (more than 100 km in diameter). Only a small number of volcanoes exceed diameters of 700 km. They are often associated with fields of radar-bright radiating lava flows with lobate margins and a large summit depression. Sometimes this depression is more of a corona-like structure, and sometimes fractures give it the appearance of something between a corona and a nova. The large volcanic structures are remarkably clustered within the upland regions of Beta-Atla-Themis Regiones as well as Eistla Regio, but almost absent from the lowland and ridged terrain. This fact leads to the conclusion that a distinct formational factor is involved (Cattermole, 1994). Moreover, although the large volcanoes on Venus occupy basal areas with large diameters, compared to terrestrial or Marsian volcanoes, the Venusian ones are remarkably low in height (Keddie and Head, 1994e).

Following their appearance, the large volcanoes are divided into nine morphologic classes. Class I describes the simple type. The volcanoes of this class are rather symmetric, as are their radial lava flows. They show a lack of prominent structures, such as summit calderas and flanking constructs. Class II volcanoes are characterized by a caldera located on the summit. Class III volcanoes have radial rift zones that cut through their flanks. They resemble the terrestrial example of Kilauea on Hawaii. An example of a Venusian volcano of class III is Nyx Mons in Bell Regio. This group is not to be confused with Class VII. In contrast to volcanoes of type III, class VII volcanoes are associated with large regional rift zones (such as Gula Mons and Guor Linea in Western Eistla Regio) or with rift zones that cut through the volcano itself (such as Theia Mons and Devana Chasma in Beta Regio). The volcanoes of class IV are characterized by an elongated summit

that often is associated with several caldera-like structures. Gula Mons in Western Eistla Regio is an example of this type. Class V volcanoes have a complex summit structure that consists of multiple constructs regarding topography and morphology. Sapas Mons in Atla Regio, for example, has twin peaks that both are associated with several small edifices and central depressions. Volcanoes of class VI are surrounded by an exterior set of usually radial fractures that generally predate lava flows that form the central part of the volcanoes. Volcanoes that also have an interior set of radial fractures belong to class VIII. These fractures usually have a high density and sometimes are the origins of flanking lava flows. Volcanoes of class IX have a corona-like interior which comprises at least 50% of the diameter of the volcano. However, lava flows that define the shield volcano are clearly discernible. Whichever morphologic type was developed first, the volcano or the corona, is not clear (Head et al., 1992a; Crumpler et al., 1993, 1997).

As mentioned before, Venus has a couple of peculiar volcanic features that seem to be quite unique to this planet with no terrestrial counterparts (Cattermole, 1994). Coronae are circular structures made up of concentric fractures and ridges (Smrekar and Stofan, 2006). Besides Venus these features are only observed on Uranus's moon Miranda (Anguita and Chicarro, 1991). Novae do not have annular faults, but they consist of a radial network of fractures with a dome in the center. Systems with concentric fracturing on the inside and radial faulting on the outside are called arachnoids. It is suggested that these types may be three different stages of evolution (Cattermole, 1994).

The amount of coronae exceeds 500 (Smrekar and Stofan, 2006). They are often associated with rift systems. Moreover, they are not randomly distributed on the Venusian surface but rather clustered around longitude 250°E. Particularly many can be found between the longitudes of Beta, Phoebe and Themis Regiones, and in the vicinity of Atla Regio. Moreover, in the lowlands, rather few coronae are located. A possible explanation is that coronae there have been obliterated by lava flows. Artemis Corona is the largest one with a diameter of 2600 km (Cattermole, 1994). The majority of the coronae, however, have a diameter of about 250 km (Smrekar and Stofan, 2006).

Following the shape of the annulus which usually is narrow with a thickness of less than 150 km (Hansen et al., 1997), coronae are divided into five groups: concentric (circular), concentric-double ring, radial/concentric (due to the presence of dominant radial fractures), multiple, and asymmetric. The concentric type is the most common one (Stofan et al., 1992). Many coronae have a raised topography with an elevation of at least 1 km (Cattermole, 1994). Regarding their topographic profile, they can be divided into nine groups: (1) simple depressions,

(2) depressions surrounded by a rim and probably an outer trough, (3) interior highs surrounded by a rim and maybe an outer trough, (4) just a rim, (5) interior highs surrounded by a rim, a trough and an outer rise, (6) interior depressions surrounded by a rim, a trough and an outer rise, (7) plateaus that may be surrounded by a trough, (8) domes that may be surrounded by a trough, and (9) no discernible topographic signature (Stofan, 1995). Rather often, volcanoes are located in the interiors of coronae. Moreover, many of them are associated with surrounding lava flows (Smrekar and Stofan, 2006).

Figure 3.2: Coronae: Idealized sketches of the five groups of coronae with a description of their most characteristic features, from Stofan et al. (1992)

It is thought that coronae are the surface manifestation of small mantle plumes that originate from shallower depths (Smrekar and Stofan, 2006). The formation of a corona would start with a dome-like uplift due to the rising plume, sometimes accompanied by radial fracturing and/or the generation of volcanic deposits

(Cattermole, 1994). As the plume head spreads and flattens, a more plateau-like structure may form. Concurrently, central subsidence can occur accompanied by concentric faulting as well as the generation of a surrounding rim and a moat. Concentric deformation will increasingly focus on the area close to the rim (Cattermole, 1994; Koch and Manga, 1996). As the plume cools and, hence, loses its buoyancy, the topography further relaxes and an outer set of concentric fractures is formed (Stofan et al., 1997). Eventually, the interior of the corona may even sink further so that it will lie deeper than the surrounding surface (Cattermole, 1994; Koch and Manga, 1996).

Throughout the entire formation, volcanism may occur. At late stage, volcanism may be intense and cover up radial fractures, flood the depressed interiors of coronae as well as the floors of moats, and build up shields and domes in the interiors. At later stages of the mantle plume activity, the plume material cools, volcanism declines and the topography relaxes. The local crust and its strength determine how much of the topography of the corona will survive later tectonic activity (Cattermole, 1994).

Gravity data suggest that many coronae are isostatically compensated, which could mean that they are inactive. It has been proposed that there are no coronae on Earth due to the presence of an asthenosphere (Smrekar and Stofan, 2006). Regarding the geologic history of Venus, the following sequence has been established: the oldest stratigraphic unit seems to be tessera material. Although it has been heavily disrupted, it has not been covered up entirely, but parts of it survived the volcanism associated with the resurfacing event (Smrekar and Stofan, 2006). Towards the end of tessera formation, early regional plains were emplaced. Heavy extensional deformation followed. While more volcanic plains were emplaced, deformation changed from extensional to compressional and the characteristic wrinkle ridges were formed. Contemporaneously to the emplacement of the regional plains, the formation of coronae started. After the formation of the regional plains had ended, coronae entered the final stages of their development. Eventually, Venus entered a stage of low activity in which rifting and volcanism associated with coronae, large shield volcanoes and lava flows dominated (Basilevsky et al., 1997).

Chapter 4

Hotspots on Venus

Whereas coronae are believed to be the surface manifestation of either small and/or weaker, shorter-lived, or secondary plumes, so-called volcanic rises seem to have the same cause, but on a larger scale (Cattermole, 1994; Hansen et al., 1997). Smrekar and Stofan (2006) argue that since Venus is lacking an asthenosphere, mantle plumes of a given size impinge on the base of the lithosphere directly and cause an uplift of the topography of larger dimensions than on Earth. Hence, hotspots on Venus are characterized by swells as well. Like terrestrial hotspots, the Venusian rises are the result of a combination of a couple of processes. On the one hand, they are caused by uplift of the thinning lithosphere due to the underlying hot mantle plume. On the other hand, the crust at hotspots is thickened due to volcanic activity (Hansen et al., 1997).

Analogous to Earth, hotspots on Venus are characterized by gravity anomalies as well, even though they are relatively mild. On Mars and the Moon, gravity anomalies of the order of 100 mGal are rather common, whereas on Venus, they generally are in the range of 40-50 mGal. Nevertheless, according to Esposito et al. (1982) the largest gravity anomaly on Venus coincides with Beta Regio with a value of about 150 mGal (Basilevsky, 2008). In contrast to Earth, on Venus large gravity highs and positive topographic features coincide, showing that the gravity field of the planet and the topography seem to be strongly correlated (Cattermole, 1994).

Following gravity-topography analysis, two different kinds of highland regions can be distinguished (Cattermole, 1994). The fist type of a highland comprises crustal plateaus. Examples of this type are Ovda and Thetis Regiones. They are characterized by flat tops and steep sides. Their origin still is a matter of debate: they may be the result of mantle downwelling (crustal shortening), or they may be the manifestation of ancient mantle plumes (hence, old hotspots) (Cattermole, 1994;

Grimm, 1994; Hansen et al., 1997). They have smaller gravity signals which reflect shallow apparent depths of compensation (ADCs). Shallow ADCs are interpreted to be a sign of topography that is supported by crustal compensation. This is also revealed by small geoid to topography ratios (GTRs). With the help of GTRs and some further assumptions it can be determined whether the topography is supported isostatically or dynamically. Large GTRs would indicate that the topography is compensated by a mass deep in the mantle or that it is not completely compensated. Deep ADCs as well as large GTRs characterize the second type of highland, the volcanic rises. Their topography (broad, dome-like) is dynamically supported by the mantle plume (Smrekar and Phillips, 1991; Cattermole, 1994; Grimm, 1994; Hansen et al., 1997).

Overall, nine topographic rises on Venus have been identified that are believed to be the surface manifestations of underlying mantle plumes due to their similarities to terrestrial hotspot swells in regard to the remnants of volcanism, their topographic appearance and large positive gravity anomalies (Smrekar et al., 2010). According to their dominant morphology, they are divided into groups as follows: rift dominated (Atla and Beta Regiones), volcano-dominated (Bell, Dione, western Eistla, and Imdr Regiones) and corona-dominated (central Eistla, eastern Eistla, and Themis Regiones). The morphologic variations are not believed to be consequences of different stages of evolution of the hotspot. They rather seem to be influenced by varying lithospheric features, plume properties, and the tectonic environment of the region. According to this, whereas volcano-dominated rises are seen as the closest equivalent to terrestrial hotspots caused by a simple mantle plume, corona-dominated rises are interpreted to be the result of a secondary plume or of a plume head that has broken up (Smrekar et al., 1997).

Within each morphological type, however, different stages of evolution are responsible for variations regarding the topography of the rises, their gravitational properties, and the characteristics of their volcanism (Stofan et al., 1995). Volcanism became manifested in large shield volcanoes, lava plains, small volcanic edifices and coronae. The nine rises also have in common that evidence for extensional deformation is present at all of them, ranging from small graben to large fracture zones (Condie, 2001).

Several models aim to explain the sub-surface structure responsible for the observed topography of the volcanic rises. There are basically three approaches (Smrekar et al., 1997). One is to numerically or analytically simulate an (axisymmetric) mantle upwelling (e.g. Kiefer and Hager, 1991; Smrekar and Phillips, 1991; McKenzie, 1994). Another approach is the isostatic compensation model. It is assumed here that thinning of the lithosphere due to the mantle plume sup-
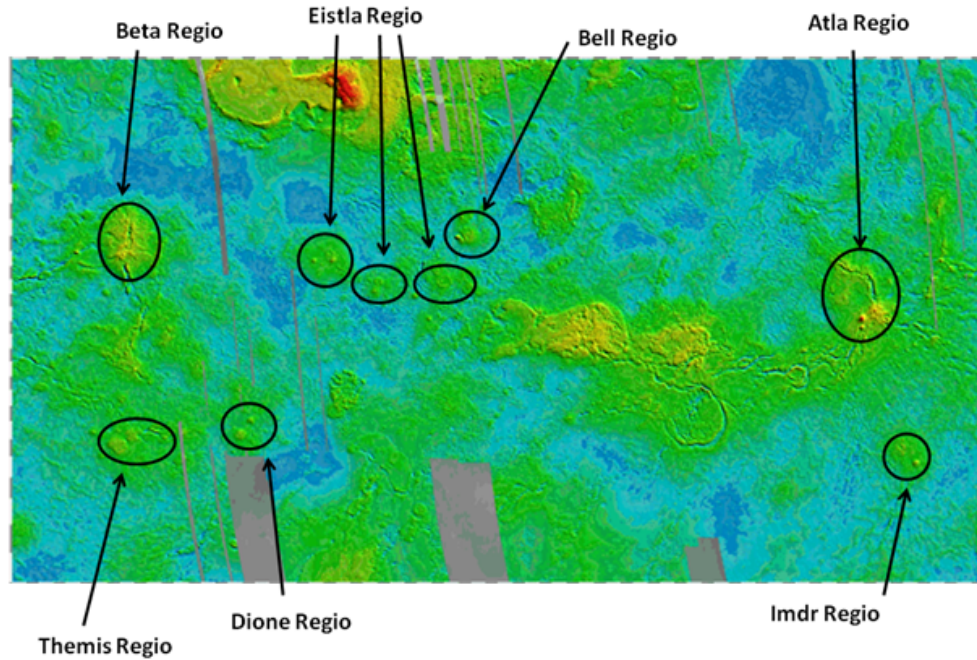
Figure 4.1: Topographic map of Venus: The blue regions are areas of the lowest elevation; red regions have the highest elevations. The gray areas have not been mapped by Magellan. The locations of the nine volcanic rises are marked (`http://www2.jpl.nasa.gov/magellan/image2.html`, retrieved: 2014-01-21).

ports the topography isostatically (e.g. Kucinskas and Turcotte, 1994; Moore and Schubert, 1995). An alternative version of this model is to assume two density contrasts in the mantle, one between mantle and crust, the other one between mantle and lithosphere. In the third group of models, the flexure of the elastic lithosphere is taken into consideration as well (e.g. Smrekar, 1994; Phillips, 1994). Due to the absence of plate tectonics and topography that resembles the intraplate environment on Earth, as well as the amount of coronae that cover the surface of Venus, plume activity may be of much more importance on this planet regarding its heat budget than on Earth where hotspot activity only plays a minor role (Cattermole, 1994). However, taken all coronae and volcanic rises together, they would still account for only a minor portion of the Venusian heat loss (Smrekar and Stofan, 2006).

The region between the three highlands of Atla (to the west), Beta (to the northeast), and Themis (to the south) Regiones (BAT region) is known for the highest density of volcanic edifices (especially large volcanoes and coronae) on Venus (Crumpler et al., 1992, 1997; Head et al., 1992b). Furthermore, the abundance of tectonically or volcanically modified craters in this region is remarkable as well.

They may be indicative of some rather recent tectonic and volcanic activity that took place in this region after the last resurfacing event (Strom et al., 1994). Another area with an unusual concentration of volcanic centers occurs in the region between Eistla Regio (to the west), Bell Regio (to the northeast) and the equator (to the south) (Crumpler et al., 1997). All those regions as well as the two regions of Imdr and Dione Regio not mentioned above are located between the latitudes 40°N and 50°S. Since no hotspot region is located in higher latitudes, the volcanic rises are broadly summarized as equatorial highlands (Crumpler et al., 1997). It is assumed that the planet's principal inertial axes and their orientation are tightly linked to the locations of volcanic centers, as may be the case on Mars and Earth, where a similar distribution is observed (Ward et al., 1979; Jurdy, 1983; Crumpler et al., 1997).

4.1   Beta Regio

Particular interest had been shown to Beta Regio, besides Atla and Phoebe Regiones, already in the 1970s. Low-frequency radio emissions in those regions had been recorded by an antenna. Scientists (e.g. Scarf, 1985) interpreted them to be lightning discharges, analogous to observations of such in the plumes associated with terrestrial volcanic eruptions. Furthermore, from 1978 until 1983, the levels of sulphur dioxide and hazes of sulphuric acid in the atmosphere of Venus decreased by about 90%. The levels that had been predicted were clearly below the levels that had been measured in 1978. The following decline led to the conclusion that large-scale volcanic eruptions must have taken place in the 1970s, enhancing the upper atmosphere with sulphur dioxide. These observations suggest that Beta Regio has been geologically active in very recent time, and probably still is (Cattermole, 1994).

Southwest of Ishtar Terra, separated by plains, such as Sedna and Guinevere Planitiae, Beta Regio is located. With dimensions of about 2,000 x 2,300 km (Stofan et al., 1989; Senske et al., 1991b) it occupies approximately the area between latitudes 12° and 40°N as well as longitudes 270° and 290°E. The rise has a minimum elevation of about 2 km (Keddie and Head, 1994a; Basilevsky, 2008). The highland is characterized by widespread volcanism and rifting. Thus, the most prominent features of this highland are Theia and Rhea Montes as well as Devana Chasma. The rift system traverses the highland from north to south. At the flanks of the rise less prominent features are located: Aikhylu Chasma in the west and Latona Chasma in the east. The north of the Beta Regio rise is

defined by Agrona Linea. The region is characterized by a large positive gravity anomaly of 150 mGal. An apparent depth of compensation of the order of 300 km is assumed (Cattermole, 1994; Basilevsky, 2008).
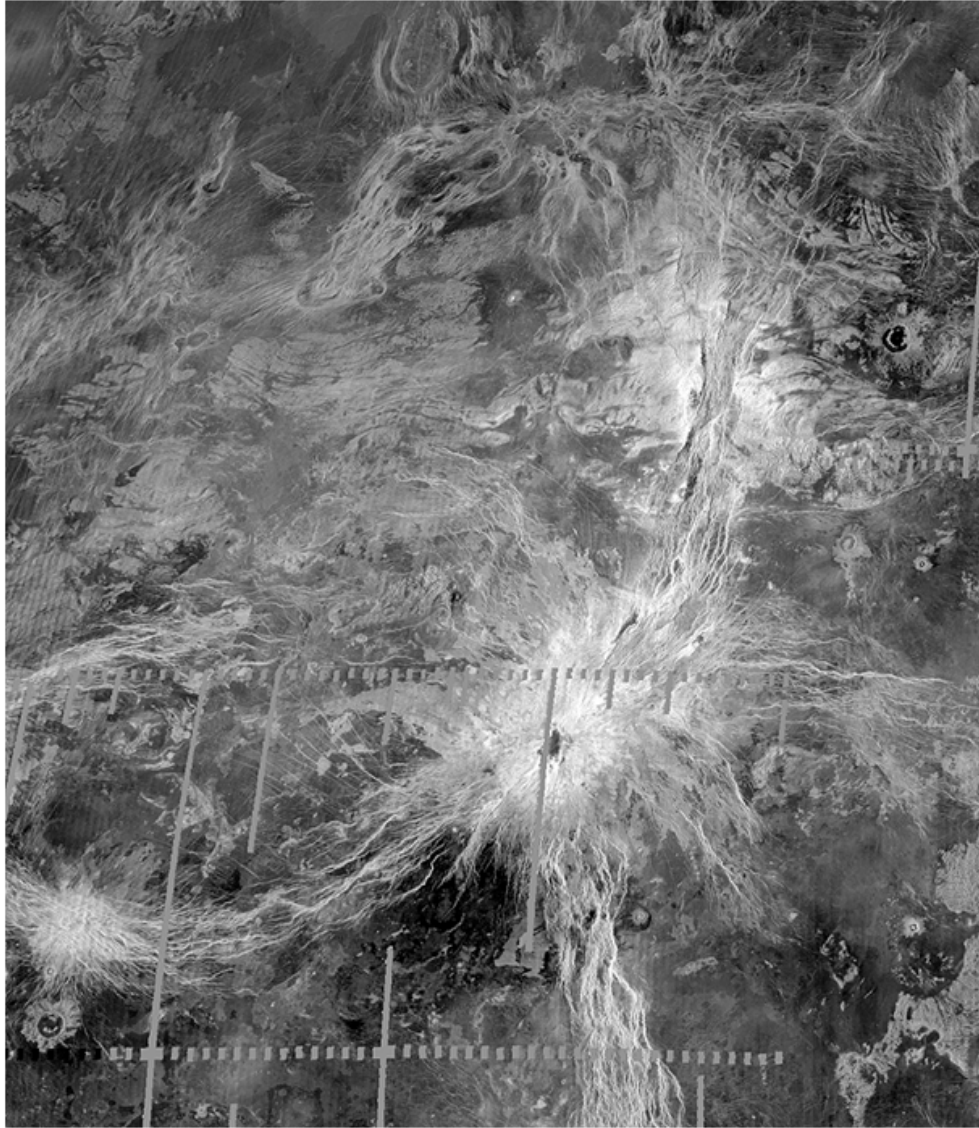
Figure 4.2: Magellan radar image of Beta Regio. Theia Mons is the bright object in the middle of the lower part of the picture; Rhea Mons is the bright feature in the right upper part (`http://nssdc.gsfc.nasa.gov/imgcat/html/object_page/mgn_c314n300_1.html`, retrieved: 2014-11-10).

The volcano Theia Mons rises with low flank slopes to a height of 5 km above mean planetary radius (MPR) of about 6,052 km at the southern end of Beta Regio,

covering an area with a diameter of 226 km (`http://planetarynames.wr.usgs.gov/Page/VENUS/target`, retrieved: 2013-09-13). Magellan imagery shows that Theia Mons is superimposed on the north-south striking rift system of Devana Chasma, but also that it has been cut by later faults. Radar-bright and mottled lava flows radiate on all sides of the volcano out from the top of the mountain for up to 1,000 km. On the east side of Theia the flows partly infill the floor of the rift (Basilevsky, 2008). This clearly shows that the lava flows are younger than the rifting. The long flows are overlain by shorter, lobate flows that cover the upper flanks of the volcano (Cattermole, 1994). According to Basilevsky (2008), the flows associated with this major volcano in general are interpreted to be lobate plains material, and therefore rather young. Regarding the Beta rise, most of this material is associated with Theia Mons. Except in the northwest part of the volcanic rise, a small volcanic construct, Copacati Mons, with a diameter of 80 km and a height of 1 km, is associated with lobate plains material as well.

There is evidence that Theia Mons partly collapsed into a 3 km deep radar-dark summit caldera with dimensions of 75 x 50 km. Therefore, the floor of the caldera lies deeper than the base of the volcano. To the north of the caldera, a high, plateau-like structure is located. Theia Mons is a junction of several features with different tectonic trends. In addition to Devana Chasma, the volcano is cut by an east-west rift, Hecate Chasma, which trends westwards and joins Asteria and Ulfrun Regiones, both of which are located west of Beta Regio (Cattermole, 1994). Moreover, Žverine Chasma trends away into southwest direction.

Rhea Mons, located farther north of Theia Mons, reaches a height of 4.5 km. It looks like a shield volcano and radar-bright signatures of early images that resemble the ones at Theia Mons were likewise interpreted to be lava flows. Therefore, Rhea Mons was thought to be a volcanic structure as well. However, Magellan data revealed that the highest situated part of the mountain is an area of tesserae that has been uplifted. Smoother volcanic deposits mantle the summit. The features that were falsely interpreted as lava flows seem to be highly deformed tesserae. Due to their lobate shape, they resemble volcanic flows. Also, Rhea Mons seems to have partly collapsed into a deep rift on its eastern flank (Cattermole, 1994). Thus, the northern part of the Beta rise, dominated by Rhea Mons, was primarily formed by tectonic activity. Volcanism that smoothed the flanks of the rise was not as important (Basilevsky, 2008).

Devana Chasma is thought to be an extensional fault complex comparable to its terrestrial equivalent, the East African Rift. However, the Venusian rift system is structurally different from terrestrial rifts, in that it is primarily composed of full-graben and not of half-graben as it is characteristic of the terrestrial coun-

terparts (Kiefer and Swafford, 2004). Nevertheless, Devana Chasma runs from Beta Regio over 2,000 km with an average width of 90 km southwards to the crustal plateau Phoebe Regio, descending about 2.5 km below the mean surface radius at its deepest point. As proposed by Kiefer and Swafford (2006), the Devana Chasma rift system may actually consist of two separate rifts that started at the two topographic rises and grew together, meeting in the middle. Close to the mountains of Beta Regio, the Devana Chasma is rather narrow (Cattermole, 1994). Near Rhea Mons the fault trough has a width of 80 km reaching depths between 2 and 2.5 km (Stofan et al., 1989; Cattermole, 1994). To the north of Theia Mons, where the volcano and the rift system intersect, the latter even narrows from a width of 200 km down to 50 km. In contrast, in the northern parts of Beta Regio, Devana Chasma is about 130 km wide. In this region, there are also several horsts that stick out in the rift center. The most extreme relief of the rift system of about 6 km can be found between Beta and Phoebe Regiones. This relief is flanked by well defined high shoulders (Cattermole, 1994).

Also the surroundings change along the rift system. In the north, Devana Chasma is surrounded by blocks of tesserae (for a description of this land form, see *chapter* 3.1). In the central and southern parts of Beta Regio, fractured volcanic plains surround the main rift. Radar-dark volcanic plains also embay tessera features in various localities. The tessera terrain that is encountered by Devana Chasma in the northern part of Beta Regio is composed of ridges and grooves, 1-2 km apart, with a north-east trend. To the east of Devana Chasma, the trend changes more to north-south. Some grooves and lineations crosscut in all directions. The tessera terrain is also cut by normal faults and graben fanning out from the main rift. In places, individual tessera blocks can be seen on the rift floor (Cattermole, 1994).

Tesserae occur all over the rise of Beta Regio. Rhea Mons turned out to be an uplifted area of tesserae. Farther north, Devana Chasma is surrounded by tessera blocks. Isolated blocks of tessera also occur at Theia Mons, beyond its summit, primarily to the east, west, and north. Furthermore, on the western flank of the topographic rise tessera blocks are located. Plains with shield fields transect this region, and fractures associated with adjacent coronae crosscut it. The interactions of the various tectonic features in this area make evident that tesserae are the oldest stratigraphic unit here. Tessera blocks have also been identified in eastern Beta Regio, but not in the southern part of the highland. They may have been covered by later volcanism (Cattermole, 1994).

To the north of Beta Regio, a chain of large coronae is linked by graben faults, Agrona Linea. The coronae Emegen and Blathnut lie at the eastern end of Agrona

Linea, and in the northern surroundings of the fault system the coronae Rauni and Urash can be found (Cattermole, 1994). However, all four coronae are located off the topographic rise of Beta Regio.

As mentioned before, Beta Regio is one of the regions that are abundant in modified impact craters, otherwise a rather rare occurrence on Venus. Basilevsky and Head (2002a) found that five out of 10 craters have been affected by the volcanic and tectonic activity associated with the highland. A good example is the crater Balch in Devana Chasma, central Beta Regio, with a diameter of 37 km. Rifting associated with the rise of the Beta highland caused the crater to split apart. The form of the crater originally was circular, but its width has been extended by approximately 11 km. Therefore, this feature gives useful information about how much extensional strain acted on this area (Cattermole, 1994). Due to the lack of a surrounding radar-dark halo, Basilevsky and Head (2002a) assume that the crater is older than 0.5 T, with T being the mean global age of the surface of Venus.

The crater Sanger is located east of Rhea Mons. With a diameter of 83.8 km, it is the largest crater of Beta Regio. Is has possibly been embayed from the southwest, which would explain its irregular ejecta blanket. Its age is suggested to be less than 0.5 T due to a clear dark halo. Outflows from Sanger in the northwest are cut by lineaments from Devana Chasma, which means that the rifts are younger than 0.5 T (Basilevsky and Head, 2002a; Matias and Jurdy, 2005).

The crater Raisa, 13.5 km in diameter, lies 350 km north of the summit of Theia Mons. It has been heavily flooded by young lava flows (belonging to the lobate plains unit), only leaving part of its rim and a small amount of ejecta to the northeast of the crater. Basilevsky and Head (2002a) estimate that the crater formed in a time more recent than 0.75 T, maybe even more recently than 0.5 T. Theia Mons is thought to have been active at that time.

The 15.5 km crater Olga lies to the northeast of Theia Mons at the eastern flank of Devana Chasma. Olga is superimposed on major episodes of rifting associated with Devana, and has locally been cut by younger faults. There may be remnants of a crater-related clear halo, which sets the maximum age of the crater to about 0.5 T (Basilevsky and Head, 2002a).

The smallest of the five craters is Tako with a diameter of 10.5 km. It is located southeast of Olga, superimposed on faults associated with Devana Chasma. Due to a faint dark halo, Basilevsky and Head (2002a) estimate the crater's maximum age to be less than 0.75 T. Regarding its small size and the fact that it is superimposed on young lobate plains material, the crater may be even significantly younger (Basilevsky, 2008).

In general, these observations make it possible to draw conclusions about the volcanic and tectonic activity of Beta Regio. Sanger and Olga show that faulting associated with Devana Chasma took place after 0.5 T. The lava flows originating from Theia Mons that flooded Raisa are younger than 0.75 T, or maybe even younger than 0.5 T. Therefore, volcanic and tectonic activity occurred within the last 0.5 T (Basilevsky and Head, 2002a).

The geological history appears as follows: The oldest unit in this area, as elsewhere on the planet, is the tessera material unit. Next, a couple of plains units were emplaced that were subsequently deformed by two deformational episodes: tessera transitional terrain and fracture belts. The fractures of the former deformation show no alignment with the topographical rise of Beta Regio, whereas the later pattern of the fracture belts widely aligns with the volcanic rise, e.g. Agrona Linea. At the time of the emplacement of the shielded plains, the growth of the Beta rise was already in process. Contemporaneously with the emplacement of the last two units (smooth and lobate plains), rifting occurred, and the Devana Chasma rift system was formed. The majority of the lobate plains originate from Theia Mons. The Beta rise may still be growing today (Basilevsky and Head, 2007; Basilevsky, 2008).

Beta Regio seems like a tessera block that has been disrupted by major mantle upwelling caused by a mantle plume. Rifting and the main phase of volcanism occurred contemporaneously. Theia Mons constituted the center of volcanism. Moreover, several tectonic trends run together at the volcano (Cattermole, 1994). This geometry is not only similar to other major volcanic centers on Venus, such as Atla and Eistla Regiones, but also to terrestrial regions, where rift-related volcanism occurs. Due to considerable volcanism and rifting and the fact that several major tectonic lines intersect at Beta Regio, the Venusian highland has been compared to the terrestrial East African Rift Valley (Stofan et al., 1989; Cattermole, 1994).

4.1.1 Venera 9 and 10

The first pictures sent from the surface of Venus were taken from Venera 9 and 10, two spacecraft in a series of missions that were developed by the Soviet Union. Venera 9 was launched on June 8, 1975, and Venera 10 was launched 6 days later. The landers of both probes touched down on the eastern edge of Beta Regio (Venera 9 on the northeastern flank at 31.01°N , 291.64°E , Venera 10 farther south) on October 22 and 25, 1975, respectively, separated by about 2,000 km (Garvin

et al., 1984; Basilevsky et al., 1992; Basilevsky, 2008).

Venera 9 landed on a steep region with a slope of about 30°. The pictures of Venera 9 show a slightly sloping landscape covered in loose rocks. The rocks are flat (15-20 cm thick) slabs with sizes ranging between 20 and 70 cm. Abundant darker fine-grained debris separates the individual rocks that show hardly any sign of chemical weathering. The landscape in the pictures of Venera 10 is gently sloped as well. It is made up of isolated outcrops scattered over a relatively flat plain. The outcrops are flat as well with sizes of the order of 1 - 3 m. The space between the rocks is also filled with darker fine-grained material which has a very low albedo. Some evidence of at least small-scale Aeolian processes can be seen in these pictures (Florensky et al., 1977; Cattermole, 1994).

The two probes measured the local rock densities and the abundances of the rocks. The former probe detected a density of < 2 g cm^{-3} in the northeastern flank of Beta Regio. Venera 10 yielded a value of 2.8 ± 0.1 g cm^{-3}. Moreover, they discovered that the rocks in this area of Beta Regio resemble terrestrial basaltic rocks relating to the concentrations of potassium, uranium, and thorium (Florensky et al., 1977; Cattermole, 1994).

Both landers neither show typical lowland area, nor highland terrain. They landed in regions in between, Venera 9 with an elevation of about 1.5 - 2 km above MPR, Venera 10 with an elevation of about 1 km above MPR (Cattermole, 1994).

Figure 4.3: Venera 9 and 10: Photographs taken by the Soviet landers showing the Venusian surface. (`http://nssdc.gsfc.nasa.gov/photo_gallery/photogallery-venus.html`, retrieved: 2013-02-23)

4.2   Atla Regio

The most extensive highland on Venus is Aphrodite Terra, covering an area comparable to the size of Africa. Aphrodite lies on and south of the equator and spans an area more than 10,000 km across (`http://planetarynames.wr.usgs.gov/Page/VENUS/target`, retrieved: 2013-08-03) between the 45° and 210°E meridians comprising various topographical and structural features. The western part of Aphrodite is dominated by two highland massifs: Ovda Regio and to its east Thetis Regio. These two regions have elevations of 3-4 km and span a distance of about 6,000 km (Cattermole, 1994).

The eastern part of Aphrodite is formed by Atla Regio. It clearly differs from the two highland regions in western Aphrodite in being dominated by volcano edifices. Atla Regio is a broad upland dome with dimensions of about 1,500 x 2,500 km and an elevation between 2 and 4 km above mean planetary radius comprising many rifts and volcanic centers. In some places, the highland rises to almost 6 km. Both, geoid and gravity anomalies for this highland are high, namely 120 m and 130 mGal, respectively. The depth of compensation has been estimated to lie between 200 and 250 km (Herrick et al., 1989; Phillips et al., 1991b; Smrekar and Phillips, 1991).

As has been mentioned before, the Beta-Atla-Themis-region stands out regarding the density of volcanic edifices and modified impact craters. In Atla Regio, three major volcanoes (Maat, Ozza, and Sapas Montes) are located. They are associated with at least five modified impact craters which constitutes the densest concentration on Venus (Strom et al., 1994).

The most prominent features of Atla Regio are the two volcanoes Maat and Ozza Montes. The former is the highest volcano and the second highest mountain on Venus. It is of all of Atla Regio's volcanoes the one that is located closest to the center of the region. There, it reaches a height between 8 and 9 km above mean planetary radius, with its basal elevation of about 2.6 km above mean planetary radius (MPR) (Keddie and Head, 1992). It has a basal diameter of 395 km enclosing an area of about 122,480 km^2. The slope of the volcano with an average grade of about 2.3° is covered by lava flows. Since they reflect radar waves efficiently, they are thought to be rather young, meaning less than 10 million years. The Venusian volcano is similar to the terrestrial counterpart Mauna Loa in Hawaii. The terrestrial volcano rises up to a height between 8 and 9 km above the surrounding sea floor, as well, but with a slope of about 4.2° (Cattermole, 1994; Faure and Mensing, 2007).

Even though the boundaries are gradational, various lava flow units originating

from Maat Mons can be distinguished. Radar bright flows, the most abundant unit, are located on the lower flanks of the shield volcano. These lava flows are interpreted to originate from large-scale effusion. Another unit is formed by mottled bright flows. The summit region shows radar-dark material with a diameter of 100 km comprising pits, flows and domes. North of the summit, a depression with a depth of about 2 km contains a field of small domes. On the summit itself, a caldera complex, 25 km in diameter, is located. Concentric graben between 5 and 10 km wide border the summit region in the south and west (Senske and Head, 1992; Cattermole, 1994).
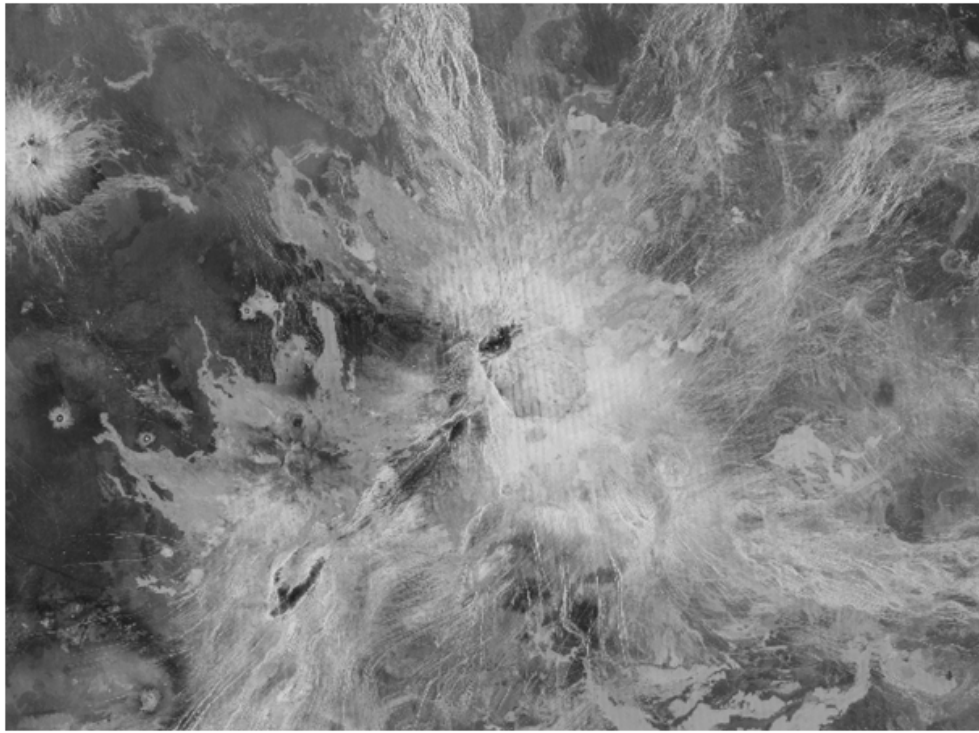
Figure 4.4: Magellan radar image of Atla Regio. The bright feature in the center is Ozza Mons. Maat Mons is located in the lower left part. Sapas Mons can be seen in the upper left corner. Also the various rift systems are clearly visible (`http://www.funkyscience.net/old/imagebank/eastaphrodite.html`, retrieved: 2014-11-10)

Northeast of Maat Mons, Ozza Mons is located, a volcanic edifice that has similar characteristics as Theia Mons in Beta Regio (Senske and Head, 1992). Superposed on the rift system Ganis Chasma (Keddie and Head, 1994d), the volcano rises up to a height of 7.5 km above MPR and about 3.85 km above the surrounding highland. It has a diameter of about 500 km at its base (Cattermole, 1994; Schinella

et al., 2011). Although it is smaller than Maat Mons, geoid and gravity anomalies are centered above Ozza Mons (Cattermole, 1994).

The two volcanoes share many characteristics. Numerous volcanic domes, flows, and small depressions can be found on the surface of Ozza Mons as well. However, the volcano does not have a summit caldera. This area rather comprises a radar-dark oval plateau that measures 50 x 100 km with an elevation of 1.5 km. The plateau contains several pits and collapse structures (Senske and Head, 1992). North of the summit, lava flows coming from a cluster of small volcanoes partially buried Ganis Chasma, which makes a clear time sequence in this area apparent. Another minor volcano, elongated in the northeast direction, is located south of the summit. Furthermore, there are many volcanic flows and fractures in this area. Many of the fractures are radial, but in general they follow the northeast trend. The locations of volcanic centers and regional faulting seem to be closely connected (Cattermole, 1994).

At least two different flow units originating from Ozza Mons can be discerned. Bright flows show no clear source region. They are often cut by faults and fractures. The second unit, mottled bright flows, appears to originate primarily from numerous vents on the flanks of Ozza Mons. In some places, this unit is crosscut by faulting as well. The two units form an embayment relationship, but in general, the mottled bright flows seem to be younger ones (Senske and Head, 1992). Farther to the west of Ozza and Maat Montes and their flow units, separated by a broad basin, about 600 km in diameter, another large shield volcano is located. Set on a local high close to Atla Regio's western margin, Sapas Mons resembles the other two volcanoes, but is smaller (Keddie and Head, 1994d). There is no consensus regarding the diameter of the volcano. Depending on where the base of the volcano is thought to be, it has a diameter between 217 km (`http://planetarynames.wr.usgs.gov/Page/VENUS/target`, retrieved: 2013-09-13) and about 600 km (Keddie and Head, 1994a; Schinella et al., 2011). Also the height of the volcano is unclear. It reaches an elevation of either about 3.6 km (Keddie and Head, 1994a) or 4.5 km (Faure and Mensing, 2007) above MPR and about 2.4 km above its base (Keddie and Head, 1992; Cattermole, 1994). The volcano is characterized by a gravity high of about 65 mGal (Keddie and Head, 1994d).

The summit region comprises two so-called scalloped-margin domes. These radar-dark, circular features are about 25 km in diameter and are surrounded by radial ridges. The centers of the domes appear in Magellan topography data as 2 to 3 km deep holes. However, this may be an overestimation due to steep scarps on the western edge that may cause radar echoes. These domes seem to be the

source regions of the youngest lava flows observed at Sapas Mons (Keddie and Head, 1994d). The volcano is surrounded by ridged plains. The formation of the ridges predated activity of Sapas. This is indicated by a lava flow to the northeast of the volcano that is diverted by a ridge and flows along it (Keddie and Head, 1992).

Sapas Mons has been built up by various flow units that can be divided by following their radar properties and morphology. The differing radar signatures and morphologies indicate that the effusing magma underwent a change in nature. Overall, six different flow units can be discerned. The younger the lava flows are, the shorter their length is. Therefore, the oldest unit can be found at the bottom, the youngest one makes up the summit region. This unit is linked with the two scalloped-margin domes in the summit region. Numerous small shields have been formed between the flows as well. They almost completely surround the center. The older units are cut by radial fractures and graben, especially on the southern and northeastern flanks. They are interpreted to be surface manifestations of deep dikes. The summit is surrounded by concentric pit chains and graben forming a partial ring that is between 75 and 100 km in diameter. Crosscutting the two youngest units, the graben appear to be rather young. However, the graben may have formed a continuous ring that has been buried partly by later eruptions. Therefore, a contemporaneous activity of erupting and rifting is suggested (Keddie and Head, 1992, 1994c).

The distribution of the lava flows on the one hand and the radial fractures and small shields on the other hand is quite asymmetrical. The lava flows dominate in the northwest and southeast of the volcano, probably reflecting the original topography. Wherever there is a lack of lava flows, fractures and shields that appear to be rather old dominate. This suggests that an original pattern may have partly been buried by lava flows (Keddie and Head, 1994c).

The oldest flow units that originated from Sapas Mons may be some smooth plains with low radar backscatter south of the volcano. They may have erupted from a vent that was to become the shield volcano. Such early-stage, radar-dark plains are often observed around large Venusian volcanoes (Keddie and Head, 1994d).

Although several large and smaller volcanoes as well as other volcanic deposits can be found on Atla Regio, the region is dominated by a different geological characteristic: major rifting. Five rift zones converge in this highland, and a series of chasmata radiates out from the common center, Ozza Mons. This makes Atla Regio, like Beta Regio, to a kind of tectonic junction. One of these has already been mentioned: Ganis Chasma to the north of Ozza Mons. The rift connects the volcano and Nokomis Montes in the northwest. The north-

ern termination of Ganis Chasma is surrounded by a region of tesserae. However, tesserae are more abundant in Beta Regio. On its way Ganis Chasma cuts through the small volcano Yolkai-Estsan Mons that has a diameter of 600 km (`http://planetarynames.wr.usgs.gov/Page/VENUS/target`, retrieved: 2013-09-13). To the east of the volcano, Ganis Chasma is met by two minor rift systems. This area is characterized by a field of rift-associated lava flows (Basilevsky, 1993). The system of fractures forming Ganis Chasma consists of numerous individual graben that are between 1 and 10 km wide and cross-cut each other. The branching network itself reaches a maximum width of 300 km and a length of about 1000 km (Cattermole, 1994). Close to Ozza Mons, the rift system narrows down to 125 km. Lava flows from Ozza Mons both, superpose and are crosscut by fractures, indicating that rifting and volcanic activity occurred contemporaneously (Senske and Head, 1992).
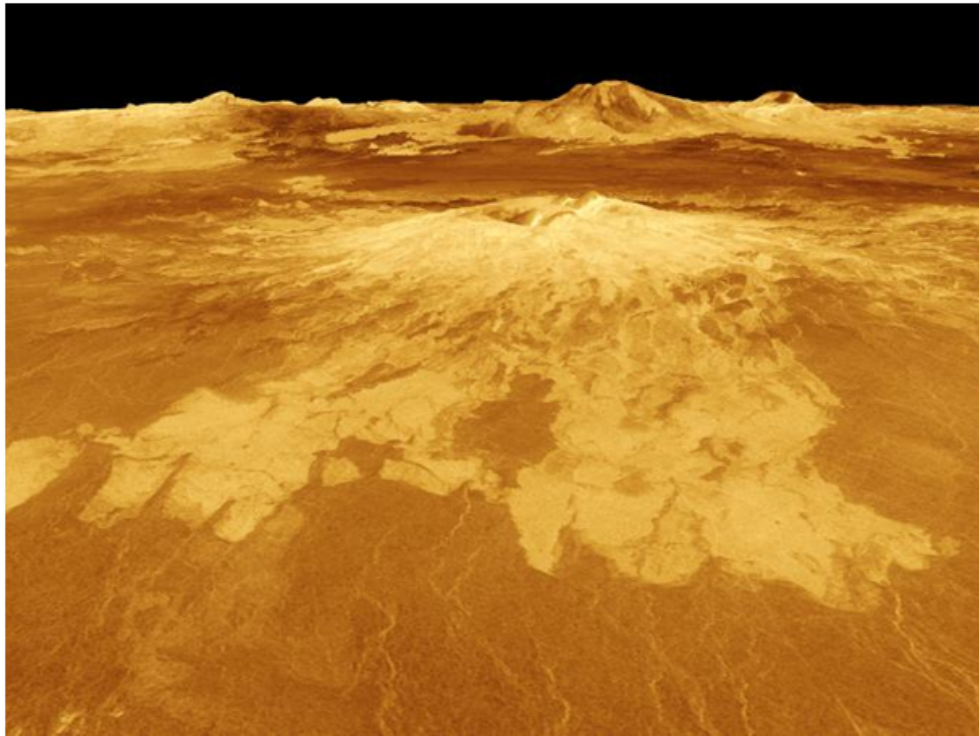

Figure 4.5: The volcanoes of Atla Regio: This computer-generated three-dimensional image shows Sapas Mons in the front and (from left to right) Ozza, Maat, and Ongwuti Montes in the back. Lava flows surrounding the volcanoes are clearly visible. The vertical scale of this image has been exaggerated ten times (`http://photojournal.jpl.nasa.gov/catalog/PIA00107`, retrieved: 2014-11-10)

Two other major rift systems radiate from Ozza Mons: Kicheda Chasma which merges into Parga Chasmata eastwards and Dali Chasma in southwest direction. The latter is among the deepest on Venus and together with Diana Chasma connects Atla Regio to eastern Thetis Regio. The rifts are up to 1,000 km long and about 100 km wide. They are at least 1 km deep and usually bounded by a ridge on one side. The height of the ridge has about the same value as the depth of the trough. The difference between the highest point of the rim and the deepest point of the trough can be up to 7 km. This region in general is characterized by a high degree of deformation (Cattermole, 1994).

The two less well-developed rift systems, Tkashi-mapa and Zewana Chasmata, to the east of Ganis Chasma complete the five rift systems (Basilevsky and Head, 2002a).

As mentioned before, Venusian lava flow fields are large compared to their terrestrial counterparts. In southern Atla Regio, one prominent example of a radar-bright flow field with a rather uniform texture can be found. About 900 km south of Ozza Mons a family of lobate flows, with a length of roughly 1,000 km, covers an area of around 180,000 km^2. The flows covering the present faulted and fractured plains were emplaced during at least four distinct episodes as can be told from superposition and intersections. They seem to originate from a series of graben that formed due to regional faulting. Some interesting details can be seen in some places. A flow channel is partly well defined by clear levees. The crust of the flow broke into numerous smaller pieces. Lava with low radar backscatter became visible underneath. Also, a small shield volcano has been flooded. Since nearby unflooded volcanoes have basal diameters of about 500 m, it is assumed that the thickness of the flow is about 100 m (Cattermole, 1994).

Besides these major volcanic edifices, Atla Regio comprises a couple of pancake domes, small domes, pits, and lava flows (Cattermole, 1994).

In addition to Beta Regio, Atla is an outstanding region with abundant modified impact craters as well (Cattermole, 1994). Basilevsky and Head (2002a) mention 9 impact craters that have been affected by local volcanic and tectonic activity that is believed to have occurred rather recently. The crater Uvaysi (formerly Luxemburg) has a diameter of 38.9 km and is located southwest of the summit of Ozza Mons. It is superposed on lava flows originating from the volcano. The flows are deformed by faults associated with Dali Chasma. Lava flows originating from Maat Mons in turn cover these faults (Basilevsky, 1993). The crater has a radar-dark parabola and therefore is estimated to be rather young, meaning younger than 0.1 - 0.15 T. Its ejecta to the west and its floor are partly embayed by lava flows originating from Maat Mons. The center of the crater is marked by

a peak (Basilevsky, 1993).

Due west of Maat Mons, two craters are located: Fossey and Piscopia, 30.4 and 26.2 km in diameter, respectively. The former has a clear dark halo which is partly flooded by lava flows from Maat Mons that post-date the formation of the crater. Due to the dark halo, Fossey is estimated to be younger than 0.5 T, which is the upper limit of the range of age estimated for lava flows from Maat Mons. 150 km east of Fossey, Piscopia is located. It shows a faint dark halo. Its age therefore is thought to lie in the range of 0.5 T and 0.75 T. It is affected by the same lava flow that approached Fossey. In the case of Piscopia, the southern part of the ejecta blanket is obscured (Basilevsky and Head, 2002a).

To the north of Maat Mons, the 21.8 km crater Melba is found. Also this crater is affected by a lava flow associated with the volcano. The flow covers the halo of the impact crater to the north and northeast and it embays the ejecta blanket. Basilevsky and Head (2002a) estimate the crater to be younger than 0.5 T, and maybe even younger than 0.15 T. Consequently, this lava flow from Maat Mons is accordingly younger.

The crater Von Schuurman (29.1 km in diameter) to the southwest of Maat Mons is superposed on lava flows associated with the Dali Chasma rift. Sitwell (32.8 km in diameter) in the north of Atla Regio is superposed on Ganis Chasma. Both craters have central peaks (Basilevsky, 1993) and prominent dark parabolas, and both postdate rifting. Therefore, rifting in Dali and Ganis Chasmata occurred before 0.1 - 0.15 T (Basilevsky and Head, 2002a).

South of Yolkai-Estsan Mons, the volcano that sits on Ganis Chasma, the 36.2 km crater Bashkirtseff is situated. It has been flooded by lava flows originating from the volcano. The crater has remnants of a faint halo and therefore is interpreted by Basilevsky and Head (2002a) to be older than 0.5 T .

In general, the craters close to Maat Mons Uvaysi, Fossey, Piscopia and Melba imply that the volcano was active until very recently. Some of its lava flows are younger than 0.5 T, some may be even younger than 0.1 - 0.15 T. There are, however, no strong constraints for lava flows from Ozza Mons. Whereas rifting and associated occasional volcanism of Dali and Ganis Chasmata predate the formation of the craters Von Schuurman and Sitwell, lava flows associated with Ganis postdate the crater Bashkirtseff (Basilevsky and Head, 2002a).

4.3   Bell Regio

To the northeast of Aphrodite Terra, there are three plains called Leda, Niobe, and Rusalka Planitiae. The former is enclosed by the two isolated upland massifs, Bell and Tellus Regiones. The latter lies about 3,000 km north of Ovda Regio. Bell Regio is located to its west. This complex highland region has an elevation of 1.5 - 2 km. Bell Regio appears as a broad crustal dome, between 1,500 km (Cattermole, 1994; Campbell and Campbell, 2002) and 1,600 km (Bindschadler et al., 1992) across, elongated along the longitude of 48°E. An apparent depth of compensation between 125 km (Smrekar, 1994) and 170 km (Smrekar and Phillips, 1991) has been estimated for Bell Regio. It is split up into two rises, each of which contains one of the two most prominent features of this region. On the southern rise, the shield volcano Tepev Mons rises up to a height of 5 km above the surrounding plains. The northern rise comprises the corona Nefertiti (Cattermole, 1994). Three other volcanic edifices besides these two are responsible for extensive effusive volcanism characteristic of Bell Regio. The lack of associated rifting clearly distinguishes this highland from Atla and Beta Regiones (Campbell and Campbell, 2002). Only a small gravity anomaly of 20 mGal is located on the northern part of the Bell Regio rise (Bindschadler et al., 1992).

Tepev Mons has a diameter of 300 km (Campbell and Campbell, 2002) and reaches a height of almost 6 km above MPR. Its twin peaks are elongated in a west-east direction. Both peaks contain two circular radar-dark features that appear to be shallow calderas. The one on the eastern peak has a diameter of 11 km and the western caldera is larger with a diameter of 31 km. Many radar-bright lava flows radiate outwards from the two foci, overlapping one another. They extend up to 200 km and originate from the calderas or from proximate fissures or pit craters. To the north of the summit area, a set of circumferential radar-bright fractures is located. Moreover, the summit region comprises collapse pits and pit crater chains. The central massif of the volcano has steep slopes with flanks of up to 40° (Cattermole, 1994; Campbell and Campbell, 2002).

To the east of Tepev Mons, on the southeast flank of the southern rise of Bell Regio, another volcanic focus, called Nyx Mons, is located. The volcano has a diameter of 875 km (`http://planetarynames.wr.usgs.gov/Page/VENUS/target`, retrieved: 2013-10-08) and rises with gentle flank slopes of less than 1° to a height between 2 and 3 km above MPR. Nyx Mons was the earliest volcanic edifice that started forming in this region. It is associated with a moat that surrounds the central bulge as well as ridges whose pattern resembles a wishbone. A small set of concentric graben occurs farther south. The volcano is also characterized by pit

crater chains that form a radial pattern (Cattermole, 1994; Campbell and Campbell, 2002).
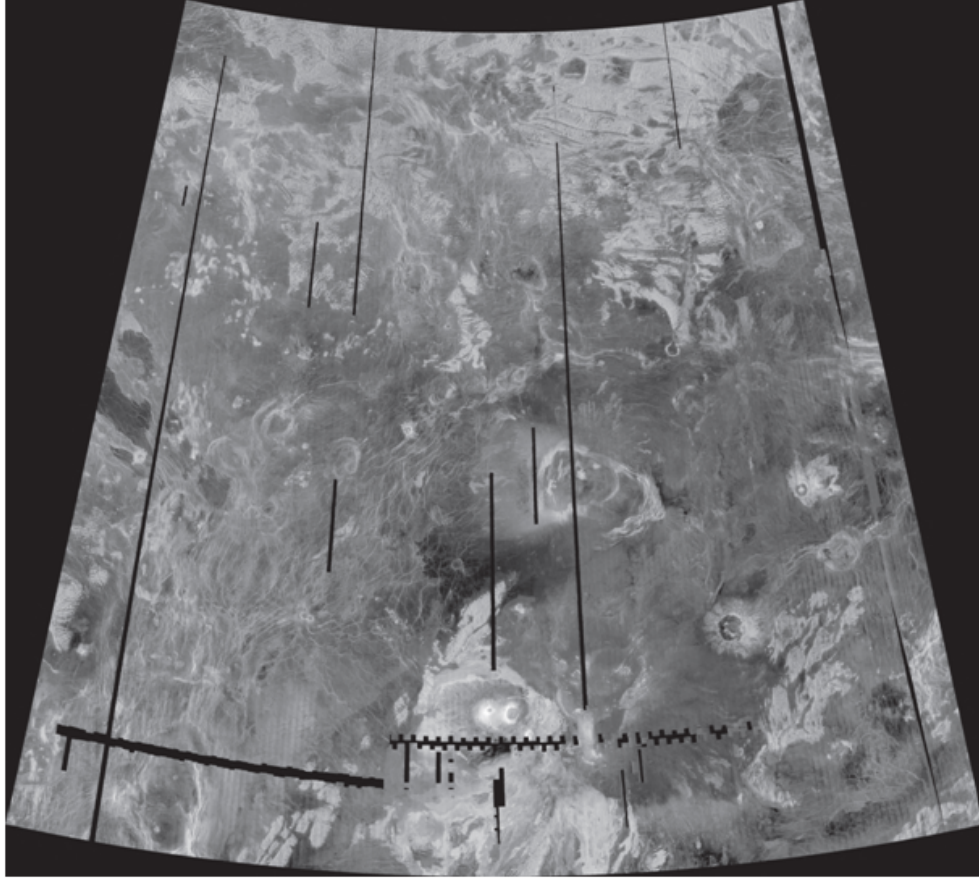
Figure 4.6: This radar image shows Bell Regio and the surrounding regions. The two calderae of Tepev Mons are clearly visible at the bottom of the image in the center. Nyx Mons is located to their east. Nefertiti Corona is situated north of Nyx Mons (`http://planetarynames.wr.usgs.gov/Page/venus1to5m_Radar`, retrieved: 2014-11-15)

Moreover, the volcano is associated with several lava flows that can be divided into three units. The oldest one with a moderate to low radar signature superposes the ridged plains to the east of the highland and embays the tesserae found south of the rise. This unit extends up to 600 km from the volcanic center. The next-youngest unit is radar-dark and extends up to 450 km, superposing the older unit. Its outcrops to the south-east have bright boundaries. They could be a result of a transition of smooth lava flows to rougher ones. They could also be higher-standing remnants of older flows that were embayed. Superposing the other two flow units, the youngest one consists of radar-bright flows to the south

and southwest of Nyx Mons, reaching even far beyond Tepev Mons. Some seem to originate from fissures concentric to the volcano (Campbell and Campbell, 2002). Nyx Mons is believed to be the oldest volcanic center of the Bell Regio rise. Rogers and Zuber (1998) propose a scenario in which the volcanic style changed with time. McGovern and Solomon (1995) suggest that the lithosphere has to be sufficiently thick to allow the formation of large shield volcanoes. They associate a thin lithosphere with rapid eruptions and, hence, the formation of volcanic centers of low relief (such as coronae or small shield volcanoes) and the emplacement of plains. Thick lithosphere, on the other hand, traps magma at depth and causes infrequent eruptions creating steep-sided edifices (Rogers and Zuber, 1998; Campbell and Clark, 2006). This suggestion is supported by modeling (Solomon et al., 1994; Smrekar and Stofan, 1997; McGovern and Solomon, 1998). Therefore, in the Bell Regio rise, Nyx Mons seems to manifest a transition from thin to thick lithosphere and, hence, from plains-forming volcanism to more shield-forming volcanism which then led to the formation of Tepev Mons (Rogers and Zuber, 1998). There may be evidence of rare pyroclastic activity. South of Tepev Mons, an area of fine-grained material superposes lava flows from Nyx Mons. It is radar dark and has feathery margins. Due to the lack of a clear crater or a discernible central area, a pyroclastic nature is possible (Campbell and Campbell, 2002).

On the southeast flank of the volcano, two small (about 80 km in diameter, `http://planetarynames.wr.usgs.gov/Page/VENUS/target`, retrieved: 2013-10-08), steep edifices called Otafuku Tholi are located. They reach heights of 4.4 and 4.9 km above MPR. The northern edifice is the source of radar-bright lava flows that superpose flows from Tepev and Nyx Montes and partly embay tesserae to the north of Tepev Mons. The flows from Otafuku Tholi seem to follow and infill a topographic moat encircling the northern side of Tepev Mons. The southern edifice is not associated with lava flows but with flow debris to its southwest and east. The southwestern debris may have been the result of the collapse of the volcano flank. Due west of the southern edifice, another steep-sided dome, 31 km in diameter, is located. It has partially been buried by flows originating from Nyx Mons (Campbell and Campbell, 2002).

The northern rise of Bell Regio is not as high as the southern one. Moreover, volcanism there is less dominant, although several lava flows can be seen. The prominent corona Nefertiti has dimensions of 500 x 230 km and is associated with numerous lava flows that cover its interior and overlie parts of its rim. The flows radiate outwards for up to about 100 km. To the north of the corona a region of higher topography with an east-west trend diverts the lava flows eastward. The corona is also defined by some concentric faults. To the south of Nefertiti Corona,

a minor rift zone made up of some ill defined fractures trending in north-south direction can be seen. Inside Nefertiti Corona, the impact crater Miriam with a diameter of 16.5 km is located (Cattermole, 1994; Campbell and Campbell, 2002). More impact craters can be found on the southern Bell Regio rise. East of the southern rise, the crater Potanina (92.4 km in diameter) is superposed on the plains that surround the highland as well as on lava flows originating from Nyx Mons. The crater is surrounded by blocky ejecta deposits and an outflow on its eastern side trending into a northeast direction. Moreover, a clear dark halo is visible, which indicates a rather young age of the impact crater (Basilevsky and Head, 2002b).

Another crater is located within the lava flows from Nyx Mons south of Tepev Mons. Gautier is 59.3 km in diameter and has been heavily flooded by the lava flows. The southern part of the crater's rim is visible for the most part as well as some of the ejecta deposit which is superposed on an underlying plain that has not been covered by lava flows. This clearly shows that the impact crater formed before emplacement of the lava flows (Basilevsky and Head, 2002b).

Numerous tessera blocks are located south and west of the southern rise. Associated with them are a few sets of lineations. In some places, the space separating the faults is flooded by lava flows originating from the volcanic rise of Bell Regio. Moreover, all tessera blocks are embayed by either plains or lava flows. This emphasizes that tesserae are the oldest geological features on Venus that predate volcanism. However, due to a lack of contact between the individual tessera blocks, it is not possible to determine the relative ages of them, nor whether they all formed around the same time or in the course of a longer time span. More regions of tessera are located north of Bell Regio. Nevertheless, no tessera block can be found on the rise (Cattermole, 1994; Campbell and Campbell, 2002).

South of Isthar Terra, there are the lowlands of Sedna and Guinevere Planitiae. These plains are disrupted by the isolated highlands of Alpha (in the south), Bell (in the east), and Eistla (central) Regiones. The latter with elevations above 1.5 km is split up into three separate massifs: western, central, and eastern Eistla Regiones. They continue the west-north-west trend of western Aphrodite Terra. Eistla Regio comprises the region between longitudes 340° and 55°E as well as latitudes 10° and 25°N. About 6,500 km to the west of Eistla Regio, Beta Regio is situated (Cattermole, 1994).

4.4   Western Eistla Regio

In general, this highland massif is characterized by radar-dark and mottled plains that occupy extensive areas. The radar-dark area is believed to be due to widespread lava flooding. The mottled plains comprise many small shield volcanoes. The topographic rise is traversed by rift zones on whose higher ground large, radarbright volcanic edifices are located. As typical for hotspot regions on Venus, also western Eistla Regio is characterized by large positive gravity anomalies: with values of 30 mGal and 25 mGal they are located above the volcanoes Gula and Sif Montes, respectively. Depths of compensation have been estimated to be in the range of 100 and 200 km, similar to Bell Regio. In general, this volcanic rise is somewhat similar to the highland of Bell Regio (Senske, 1992; Grimm and Phillips, 1992; Cattermole, 1994).

Western Eistla Regio, a rhombic shaped highland rise with dimensions of about 3,200 x 2,000 km and an elevation of about 1.8 km (Stofan et al., 1995; Copp and Guest, 2007), is dominated by the two peaks of the large volcanoes Sif and Gula Montes. The latter is the larger of the two with a height of 4.6 km above MPR. It rises up to 3.2 km above the surrounding region, occupying an elliptical area with the dimensions of about 400 x 250 km. Like many other hotspot volcanoes, Gula Mons is a shield volcano with an upper flanks slope between 2° and 4° and a lower flanks slope between 0.25° and 1.4° (Senske et al., 1992; McGill, 2000; Stofan et al., 2001). The steep flanks indicate that eruptions associated with low mass or a short period of time occurred. The flanks are covered with radar-dark sheet-like and radar-bright digitate lava flows. The varying types of flows hint towards different styles of volcanism. The flows extend outwards for a few 100 km superposing the radar-dark and mottled plains of this highland (Senske, 1992; Cattermole, 1994). Nevertheless, a few distal flows that reach a length of up to 600 km are cut by wrinkle ridges. Most lava flows are of a digitate shape. Common appearances at Gula Mons, especially on its southern flank and the outer apron, are flows with radar-dark interiors indicative of smooth surfaces and radar-bright margins indicating a rougher texture. Pits, fractures as well as small edifices are the sources of flank eruptions. However, at Gula Mons they are less common than flows originating from vents along the summit rift (Stofan et al., 2001). Gravity data reveal a positive free-air gravity anomaly of 60 mGal centered on the volcano (Bindschadler et al., 1992).

The summit of the volcano is not a single peak, but consists of a number of volcanic centers as well as a rift striking northeast with a length between 100 and 150 km and a width of 25-30 km (Stofan et al., 2001; Copp and Guest, 2007).

Both ends of the rift terminate at caldera complexes. At least three collapsed structures with diameters between 19 and 25 km are located at the northeastern end. The calderas are surrounded by radial fractures and pits. The southwestern end comprises a construct with a height of about 500 m. Within this construct, several partly filled calderas are located. The caldera at the far southwestern end comprises a dome with a diameter of 25 km. Since the rift partly cuts the caldera, but is also filled with lava, contemporaneous rifting and volcanism is suggested. Radar-dark lava flows originate from all volcanic centers in the summit region (Stofan et al., 2001).

In the vicinity of Gula Mons, extensional fractures can be found. They crosscut the lava flows from the volcano and continue on the adjacent plains. To the northwest, east, and southwest, the volcanic edifice is partly surrounded by radial fractures. Moreover, a group of several hundred kilometers long but less than 1 km wide curvilinear lineaments can be seen on the lava flows of Gula Mons. These are believed to be dikes that did not reach the surface and became manifested in graben (McKenzie et al., 1992; Copp and Guest, 2007).

The most prominent fractures, however, of this area are located to the southeast of Gula Mons. The rift valley Guor Linea extends for at least 1,000 km and reaches a width of up to 150 km (Grimm and Phillips, 1992; Keddie and Head, 1994a). It is associated with a topographic rise that strikes northwest-southeast and connects the highlands of western and central Eistla Regio. The rift system is a result of local extension and lithospheric thinning. According to detailed analysis by Grimm and Phillips (1992), the whole rift system consists of at least three major fracture families. Some of the fractures are approximately 300 km long, but most of them are clearly shorter. Due to superposition and transactions, an age relationship can be established. The probably youngest fractures strike west-east. They form a deep trough which transects older faults with a northwest-southeast trend. These faults represent the main pattern of the rift. The third of the major fracture families is less prominent. It strikes north-south and seems to be the oldest one that has been reactivated and therefore crosscuts the youngest fractures and Gula Mons. The outermost lava flows from the volcano superpose the rift system, which shows that the main rifting predates the formation of the volcano (Copp and Guest, 2007). However, the fractures that crosscut the lava flows from Gula Mons show that also after volcanic activity extensional deformation occurred (Cattermole, 1994). A graben-like rift on the northern flank of Gula Mons connects the volcano with the corona Idem-Kuva. This rift shows the same trend as Guor Linea (Copp and Guest, 2007).

Sif Mons has, in contrast to Gula Mons, only one peak. With a diameter between

200 km (Senske, 1992) and 300 km (Cattermole, 1994; Francis and Oppenheimer, 2004; Copp and Guest, 2007) and a height of about 3.4 km above MPR (about 1.7 km above the surrounding highland), it is smaller than Gula Mons. Its gentle lower flanks have a slope of 0.15 - 0.25°. Closer to the summit they are steeper with a slope of 1 - 3°. Along this change in slope angle which is in a distance of about 100 km to the summit, numerous small edifices have formed. Many of them are associated with surrounding flows (Cattermole, 1994; Stofan et al., 2001). Not far from the volcano, northwest-striking fractures form an area with a width of about 125 km. Radial fractures are situated northwest of the volcano. In general, the fractures associated with Sif Mons are not as prominent as those of Gula Mons (Senske, 1992; Cattermole, 1994).

Most of the volcanism originating from Sif Mons occurred after the emplacement of the radial fractures. This is apparent from a field of radar-bright lava flows which are about 15-30 km wide and at least 250 km long that flowed down the northern flank of the volcano and on their way flooded a group of small shield volcanoes. The sources of these flows can often be discerned. Therefore, a large dome seems to be the source of the westernmost flow. On the same flank an older series of radar-dark flows with a length of at least 400 km can be observed. Their sources, however, are not visible. They end in a fault trough. Such extensive flows occur either due to high mass-eruption rates or magma with low viscosity, or both. More flows with radar-bright signatures originated from the summit region and flowed down east and southwards (Senske, 1992; Cattermole, 1994). Especially the lava flows to the east are associated with flow channels. In general, lava flows from Sif Mons are not as long and sinuous as flows from Gula Mons. Distal flows of Sif Mons, the longest with lengths of about 600 km, superpose the regional plains units. Thus, a clear age relationship can be established (Stofan et al., 2001). Also flank eruptions that are typical for Hawaii occurred at Sif Mons. Considering the whole size of the Venusian volcano, it has a striking similarity to the Hawaiian shield volcanoes, such as Kilauea (Senske, 1992; Cattermole, 1994). However, the central, steeper part, a cone 170 km in diameter, resembles Mount Etna in Sicily according to Copp and Guest (2007).

A relatively flat-floored caldera structure with a diameter of about 45 km is located on the summit. The caldera is filled with young, smooth flows of variable back-scatter that partly flowed over the edge in the north and east. In the west and south of the floor, marginal ridges are located. The depression itself is surrounded by abundant radar-bright lobate flows that form an apron with a width in the range of 100 and 150 km. There is also a chain of collapse pits (3-10 km in diameter) within the depression as well as on the southern and southwestern

flanks. They were probably generated as a consequence of flank eruptions and activity relating to dykes along the flank. These smaller depressions reflect the general northwest-southeast trend that is associated with this highland (Cattermole, 1994; Stofan et al., 2001). Copp and Guest (2007) identify deposits of low radar backscatter that surround these depressions and interpret them as evidence of pyroclastic activity. Stofan et al. (2001), however, did not classify any such evidence.
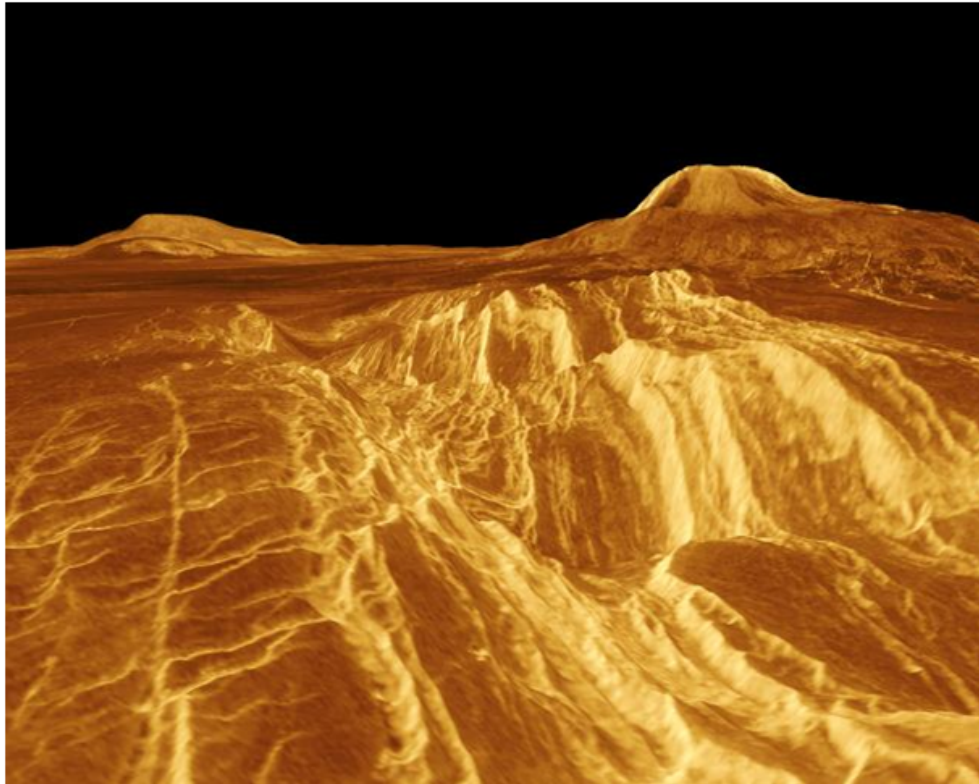
Figure 4.7: The volcanoes of Western Eistla Regio: A computer-generated three-dimensional picture of Sif (to the left) and Gula (to the right) Montes (`http://photojournal.jpl.nasa.gov/catalog/PIA00200`, retrieved: 2014-11-15)

Besides volcanoes, other volcanic structures are located on western Eistla Regio. Nissaba Corona with intermediate radar signature is situated north of the two volcanoes. Nissaba Corona is irregularly shaped with a 320 km long northwest-southeast axis and a 220 km long north-south axis. A small, circular topographic high forms the northwest of the corona. This rise is surrounded by a trough in the west and southwest. Outside of the trough, a discontinuous ridge is located. The ridge stops flows from the volcanoes from entering the corona. There does

not appear to be an outer trough. Nissaba Corona is surrounded by several flows. One flow unit superposing the northwestern part of the corona originates from a small volcano which is associated with the formation of the corona. More flows originate from fractures surrounding a small depression in the interior of Nissaba Corona (Copp and Guest, 2007).

Due east of Nissaba, Idem-Kuva Corona is located between two radar-bright lava flows originating from Gula Mons (Senske, 1992; Cattermole, 1994). The corona is about 250 km in diameter. Like Nissaba Corona, a central plateau with a diameter of about 100 km is located in the interior. This rise has an elevation of about 600 m and is surrounded by a moat which, in turn, is surrounded by a semicircular ridge. The corona is also associated with various fractures. Concentric fractures with little space between them cut the ridge and the moat. Graben to the southwest of the corona, offset from the topographic ridge, indicate a protracted formation of the volcanic structure. Two radar-bright lava flows are located in the interior of the corona. The source of the western one is a small volcanic construct, whereas graben are the source of the eastern flows. The lava flows follow the pre-existing topography (Copp and Guest, 2007).

Even though there are several superposition relations between the four volcanic constructs, a determination of the relative ages is difficult. Nissaba Corona seems to be older than Sif Mons. Lava flows from the volcano are deflected by Nissaba Corona and overlay some of its flows, indicating that they formed later. Nevertheless, some of Nissaba's late volcanism may have occurred after early activity of the volcano, as some lava flows from the corona indicate. The southern part of Idem-Kuva Corona, however, seems to be younger than Gula Mons, since it cuts the flanks of the volcano. The formation of both coronae began before or during the emplacement of the regional plains unit. Fracturing and volcanic activity at Idem-Kuva Corona continued after Gula Mons had formed (Copp and Guest, 2007). It has not been established yet, whether Gula or Sif Mons is the older volcano.

To the southwest of Sif Mons, a small impact crater is located on the volcano's flow apron. Veriko has a diameter of about 5.2 km (`http://planetarynames.wr.usgs.gov/Page/VENUS/target`, retrieved: 2014-05-09). It is surrounded by radar-bright ejecta material which, in turn, is surrounded by a radar-dark halo consisting of fine-grained material. No outflow material is associated with this crater (Copp and Guest, 2007).

Another impact crater is located southeast of Sif Mons. The crater itself does not seem to be superposed on lava flows, whereas parts of its ejecta material are. De Lalande has a diameter of 21.3 km (`http://planetarynames.wr.usgs.gov/`

`Page/VENUS/target`, retrieved: 2014-05-09). The floor in the interior of the crater appears radar-dark. Copp and Guest (2007) mapped a radar-bright central crater peak surrounded by a hummocky rim. Also this crater is encircled by radar-bright ejecta deposits which especially to the north and east appears flow-like. A radar-dark halo is visible as well.

There are two regions of tessera material on the topographic rise. One is completely surrounded by volcanic flows originating from Gula Mons, the other one close by is partly surrounded by flows from Sif Mons. Copp and Guest (2007) list another plains unit which resembles tessera material in that it is radar-bright and highly fractured as well. However, since the identification is not without doubt, they named this unit "deformed plains material" instead. Also large areas of the extensive regional plains characterized by wrinkle ridges can be found on the topographic rise.

Surrounding the rise but also on the rise itself are extensive regions containing numerous small volcanic domes, cones, and shields with diameters less than 10 km. In general, their flank slopes are below 5°. Some volcanic edifices are clustered in groups, others are isolated. An edifice field generally has a diameter of 100 km and comprises about 75 edifices. A flow apron with a width of up to 275 km surrounds such a field. The formation of these plains seems to have predated the volcanic activity of Sif Mons. However, there are also clusters that are superimposed on fracturing that occurred later on. These domes seem to have formed due to volcanic activity that was locally concentrated but whose partial melts only had limited access to the Venusian surface (Cattermole, 1994; Copp and Guest, 2007). The plains are additionally characterized by parallel faults and ridges with little space in between as well as narrow wrinkle ridges and lineaments. Fracturing and the formation of these volcanic edifices occurred concurrently (Copp and Guest, 2007).

The geologic history is similar as in other regions on Venus. Tessera material appears as the oldest material. Similar to tessera material is the deformed plains material which seems to be younger. The subsequent plains unit is the mottled one containing numerous small shields, cones, and domes. As a part of the western Eistla rise, large areas of this unit have been uplifted. Since the formation of the small volcanic edifices was rather protracted, some of them postdate the next unit which is characterized by wrinkle ridges. Before the plains material unit with abundant wrinkle ridges was emplaced, Idem-Kuva Corona started to form. However, its activity was protracted as well, and therefore some of its lava flows overlie wrinkle ridged plains material. After the emplacement of these plains units, isolated edifices with diameters less than 100 km erupted and produced a

few scattered lava flow fields. Their age, however, is not constrained. Eventually, the major volcanoes formed. But also the formation of Sif and Gula Montes may have started a lot earlier and older lava flows from them may even predate the emplacement of the wrinkle ridged plains unit (Copp and Guest, 2007). This is insinuated by wrinkle ridges that are concentric to the rise, which shows that at the time of the formation of the wrinkle ridges, some kind of topographic rise already existed and deflected the ridges (Basilevsky, 1994).

As for Bell Regio, also for western Eistla Regio thickening of the lithosphere and accompanying change in style of volcanism is proposed. Therefore, in the early stages of evolution, rapid eruption was possible and the coronae formed. As the lithosphere thickened, the construction of large shield volcanoes, such as Sif and Gula Montes, became possible (Campbell and Clark, 2006).

4.5   Central Eistla Regio

The middle highland massif with a mean elevation of about 1 km is similar to its western neighbor and Bell Regio (Cattermole, 1994; McGill, 1998). Extensive areas are occupied by radar-dark and mottled plains that are cut by rift zones. Large volcanic structures can be found on higher ground. The positive gravity anomalies (about 15 mGal above one of the volcanic centers) and the estimated depths of compensation (about 110 km) show similar values as well (Grimm and Phillips, 1991; Cattermole, 1994).

The middle rise of Eistla Regio was originally called Sappho due to a distinctive radar-bright feature seen on early images. This later turned out to be a caldera, Sappho Patera, on a volcano called Irnini Mons, 1.75 km elevated above MPR (Cattermole, 1994; McGill, 2000). There is no consensus about the diameter of the volcano. It lies somewhere in the range of 300 km (Cattermole, 1994) and 525 km (`http://planetarynames.wr.usgs.gov/Page/VENUS/target`, retrieved: 2013-10-19). With a diameter of 225 km and a depth of several hundred meters the caldera is one of the largest on the planet. Moreover, it shares many characteristics with coronae. The volcano is marked by concentric fractures. East of Irnini Mons, a few patches of areas with a rather homogeneous surface are located. The transition between these areas and the surrounding plains appears wispy. McGill (2000) interpreted this wispy nature to be of Aeolian activity. Besides these homogeneous areas, some textured plains material with ridges occurs east of Irnini Mons as well. These plains could be the remnants of a ridge belt that has been

buried by lava flows from the volcano.

Another volcanic edifice can be found to the south of Irnini. Anala Mons has a diameter of about 550 km. The volcano is less well defined and rises up to about 2.25 km above MPR. Both volcanoes have average flank slopes of about 0.5° that are covered in lava flows (McGill, 2000). These flows extend outwards well beyond the base of the volcanoes for up to 250 km. Those from Anala Mons partly overlap lava flows originating from Irnini Mons indicating the age relationship (Cattermole, 1994; McGill, 2000). Due to the shield shape of the volcanoes and the lengths of the lava flows the magma is assumed to be basaltic with low viscosity. To the west of Irnini Mons, flows from the volcano are bounded by a preexisting valley suggesting older topography (McGill, 2000).
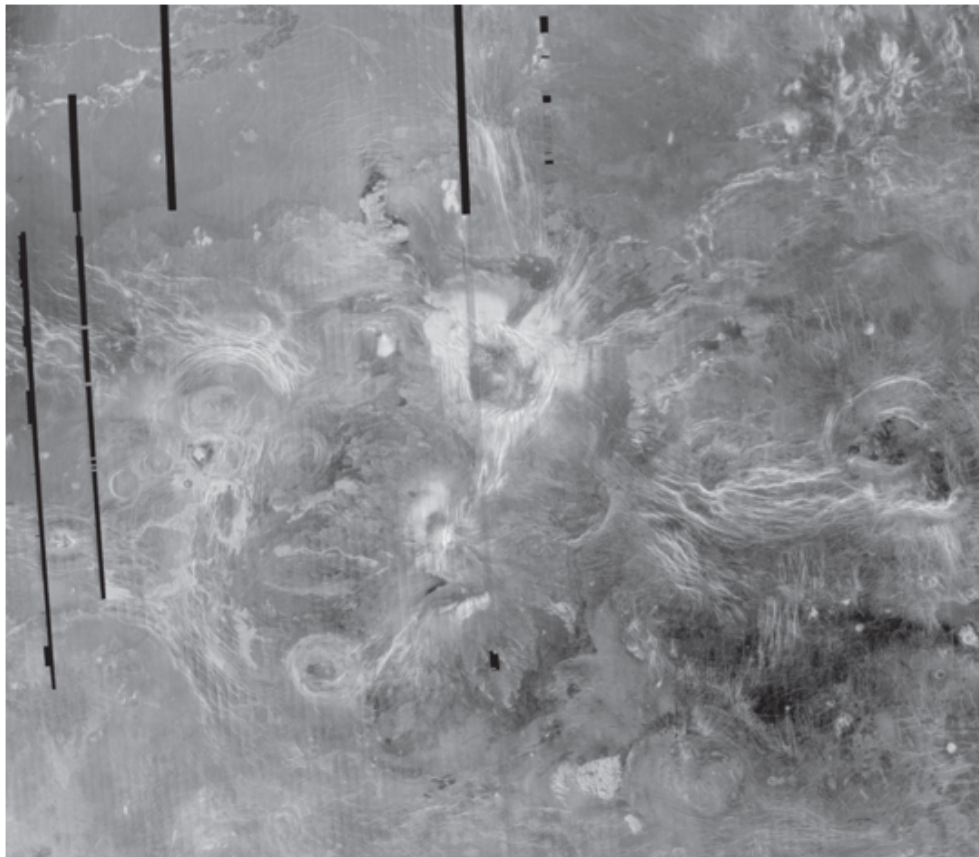

Figure 4.8: Magellan radar image of Central Eistla Regio. This volcanic rise consists of Irnini Mons with Sappho Patera, located just above the center of the image, and Anala Mons to the southwest of the former volcanic center (`http://planetarynames.wr.usgs.gov/Page/venus1to5m_Radar`, retrieved: 2014-11-15)

The summit regions of Irnini and Anala Montes are surrounded by very radar-bright halos that are superposed on flow material. The halo material is interpreted to be rare pyroclastic deposits with a roughness on the centimeter-scale. Between the halos and the surrounding flow materials, transitional units occur that are almost as radar-bright as the halo material. Flows originating from the two volcanoes are superposed on regional plains showing that the volcanic edifices are younger. In the summit regions of both volcanoes mottled plains abundant in small shields and domes with diameters between one and five kilometers are located. Since these plains seem to embay the pyroclastic deposits, they are interpreted to be younger (McGill, 2000).

Irnini and Anala Montes are very unique in that they are hybrid structures of shield volcanoes and coronae (McGill, 2000). Indeed, Stofan et al. (1992) list both Sappho and Anala as coronae and they classify central Eistla Regio as corona-dominated. However, it is not known whether the two volcanic edifices first formed as coronae which then have been uplifted, or whether they are shield volcanoes whose summit evolved corona-like features (McGill, 1998). Considering the probable development in Bell and western Eistla Regiones, where the lithosphere is believed to have cooled and thickened with time, the first case seems more likely (McGill, 1994). Moreover, the first hypothesis is favored by most models of the formation of coronae (e.g. Smrekar and Stofan, 1997). However, the second hypothesis is supported by the geology of the topographic rise. Fractures and faults associated with the corona-like features cut the youngest lava flows of the shield-like volcanoes. The development of a volcano into a corona by thinning of the lithosphere caused by an impinging mantle plume is not unlikely (McGill, 1998). The topographic rise is flanked by several coronae (Cattermole, 1994). Located to the west of the rise is Nehalennia Corona with a diameter of 345 km. Its internal topography is rather complex with parts lying higher and parts lying lower than the surrounding plains. Flows originating from the corona are embayed by flows from both volcanoes indicating that the corona is older than the volcanoes. Nehalennia Corona has some radial structures. Southwest of Anala Mons, Sunrta Corona is located. The corona, a large depression with a diameter of 170 km surrounded by a rim, is embayed by flow material from the volcano close-by. Both, Sunrta and Nehalennia Coronae are characterized by prominent concentric structures that have been partially buried by material from Anala Mons. Another smaller corona is located east of Nehalennia and has been partially buried as well (McGill, 2000).

Like western Eistla, the central highland is very abundant in fractures and faults as well. The main trend runs in a north-south direction (Cattermole, 1994). Badb

Linea extends from north of Irnini Mons southward and terminates at Sunrta Corona. The deformation zone consists mostly of graben that are often cut short by flows from Irnini Mons. However, other graben crosscut lava flows and the summit regions of both volcanoes that suggest that Badb Linea was also active after the youngest lava flows had been emplaced. In addition to fractures parallel to Badb Linea, both volcanic constructs also show radial structures, and Irnini Mons even concentric ones (McGill, 2000).

Another major fracture system, the Guor Linea rift system coming from western Eistla, is stopped about 900 km west of Sappho Patera by Nehalennia Corona, suggesting that the corona is younger (Cattermole, 1994; McGill, 2000). The rift system continues east of Irnini and Anala Montes with an east-west trend, until it finally terminates at Libera Corona. Lava flows from the volcanoes truncate the faults of Guor Linea. Moreover, no such faults occur on the volcanoes. Therefore, part of a once probably continuous rift system has been completely buried by lava flows from Anala and Irnini Montes, splitting the system apart. The eastern part of the rift system is now called Virtus Linea. The complete rift system had a length of about 2,000 km. Its rifts were emplaced in the course of several episodes. They are younger than the surrounding plains materials (McGill, 2000).

There are a few patches of tessera material scattered around the topographic rise. Like most of the plains, the tesserae show intermediate radar brightness. However, the oldest and the youngest plains materials have different radar signatures. Some patches of so-called lineated plains materials situated off as well as on the rise are characterized by extreme radar brightness. This brightness is attributed to a highly rough and deformed surface. Since these plains embay tessera material, but are otherwise embayed by all other plains materials, they are believed to be the oldest. One patch of lineated plains is located south-southeast on the high flanks of Anala Mons. Its presence at this location indicates that a rise was formed already prior to eruptions showing that Anala Mons is not a mere volcanic construct. This rise is almost coincident with the volcanic topography itself (McGill, 2000).

The regional plains, characterized by a set of east-west-oriented wrinkle ridges, surround the topographic rise of central Eistla Regio. Several patches also occur on the rise. Therefore, the uplift of the rise must have occurred after the emplacement of these plains. A younger set of wrinkle ridges, encircling the topographic rise almost entirely, supports this idea. However, a phase of early uplift is suggested similar to western Eistla Regio (McGill, 2000). Immediately west of Irnini Mons, an area is covered by flows that originate from Nehalennia Corona. These flows are characterized by a higher density of small scale wrinkle ridges than the

regional plains. Several wrinkle ridges are embayed and truncated by the regional plains (McGill, 1998, 2000). This confined area very likely was uplifted before regional plains material was emplaced (McGill, 2000).

The majority of the rise is covered by flows originating from the volcanic centers of Irnini and Anala Montes. No wrinkle ridges are located on these flows indicating that the lava flows were emplaced after the wrinkle ridges had formed. Also very few patches of smooth plains material, the youngest unit, can be found on the rise. Its radar darkness is a consequence of the smoothness of the surface which could be a consequence either of deposited fine-grained material originating from pyroclastic volcanic activity or of low-viscosity lava (McGill, 2000).

Senske et al. (1992) state that volcanic construction usually occurred after topographic uplift. However, on western and central Eistla it becomes apparent that fracture systems cross-cut volcanic edifices, but also are flooded by them. This shows that volcanic and tectonic activities mostly co-occurred (Cattermole, 1994). In general, the formation of the Eistla Regio rise was accompanied by progressive deformation (McGill, 1998). The uplift of the topographic rise of central Eistla Regio began already during the emplacement of the regional plains material and continued afterwards. Thus, some patches of these plains and even older topography formed by early episodes of deformation are located on the rise. The emplacement of regional plains material was followed by more episodes of extensional deformation forming the major rift zones. In addition, contemporaneous volcanism built up large edifices (McGill, 2000).

Central Eistla Regio is devoid of impact craters (Phillips et al., 1991a). The distribution and condition of impact craters and wrinkle ridges imply that regional plains were emplaced within a rather short period of time. This is true for the plains surrounding central Eistla Regio. If this is true on a global scale, McGill (2000) estimates the emplacement to have lasted less than one million years.

Whereas the age relationship of the volcanic constructs somehow can be established for both rises (western and eastern Eistla Regiones) separately, the age relationship between the two rises is more difficult to determine since direct evidence such as superposition and intersections are missing. Nevertheless, according to Grimm and Phillips (1992), the volcanic edifices in central Eistla appear older due to volcanic styles that seem more evolved than the ones in western Eistla.

4.6 Eastern Eistla Regio

The easternmost part of the Eistla Regio topographic rise, partly located due south of Bell Regio, clearly is corona-dominated. Five major coronae are located on the rise: Didilia, Pavlova, Ninmah, Isong, and Calakomana Coronae. The rise has a diameter of about 1,700 km (Smrekar and Stofan, 1999) and a mean elevation of about 1 km. The highest points reach almost 4 km above MPR (Campbell and Clark, 2006). With a value of about 65 km, the estimated apparent depth of compensation (ADC) of eastern Eistla Regio is comparatively shallow (Smrekar et al., 1997). Four of the five coronae are characterized by gravity highs between 45 mGal (Schubert et al., 1994) and 66 mGal (Stofan et al., 1997).
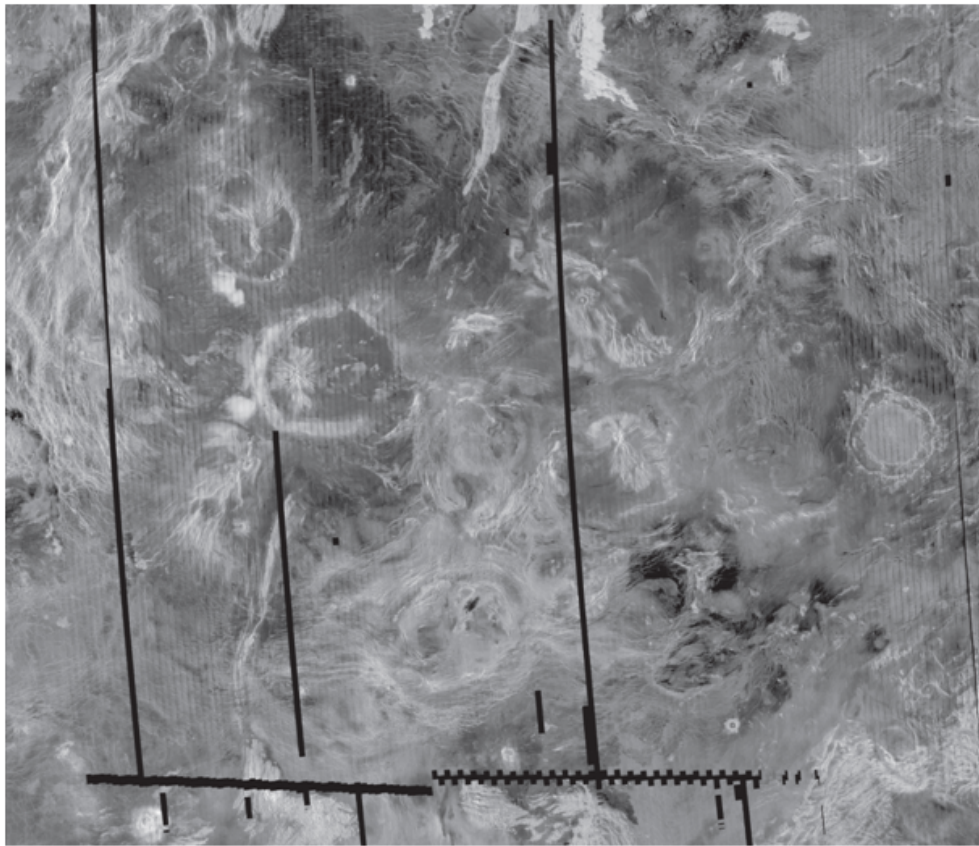

Figure 4.9: Eastern Eistla Regio with five coronae. Also Mead crater to the east is clearly visible (`http://planetarynames.wr.usgs.gov/Page/venus1to5m_Radar`, retrieved: 2014-11-15)

In the south of the rise, Calakomana Corona is located. It has a diameter of 575 km (`http://planetarynames.wr.usgs.gov/Page/VENUS/target`, retrieved:

2013-10-15) and a low topographic relief with parts of a rim in the north. The corona is surrounded by concentric fractures. As opposed to the other coronae in this area, Calakomana Corona has a lack of dominant radial fractures. The corona seems to be the oldest of its kind in this region. This statement is based on the presence of regional plains wrinkle ridges in the interior of the structure. Moreover, the wrinkle ridges surrounding the corona have been deflected by its annulus. This indicates that as the wrinkle ridges of the regional plains were formed, the annulus of the corona already existed (Fleming and Stofan, 1998). In the interior of the corona as well as to its east, volcanic flows are discernible. Some of them are cross-cut by wrinkle ridges, whereas others cover them up indicating that they were emplaced after the wrinkle ridges had formed (Fleming and Stofan, 1998; Campbell and Clark, 2006).

Due south of Bell Regio, the corona Ninmah is located. This corona has an elongated shape with a length of 700 km and a width of about 350 km. Due south of Ninmah, Isong Corona is situated with a more circular form and a diameter of about 500 km (Fleming and Stofan, 1998). Both coronae are surrounded by partial rims that are cut by radial fractures and the interiors of both are partly covered by an area of elevated, dense radial fractures (Fleming and Stofan, 1998; Campbell and Clark, 2006). In the interior of Isong Corona these fractures form a wishbone-like pattern (Campbell and Clark, 2006). Extensive lava flows are associated with both coronae. The radial fractures in the interior of Ninmah Corona are embayed by flow material. Since the rims of both coronae are not continuous, it is hard to distinguish between interior and exterior flows. In fact, they may all originate from their interiors (Fleming and Stofan, 1998). East of Isong Corona, the crater Mead with a diameter of about 270 km is located. Lava flows from Isong Corona partly embay and superpose the ejecta of the crater (Campbell and Clark, 2006).

The wrinkle ridges north of Ninmah Corona are deflected by its rim or terminate there, indicating that at the time of wrinkle ridge formation, the corona rim already existed. Therefore, it is assumed that the two eastern coronae formed after Calakomana Corona but prior to the two western ones. Some of the northern flows of Isong Corona superpose the southern flows of Ninmah Corona. Thus, at least in this region, volcanism at Ninmah Corona ceased prior to volcanism at Isong Corona (Fleming and Stofan, 1998). To the south and southeast of Isong Corona, a large part of its flows is covered by fine-grained material which was probably produced during impacts. The radar-dark material is characterized by feathery margins. It smoothes the surface and in some areas even appears fluid-like (Campbell and Clark, 2006).

Also in the western part of the eastern Eistla rise, two coronae are located. Didilia Corona is the northernmost structure with a diameter of about 320 km. To its southeast, Pavlova Corona is situated with a diameter of 500 km. Both coronae have almost continuous rims as opposed to the eastern two coronae. The rims of the western coronae are cut by radial fractures, as well. More radial fractures can be found in the interiors of the coronae near their centers. These fractures are located on small topographic rises (Fleming and Stofan, 1998). The radial fractures of Pavlova Corona are of stellate shape, the ones in Didilia Corona of wishbone shape (Campbell and Clark, 2006). Some of these fractures even cut the surrounding rims that are embayed by volcanic flows. Both coronae are surrounded by extensive volcanic flows. They generally originate from edifices located on the rims of the coronae. Didilia Corona shows a few concentric fractures on its eastern rim (Fleming and Stofan, 1998).

Fractures at Pavlova Corona are located only in elevated areas. This indicates that fractures in lower topography were covered by lava flows. Regarding Didilia Corona, however, fractures cover the entire volcanic center showing that uplift of the corona and volcanism occurred concurrently. Southwest of Pavlova Corona as well as southeast of Isong Corona fractured isolated areas that resemble the interiors of the coronae are located. Campbell and Clark (2006) interpret them to be remnants of coronae that have been flooded by lava flows for the most part. The rims of the western two coronae (as well as those of the eastern coronae) seem to be of a different material than the surrounding exterior volcanic flows (Fleming and Stofan, 1998; Campbell and Clark, 2006). Since these flows extend away from the rims, it is assumed that their emplacement postdates fracturing and uplifting of the rims. The central radial fractures, however, cross-cut the smooth volcanic flows in the interior of the coronae. Therefore, in the interiors, volcanism occurred prior to radial fracturing which may have been caused by central upwelling (Fleming and Stofan, 1998).

Volcanism at the two western coronae occurred contemporaneously. West of the coronae, flows from Didilia Corona seem to postdate flows from Pavlova Corona, whereas east of them, it appears the other way around (Fleming and Stofan, 1998). In this area, the older flows are radar-bright and rather narrow forming central channels which is indicative of high-volume eruption rates or magma with increased viscosity. The younger flows, on the other hand, are radar-dark and of a sheet-like appearance suggestive of lower eruption rates or magma with less viscosity. These diverse appearances indicate a complex history concerning the composition of magma and eruption rates (Campbell and Clark, 2006). However, a few lobes from Didilia also seem to overlay flows from Pavlova in the east.

These relationships show that the coronae experienced several episodes of volcanism (Fleming and Stofan, 1998). North and northwest of Didilia Corona off the rise, its flows superpose flow material that originates either from small shield volcanoes or from depressions that resemble calderas (Campbell and Clark, 2006). Except for Calakomana, the coronae in this area are very similar. They have comparable sizes, their topography is similar (a rather flat interior with a dome or ridge in the center surrounded by an uplifted rim) and they all have radial fractures in their interiors unlike most coronae (Fleming and Stofan, 1998; Smrekar and Stofan, 1999; Campbell and Clark, 2006). Moreover, gravity anomalies peak above the four younger coronae indicating that they are not fully compensated (Schubert et al., 1994; Stofan et al., 1997; Campbell and Clark, 2006). Calakomana, on the other hand, is of low relief with a discontinuous rim and its interior is a combination of depressions and low domes in between (Fleming and Stofan, 1998; Campbell and Clark, 2006). Moreover, this corona is not characterized by a significant gravity signature (Smrekar and Stofan, 1999). Therefore, it may be gravitationally relaxed (Fleming and Stofan, 1998). Gravity data also suggest that the eastern coronae are older than the western ones. However, there is no geologic proof in terms of overlapping or interfingering interactions of the lava flows to confirm this. The only such relation is provided by northern flows originating from Pavlova Corona. These flows partly overlay the wrinkle ridges that are deflected by the rim of Ninmah Corona or terminate at it. However, since the rim of Ninmah Corona is known to have formed early, and since the other coronae cannot be correlated to this interaction, this relationship can be neglected. It could just as well be the case that all four coronae formed at the same time, but the western two are characterized by more extensive volcanism (Fleming and Stofan, 1998).

To the east of Pavlova Corona, 800 km north of Calakomana, a caldera-like structure is located. Situated on a low topographic rise, it is shaped like a lens and shows heavy fractures and a central depression. The feature is surrounded by plains and volcanic flows originating from Pavlova, Ninmah and Isong Coronae. The plains do not have any wrinkle ridges. Thus, they formed after wrinkle ridges were emplaced. However, since they are embayed by lava flows from the coronae, they were formed prior to corona volcanism. The caldera-like structure may even have been the origin of extensive, plains-like flows that are not visible anymore. In this case, the structure would be the oldest volcanic feature in this region (Fleming and Stofan, 1998).

No major shield volcanoes can be found on the topographic rise of eastern Eistla Regio. There are numerous small ones, for example, northeast of Isong as well as

of Pavlova Corona (Fleming and Stofan, 1998; Campbell and Clark, 2006). According to Fleming and Stofan (1998), shield volcanism in general occurred after volcanism associated with the coronae.

Also, a few impact craters occur on the eastern Eistla rise. Due north of Didilia Corona, Karo is located, which is a quite small impact crater with only about 7 km in diameter. Superposed on lava flows originating from Didilia Corona, the crater is associated with a small outflow. Superposed on partly Didilia flows, partly regional plains is the impact crater Corinna, located northeast of Didilia Corona. This crater has a diameter of about 20 km and is surrounded by a radar-bright ejecta blanket. Southeast of Didilia Corona, another crater is situated on its flows: Gwynn crater has a diameter of 32 km (Campbell and Clark, 2006). Gwynn was one of the many craters that were examined by Basilevsky and Head (2006). They found that Gwynn was emplaced after the regional plains had formed. This is evidenced by crater outflow material that has been deflected by wrinkle ridges. Bradstreet crater is located in the interior of Ninmah Corona. It has a diameter of 36 km and is associated with outflow material to its north and east as well as a central uplift (Campbell and Clark, 2006). The craters in general postdate emplacement of the regional plains as well as of volcanic flows from the coronae. As for Bradstreet, situated close to the radially fractured rim of the corona, the impact crater appears to have been emplaced after the formation of the rim. Fractures are not deflected and partly covered by the rim of the crater. Moreover, the crater outflow went downslope into the interior of the corona, away from the rim as can be seen on the radar map.

The majority of the rise is covered by volcanic flows from the coronae. However, a few patches of tesserae can be found as well. Compared to the surrounding plains material, the tesserae are topographically high (Fleming and Stofan, 1998). As in other regions on Venus, due to a lack of contact between the individual tessera blocks, it is not possible to determine the relative ages of them, nor whether their formation was contemporaneous or protracted (Campbell and Campbell, 2002). However, Campbell and Clark (2006) suggest a common period of deformation of the tessera material on and close to eastern Eistla Regio. They base their statement on the fact that all tessera material, even separated by up to 1,000 km, shows the same structural patterns. There even may have been an early tessera fabric which extended across eastern Eistla Regio (including Gbadu, Mafdet and Mamitu Tesserae) northwards into Bell Regio.

The regional plains, mostly surrounding the topographic rise of eastern Eistla Regio, but also situated on the rise itself, are characterized by wrinkle ridges with an east-west orientation. Minor sets of wrinkle ridges show a more northwest-

southeast trend (Fleming and Stofan, 1998). There are also at least seven separate, radar-bright patches mostly close to the coronae. These areas have rather feathery edges and hardly any internal texture. They are believed to be coarsely grained (particle sizes of at least 4 cm) material that has been emplaced by pyroclastic flows associated with explosive volcanism. The sources, however, are not discernible. It is, nevertheless, not excluded that these areas could be dune structures associated with impact craters even though no craters are visible (Campbell et al., 1998; Campbell and Clark, 2006). Similar areas were mentioned in the central Eistla Regio in association with Irnini and Anala Montes.

Whereas central Eistla Regio and Bell Regio are very similar in that both are associated with a thickening of the lithosphere and, as a consequence, the evolution of corona-like structures to shield volcanoes, the geologic history of eastern Eistla Regio seems to differ largely. Thus, no young volcanic edifices, such as Tepev Mons and the steep-sided Otafuku Tholi in Bell Regio, are located in eastern Eistla Regio. Such discrepancies are attributed to either different ages of the topographic rises (Bell Regio may be older than eastern Eistla), or to a varying mechanism of the rising plume and related eruption. However, Campbell and Clark (2006) note similarities as well. Therefore, the initial stages of volcanic activity of Bell Regio's Nyx Mons resemble volcanism at the coronae of eastern Eistla Regio which produced sheet-like flow fields. Moreover, in both regions magma has undergone a complex evolution with time.

The geologic history of eastern Eistla Regio can be summarized as follows: as elsewhere on Venus, the oldest stratigraphic unit is tessera material embayed and superposed by regional plains. Subsequent tectonic deformation created the widespread wrinkle ridges. Ridge belts were formed that confined the lava flows originating from the coronae of eastern Eistla Regio (Campbell and Clark, 2006). This deformation could be a consequence of the uplift of the topographic rise (Bilotti and Suppe, 1999). However, volcanism and tectonism hid any evidence of an early uplift. The formation of Calakomana Corona occurred concurrently with or shortly after the tectonic deformation. Later on, the other coronae in eastern Eistla Regio formed. This formation was a combination of uplift, volcanism and tectonic deformation. The remnants of earlier coronae suggest a mixture of subsidence and burial by volcanic flows. The relative ages of the major coronae cannot be determined. However, Didilia Corona seems to have been the most recent active region. The youngest unit appears to be very radar-bright, coarse-grained deposits that are associated with pyroclastic events.

4.7 Themis Regio

This volcanic rise has dimensions of about 1,650 km x 2,300 km and a height of approximately 1.5 km. The apparent depth of compensation (ADC) of the rise is estimated to be about 100 km (Smrekar et al., 1997). Themis Regio lies at the southernmost extension of Parga Chasmata which is a roughly northwest-southeast trending rift system originating from Atla Regio. These two rises (Beta and Themis Regiones) form together with Atla Regio the BAT region that stands out due to an abundance of volcanic features. However, in contrast to Beta and Atla Regiones, Themis is not rift-dominated, but rather corona-dominated. No less than thirteen coronae are located on the topographic rise. However, this corona-dominated rise is the only one of the three (besides central and eastern Eistla Regiones) that shows distinctive deformation of extensional origin. Rifting and corona formation occurred, at least partly, contemporaneously (Stofan et al., 1995; Stofan and Brian, 2012).

The thirteen coronae located on the rise are (roughly from west to east): Parvati Corona, Rigatona Corona, Shiwanokia Corona, Erigone Corona, Shulamite Corona, Latta Corona, Ikas Coronae, Santa Corona, Tacoma Corona, Zywie Corona, Semiramus Corona, Ukemochi Corona, and Tamiyo Corona. Many coronae are associated with flow material, some even with more than one separate flow unit. These flows emanate from the inside of the coronae. The flanks of the coronae as well as their rims are the sources of more lava flows. The morphology of the flows covers a wide range, from sheet-like to digitate. Also, deformation occurred contemporaneously and thus some flows embay and others are cut by deformation associated with coronae. The annuli surrounding the coronae are made up of fractures, faults, and some ridges. They are spaced between a few and tens of kilometers apart (Stofan and Brian, 2012).

Ikas Coronae is a multiple type that has only a rim with a flat interior. It has a diameter of 127 km. Following Stofan and Brian (2012), Ikas Coronae seems to be the oldest one in this region. Originating from the corona's rim and interior and deformed by faults, its flows are superposed by various other flows originating from Tacoma, Zywie, Shulamite, Latta, Semiramus, and Shiwanokia Coronae. In the case of the latter two coronae, the superposing flow units are the younger of two.

Tacoma Corona is a concentric corona with a plateau and a diameter of 500 km. Restricted to the Themis rise, Tacoma is the second oldest corona. Its flows, originating from the interior of the corona, superpose the ones from Ikas Coronae, but they themselves are superposed by the flows emanating from four other coronae.
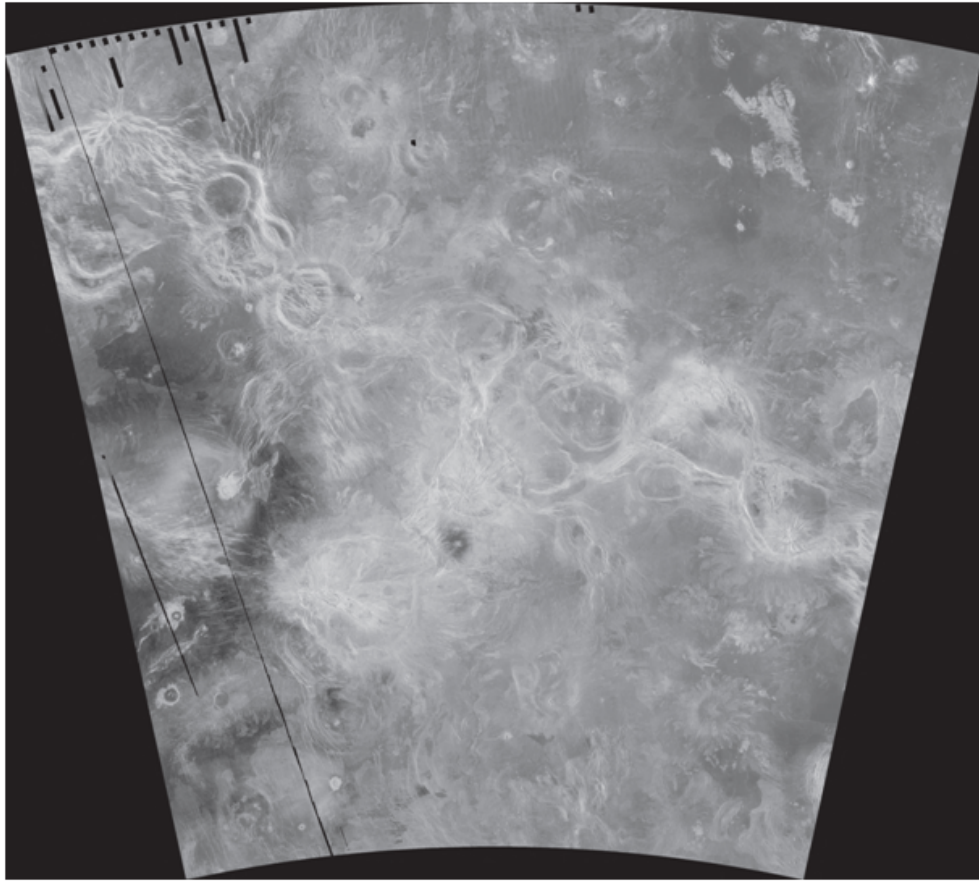
Figure 4.10: Themis Regio comprising numerous coronae (`http://planetarynames.wr.usgs.gov/Page/venus1to5m_Radar`, retrieved: 2014-11-15)

Moreover, Tacoma's flows are deformed by rift faults (Stofan and Brian, 2012). Erigone Corona, next in the time sequence, is a multiple type with a partial rim, but a flat interior. Its diameter is 325 km. Its flow unit emanates from the interior and is deformed by rift faults (Stofan and Brian, 2012).

Santa Corona, a radial/concentric corona with a plateau, has a diameter of 200 km. Two flow units extend from this corona: the older one is deformed by rift faults, and the younger one originates from the rim and the interior of the corona (Stofan and Brian, 2012).

Latta Corona, located in the center of the Themis rise, is a concentric double ring corona with a rimmed depression and a diameter of about 200 km. Its flow unit extends from both, the rim and the corona's interior, and it is deformed by rift faults (Stofan and Brian, 2012).

Rigatona Corona is a concentric corona with a double ring and a plateau in the interior which is surrounded by a rise, a trough, and a rim. The corona is located

at the northwestern edge of the highland. It has a diameter of 300 km. The impact crater Maret, 11.7 km in diameter (`http://planetarynames.wr.usgs.gov/Page/VENUS/target`, retrieved: 2013-11-12), is superposed on its flow unit. The flows emanating from the rim and the rift are deformed by rift faults. Moreover, its flows overlie flow material originating from Erigone Corona. However, they are also superposed by lava flows emanating from the volcano Mielikki Mons which is located further north of the corona and off the rise (Stofan and Brian, 2012). Ukemochi Corona is associated with five flow units, and Tamiyo Corona with four. While Ukemochi is an asymmetric corona with a plateau in its interior that is surrounded by a rise and a trough, Tamiyo is concentric with an interior plateau. Their diameters are 300 and 400 km, respectively. One flow unit of Tamiyo Corona originates from the interior and the rim of the corona. It has been deformed by the rim and rift faults. It is superposed on a flow unit of Ukemochi that extends from the interior and the rim and is deformed by the corona's rim and rift faults. However, another flow unit of Ukemochi, originating from the rim and the interior as well, but only deformed by rift faults, superposes this very Tamiyo flow unit. Both of these two flow units are superposed by flow material extending from the off-rise volcano Tefnut Mons. Another flow unit of Ukemochi Corona, emanating from the corona's rim, is superposed by flow material from yet another off-rise volcano, Chloris Mons. Two more flow units of Ukemochi Corona can be found in its interior. Regarding Tamiyo, one flow unit is in the interior of the corona as well, deformed by rift faults, and two more units originate from the corona's rim (Stofan and Brian, 2012).

The interactions between Tamiyo and Semiramus Corona are very similar. The latter is an asymmetric corona with a plateau which is surrounded by a partial rim. It has a diameter of 375 km. The older flow unit of Semiramus that is deformed by rift faults underlies one of Tamiyo's flow units. However, the younger flow unit which has been deformed by rift faults but also by rim fractures is superposed on the flow of Tamiyo. Stofan and Brian (2012) do not mention any interaction between Ukemochi and Semiramus Coronae. In the time sequence, they estimate Semiramus to be older than Ukemochi which again is older than Tamiyo Corona.

Zywie Corona, with a diameter of 200 km, is a concentric corona with a dome. It has one associated flow unit that originates from the rim and the corona's interior. Its flow unit is superposed by flow material associated with Rohina Tholus (Stofan and Brian, 2012).

Shiwanokia Corona is a concentric corona with a plateau in the center. It has a diameter between 400 km (Stofan and Brian, 2012) and 500 km (`http://`

`planetarynames.wr.usgs.gov/Page/VENUS/target`, retrieved: 2013-11-12). According to Stofan and Brian (2012), this corona is one of the younger ones. It comprises the highest point of the Themis rise (6,054.25 km). Two flow units can be discerned. Both units extend from the rim and the interior of the corona. The older unit is deformed by rift faults and, in return, partly covers them. The younger flow unit superposes flows of several other coronae, such as Shulamite and Ikas Coronae. Both flow units from Shiwanokia comprise two impact craters. Sabin (33.1 km in diameter) is superposed on the older unit, Bernadette (12.8 km in diameter) on the younger one. This younger flow unit superposes flow material related to Abeona Mons, a volcano that is located to the southwest of the rise.

Shulamite Corona is 275 km in diameter. It is a concentric corona with a plateau. It appears as a rather young corona with one associated flow unit that emanates from the rim and the interior of the corona. Rifting occurred contemporaneously with volcanism: rift faults are covered by flows but also superpose them. Superposed on flows of Shulamite Corona is a radar-dark and diffuse material whose origin is not clear. Stofan and Brian (2012) interpret this material to have been emplaced by an impactor that broke up in the atmosphere (Phillips et al., 1991a). The break up produced a shockwave which pulverized a rather circular area of the surface (Zahnle, 1992). However, flows from Shulamite also overlie flow material from, among others, Erigone and Rigatona Coronae.

Shiwanokia and Shulamite Coronae both are associated with topographic ridge crests, 10-20 km in width and several hundred kilometers in length, that are part of the rims of the coronae. Both coronae also comprise several graben in their interiors. They are believed to be of extensional origin (Stofan and Brian, 2012).

Parvati Corona is concentric with a rimmed depression. It is the westernmost corona on the highland with a diameter of 173 km. Parvati is the only corona on the Themis rise that has no associated flow units (Stofan and Brian, 2012).

Many coronae are associated with several periods of volcanism and deformation. Ukemochi Corona, for example, first underwent interior deformation, after which the annulus was formed, and then another episode of interior deformation followed. Crosscutting relations indicate this deformation sequence. Also, the style of volcanism changed over time. The initial flows were sheet-like, whereas later flows were more digitate (Stofan and Brian, 2012).

Care has to be taken by establishing relative age relationships among the coronae. If a flow unit from one corona superposes a flow unit from another corona, it is quite possible that the seemingly older corona actually formed after the seemingly younger one, but ceased activity sooner (Stofan and Brian, 2012).

Themis Regio does not comprise any large volcanoes, but only smaller ones and

steep-sided domes. Rohina Tholus has a diameter of about 30 km (`http://planetarynames.wr.usgs.gov/Page/VENUS/target`, retrieved: 2013-11-12) and is located on the southeast edge of the rise, sitting upon Ukemochi Corona. It was formed during a later stage of volcanism, and later on deformed as the annulus of the corona continued to deform. Other volcanic edifices with diameters exceeding 5 km can be found in Shiwanokia Corona, on the rim of Shulamite Corona, southeast of Parvati Corona, and close to Ikas Coronae. However, several prominent volcanoes are situated off the rise, such as Mielikki, Siduri, Tefnut, and Chloris Montes, each with a diameter of at least 100 km (Stofan and Brian, 2012).

The Parga Chasmata rift system, extending for more than 10,000 km from the southeast of Atla Regio, continues across Themis Regio, until it eventually dies out about 600 km into the plains of Lavinia Planitia, east of Themis Regio. On the rise, the rift has a width between 50 and 100 km. The discontinuous system consists of faults and fractures, extensional in origin, forming several branches. The faults and fractures are several hundred kilometers long, but very narrow. They are spaced between a few and tens of kilometers apart. The rift system is characterized by many coronae along its length. In the vicinity of a corona, fractures are either deflected around them, or they terminate. The troughs around Tacoma Corona are associated with the lowest point of the Themis rise. They reach a depth of about 1 km below MPR. Whether the troughs near large coronae are due to rifting or corona formation is not clear. Furthermore, it seems, as if coronae associated with Parga Chasmata off the rise have been less active than the coronae on the Themis rise. A fact that may be explained by the presence of a mantle plume beneath the rise. However, the origin of the Parga Chasmata rift system, as the origin of rift systems in general, is a matter of debate (Martin et al., 2007; Stofan and Brian, 2012).

There is no tessera material in Themis Regio. The oldest plains on the Themis rise are heavily fractured. It cannot be established whether this material represents regional plains unit that was deformed due to the growth of the rise, or whether it was emplaced by coronae and volcanoes and subsequently deformed. The fact that flows from coronae generally overlie the plains units surrounding the Themis rise as well as the plains units within the rise suggests that formation of these coronae and of the rise generally postdated formation of the plains. Therefore, the Themis rise may be quite young (Stofan and Brian, 2012).

There are numerous volcanic flows with lobate margins found on the rise. However, their source is not clear: they may originate from rift fractures or unknown coronae and volcanic edifices. Periods of formation of coronae, volcanoes, and plains occurred throughout the geologic history and overlapped with periods of

extensional deformation. There is evidence for various episodes of deformation given by the rift and different plains units (Stofan and Brian, 2012).

Since the Themis Regio rise clearly is corona-dominated, it has been suggested by Smrekar and Stofan (1999) that it is not the consequence of a single large-scale mantle plume that impinges upon the lithosphere, but rather the consequence of several small-scale plumes. They suggest a similar scenario for central and eastern Eistla Regiones. Furthermore, they propose that eastern Eistla Regio and its coronae are in a late stage of their evolution, whereas Themis and central Eistla Regiones appear younger.

4.8   Dione Regio

Situated in the southern hemisphere, Dione Regio is located in between the lowland Lavinia Planitia, the crustal plateau Phoebe Regio, and the volcanic rise Themis Regio. Dione Regio has dimensions of 2,700 x 1,200 km, elongated in a north-south direction, occupying the area between 20° and 45°S as well as 315° and 340°E (Keddie and Head, 1994b). The topographic rise is a very low one of its kind, with a mean elevation of less than 500 m (Stofan et al., 1995). Also, its gravity anomaly is, in contrast to the other volcanic rises, diffuse and small with a value of 20 mGal (Bindschadler et al., 1992; Keddie and Head, 1995). However, with an estimation of about 130 km the ADC is rather deep (Smrekar et al., 1997).

Dione Regio resembles other volcanic rises, such as western Eistla and Bell Regiones, in that it lacks large-scale rifting as well. It is rather volcano-dominated, as show the four large shield volcanoes: Hathor, Ushas, Innini and Nephtys Montes (Bridges, 2001). The volcanoes surmount the surrounding rise by 1 two 2.5 km (Keddie and Head, 1994b).

Ushas Mons is located in the north of Dione Regio. It occupies a triangular-shaped area with an average basal diameter of 413 km (`http://planetarynames.wr.usgs.gov/Page/VENUS/target`, retrieved: 2013-12-14) and a height of about 1.4 km above the surrounding terrain (Keddie and Head, 1995). On average they have a slope of about 3°. The Venusian volcano resembles Sif Mons in western Eistla Regio a lot. Near the radar-dark summit region which is about 200 km across, bright and dark flow episodes overlap each other suggesting that several eruptions took place. On the flanks, small cones are embayed and partly buried by distal lobate lava flows. To the northwest of the summit, lava flows infill older

fractures. The flows to the south of the volcano seem to have been confined by the local topography and are diverted to the west and east (Senske et al., 1991a; Keddie, 1993; Keddie and Head, 1994a).
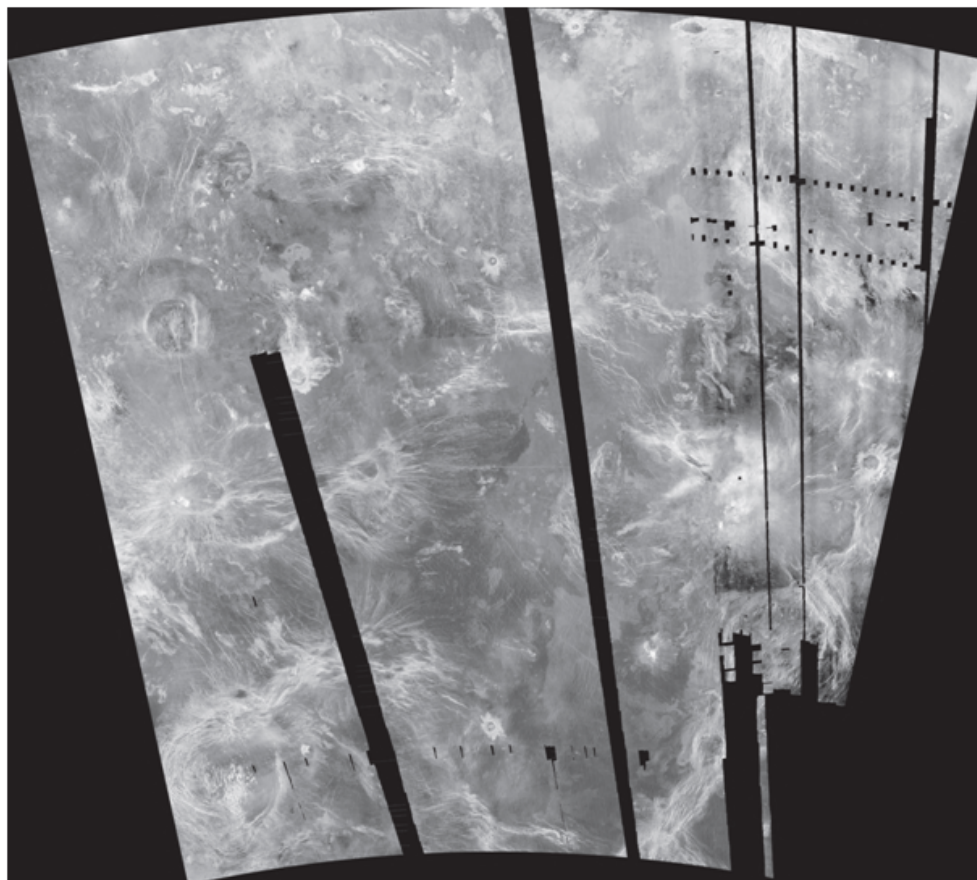
Figure 4.11: Magellan radar image of Dione Regio. Irnini Mons is located north of the impact crater in the center of the right edge of the image. Hathor Mons is situated due west of this crater. To the northwest of Hathor Mons, Nepthys Mons is located. A small part of Ushas Mons can be seen in the upper right part of the image (`http://planetarynames.wr.usgs.gov/Page/venus1to5m_Radar`, retrieved: 2014-11-15)

At least four different flow units can be discerned. The oldest unit has a radar-dark appearance and is located to the northeast of the volcano. It embays a couple of small shields. The second-oldest flow unit occurs around the entire edifice. It is of intermediate radar brightness and mostly consists of narrow (less than 1.5 km in width) and sinuous flows. Confined by pre-existing fractures, the flows of unit 2 reach lengths of up to 350 km. Flow unit 3 is surrounding the summit within a distance of 100 km. It shows a NW-SE trend. Its appearance is smooth and its

radar brightness is darker than the one from unit 2. There are only a few patches of the youngest unit, unit 4. They are located in the summit region and show a NE-SW trend. The patches are between 13 and 27 km across and very radar dark. They could also be ash deposits (Keddie and Head, 1995).

In contrast to Sif Mons, Ushas lacks a summit caldera. The summit region comprises only some small pits, less than 2 km in diameter, and domes. Two zones of radial fractures that are tens of kilometers long can be found to the north and south of the volcano, forming small rift zones. More radial fractures cut the flanks of the volcano as well as the adjacent regions. Some of the fractures are superposed by lava flows, suggesting that fracturing and volcanism occurred contemporaneously. These fractures and their relation to lava flows are associated with dike emplacement (Senske et al., 1991a; Keddie, 1993; Keddie and Head, 1994a).

About 1,050 km south-southeast of Ushas Innini Mons with a diameter of 339 km and a height of about 2.2 km above the surrounding rise is situated (`http://planetarynames.wr.usgs.gov/Page/VENUS/target`, retrieved: 2013-12-14). The lower flanks of the volcano have slopes of 3.5 - 5°, while the summit is less steep with slopes of 2 - 3° (Keddie and Head, 1995). Innini Mons appears radar-dark with a diffuse summit region about 150 km in diameter. The complex summit comprises a dome with scalloped margins (due to its appearance also called "tick"), as well as an irregular and a mesa-like dome (Aubele, 1993; Keddie, 1993). The latter is surrounded by radar-bright deposits (Keddie, 1993). The distribution of the lava flows originating from Innini Mons is not uniform. The flows covering the flanks of Innini Mons are diffuse and indistinct. However, some of them are well defined with brighter edges which may be a sign of rougher flow margins. The oldest discernible flow unit with low radar backscatter occurs to the northwest of the volcanic edifice (Keddie, 1993; Keddie and Head, 1995). Some lava flows, predominantly west and north-east of the volcano, reach lengths of 600 km and widths between 20 and 120 km (Senske et al., 1991a). A family of fractures extends southwards and then turns westwards towards Hathor Mons. These fractures, however, are shorter and less well-defined than those at Ushas Mons (Keddie, 1993).

Hathor Mons is located about 500 km southwest of Innini Mons (Keddie and Head, 1995). The flanks of the volcano are poorly defined. Therefore, the diameter of the volcanic edifice is estimated to lie in the range of 333 km (`http://planetarynames.wr.usgs.gov/Page/VENUS/target`, retrieved: 2013-12-14) and about 500 km (Keddie, 1993). The volcano reaches a height of about 2.2 km above the surrounding region (Senske et al., 1991a). The summit region is diffuse and

radar-bright. It is dominated by a large tick, 20 to 25 km in diameter, located in the southwest. To the north and east, the summit also comprises a couple of small pits with diameters between 2 and 12 km and a nested depression that resembles a caldera. The depression is surrounded by radar-bright flow deposits (Keddie, 1993; Keddie and Head, 1994a). Especially to the north and west of the volcano, distal flows are visible (Senske et al., 1991a). However, lava flows are not well defined. Older flows appear radar dark, younger flows are brighter (Keddie and Head, 1995).

South from the summit depression, a set of graben fans out. Material originating from the tick partly superposes these graben. A well-developed rift system cuts Hathor Mons in a northwest-southeast trend. To the southeast of the summit, the fractures are not as strongly developed, and in the summit region itself, the rifts are obscured by volcanic deposits. The northwestern part of the rift zone is 100 km wide and about 300 km long (Keddie, 1993; Keddie and Head, 1994a). Another zone of fracturing is located to the northeast of the summit. Near the base of the volcano a rift zone begins and strikes southward (Senske et al., 1991a).

900 km west-northwest of Innini, Nepthys Mons, the smallest of the four major volcanoes, can be found, between 250 km and 350 km in diameter (`http://planetarynames.wr.usgs.gov/Page/VENUS/target`, retrieved: 2013-12-14). It reaches a height of about 1.1 km above the surroundings. The flanks have slopes of about 3.1°. They are covered by lava flows with widths between 3 and 6 km and lengths up to 270 km. In contrast to the sinuous flows at Ushas Mons, the ones originating from Nepthys Mons are straight. The younger Nepthys flows are characterized by bright margins, whereas the older flows appear radar dark. Their distribution is controlled by the fractures of a ridge with an east-west trend. However, the lava flows are also cut by those fractures suggesting a contemporaneous formation (Keddie and Head, 1995). On the southeast flank of the volcano, fractures fan out radially and meet the rift zone to the northwest of Hathor Mons (Keddie and Head, 1994b).

The summit region of Nepthys Mons comprises a field of small shields which is a rather unique feature among the Venusian volcanoes. The field has a minimum diameter of about 30 km and is surrounded by a radar bright region about 40 km across. The shields are often surrounded by small aprons with high radar backscatter (Keddie and Head, 1995).

For the volcanic edifices at western Eistla Regio, age relationships could be established due to superposition. So far, this is not possible for the volcanoes of Dione Regio owing to the lack of overlapping flows. However, different histories of the volcanoes have been suggested. On the one hand, the radar-bright well-defined

lava flows of Ushas Mons may hint towards rather effusive eruptions, whereas the deposits in the summit regions of Innini and particularly Hathor Mons may be signs of explosive eruptions (Keddie, 1993). On the other hand, fracturing affected the volcanoes in varying degree (Keddie and Head, 1994a).

Besides the four large shield volcanoes, there are also four minor volcanoes in this area. Two of them are located near Hathor Mons, southwest and northwest of the volcano. The lower flanks of the latter are heavily cut by rifting associated with the well-developed northwest-southeast trending rift zone associated with Hathor Mons. This volcanic edifice covers an area with dimensions of 130 x 200 km and has an elevation of 1.7 km measured from its base. The minor volcano to the southwest of Hathor Mons, Rakapila Mons, has a diameter of 270 km and a height of 1.4 km above the surrounding region. Its summit with a diameter of 12 km is rather flat. This volcano clearly started its activity before Hathor Mons. This is evidenced by wrinkle ridges that cut the radar-dark flows originating from the volcano and that are so characteristic of the surrounding plains. Moreover, to the north of the Rakapila Mons the flows are superposed by flows as well as fractures associated with Hathor Mons (Keddie and Head, 1994a,b, 1995).

Another minor volcano with a diameter of 65 km is located west of Innini Mons. It covers early radar-dark flows from Innini, but deflects later radar-bright ones. The volcanic edifice has a clear summit area which comprises a pit 17 km across. It reaches a height of 1.5 km above the surrounding flows and about 2.2 above MPR (Keddie and Head, 1994a,b, 1995).

The fourth minor volcano is situated about 625 km southwest of Ushas Mons. It has a diameter of 75 km and a height of about 800 m. An asymmetrical radar-dark apron of lava flows covers its flanks. The summit comprises several small pits. Some of its distal flows are cut by wrinkle ridges suggesting that this volcano was characterized by early activity (Keddie and Head, 1995).

Dione Regio is also abundant in impact craters. On the rise itself as well as on the adjacent plains 11 impact craters (e.g. Danilova) are located (Keddie and Head, 1994b). One crater, for example, is located south of Innini Mons. Dix has a diameter of 63.3 km (`http://planetarynames.wr.usgs.gov/Page/VENUS/target`, retrieved: 2013-12-15). Radar-bright flows 250 km long run down the crater's slope to the northeast (Senske et al., 1991a; Keddie, 1993). In the plains, the flows are confined by narrow ridges. Another crater, Oma, is located on the rift system extending from Hathor Mons to the southeast. Due to their locations as well as the fact that the craters do not appear to be embayed by lava flows, they likely formed after uplift of the rise and associated activity. However, north of Ushas Mons, the crater Hansberry is cut by radial fractures related to the large volcano

(Keddie, 1993; Keddie and Head, 1994a).

Dione Regio is associated with a few small and isolated patches of tesserae. Most of them are located in the northern part of the rise, predominantly on its flanks. Another unit with mostly only one period of deformation has been identified. The most abundant plains unit in Dione Regio, however, is, as with the other volcanic rises, the regional plains unit. Wrinkle ridged plains particularly occur in the south. Shielded plains are chiefly located south of Ushas Mons, on its flanks, to the northwest of Nepthys Mons, and in the summit region of the volcano. Some shields are embayed by the lava flows originating from Ushas Mons. Many of the small shields possess a central pit. Interesting to note is that in general the shielded plains superpose and therefore postdate the ridged plains. This is a unique feature of Dione Regio which distinguishes it from the other volcanic rises. There are also some smooth, dark, and fractured plains that appear younger as well as a few coronae. Their diameters lie in the range of 50 and 100 km. Although they have clear tectonic annuli, they appear rather degraded. Furthermore, they are associated with small-scale volcanism (Keddie and Head, 1994a,b, 1995).

Regarding the geologic history of this region the following can be said: Tectonic deformation that produced the tesserae, was followed by emplacement of the regional plains. Already during their formation, the coronae started to develop. At the time of the formation of the wrinkle ridges, the uplift of the topographic rise had already started. This is indicated by wrinkle ridges of the surrounding plains that are circumferential to the volcanic rise, for example southeast of Innini Mons and to the east and southeast of Hathor Mons. Moreover, early volcanism associated with the four minor volcanoes had occurred as well. Some of their lava flows are cut by wrinkle ridges or fractures. The major volcanoes seem to be the youngest units (Keddie and Head, 1994a,b, 1995).

Although Dione Regio is listed as a volcano-dominated hotspot (Stofan et al., 1995), it is not associated with a simple mantle plume. Due to the poorly defined topographic uplift, a secondary plume or several small plumes that rise almost concurrently are favored. Another explanation is that the plume below Dione Regio is in a late stage of its development with only little thermal anomaly left (Keddie and Head, 1995; Smrekar et al., 1997).

4.9   Imdr Regio

The last-mentioned volcanic rise on Venus is Imdr Regio. With a diameter of
about 1,300 km and an elevation of approximately 1.6 km (Smrekar et al., 1997),
the volcanic rise is located roughly 3,000 km south of Atla Regio. It is the least
well investigated of the volcanic rises. The estimated apparent depth of compen-
sation for the topographic rise is comparatively large with a value of about 260 km
(Stofan et al., 1995; Smrekar et al., 1997).
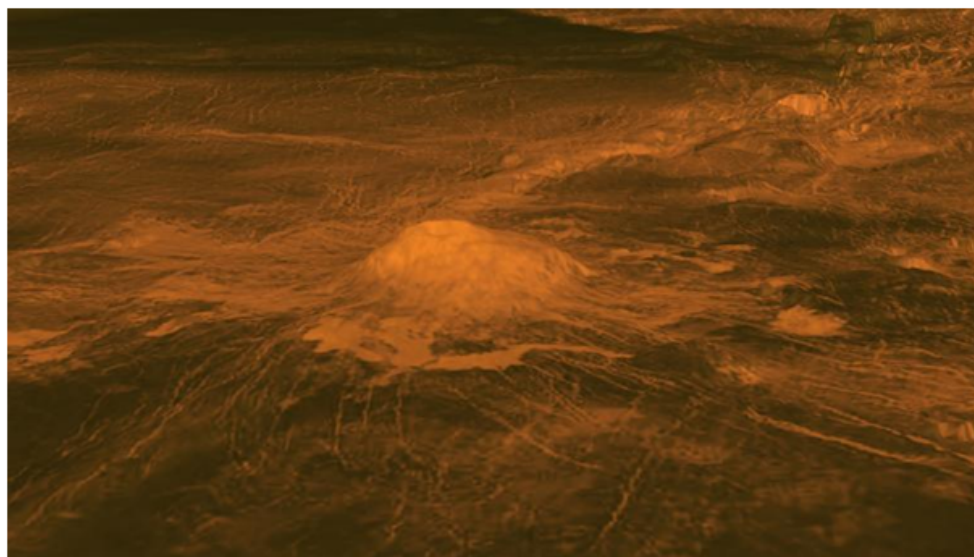
Figure 4.12: Idunn Mons in Imdr Regio. The vertical scale in this image is exaggerated
30 times (`http://photojournal.jpl.nasa.gov/catalog/PIA13001`, retrieved: 2014-11-
15)

Imdr Regio is characterized by a single large volcano, Idunn Mons, located on
the southeastern end of the rise. The volcano has a diameter of approximately
200 km and a height of about 2.5 km above MPR (`http://photojournal.jpl.`
`nasa.gov/catalog/PIA13001`, retrieved: 2014-01-27). The summit region ap-
pears diffuse and radar bright. The flanks of the volcano as well as the adjacent
area are covered by radar -bright and dark lava flows. The bright margins of the
longer flows are of a lobate appearance. Some of these flows superpose radial
fractures, others are cut by them. To the northwest of the volcano, the fractures
merge into the rift zone Olapa Chasma which, with its northwest-southeast trend,
follows the orientation of the local topography. The northwestern end of the rift
system terminates at a shield field. Another field of small shields is located to

the northeast of Olapa Chasma clearly visible on the radar map. The majority of the swell possesses sinuous ridges that resemble wrinkle ridges of the regional plains. Therefore, they are interpreted to be such (McGill, 1993; Stofan et al., 1995). The presence of such wrinkle ridges suggests that uplift of the topographic rise started after the formation of the ridges (Stofan et al., 1995).

Imdr Regio is associated with rather little volcanism that is largely limited to Idunn Mons (Stofan et al., 1995). Near the volcano, two small impact craters are located, Yelya to the southwest and Sandel to the west. The latter has a diameter of about 18 km and is surrounded by radar-bright deposits.

Smrekar et al. (1997) compared the four volcano-dominated rises based on gravity data. They suggest that whereas western Eistla and Imdr Regiones are underlain by still active mantle plumes, the activity of the plumes beneath Bell and Dione Regiones is ceasing (Smrekar, 1994; Smrekar and Parmentier, 1996).
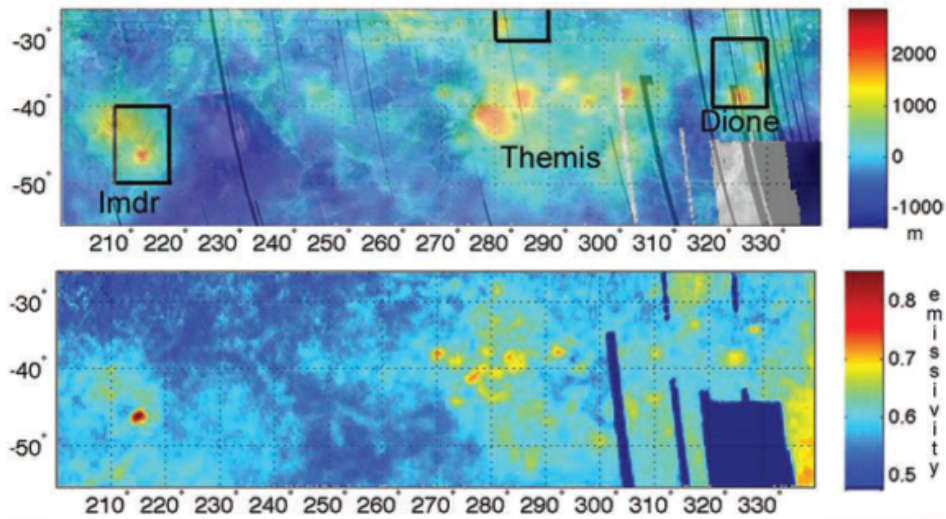
Figure 4.13: Thermal emissivity of Venus: The map on top is a Magellan synthetic aperture radar image, the one on the bottom shows the thermal emissivity as observed by VIRTIS, from Smrekar et al. (2010)

In recent years, some attention has been paid to Imdr Regio. The Visible and Infrared Thermal Imaging Spectrometer (VIRTIS) on the Venus Express spacecraft provided scientists with a map of thermal emission. This map includes most of the southern hemisphere of Venus. The southernmost three hotspots (Themis, Dione, and Imdr Regiones) stand out in this map (*fig. 4.13*). They are sites of anomalously high thermal emissivity, which could be a sign of unweathered and, hence, rather young lava flows. Idunn Mons in Imdr Regio dwarfs the other two hotspots

with an emissivity anomaly that is almost a factor of 2 greater. In Dione Regio, two of the four volcanoes show an anomalously high thermal emissivity: Innini and Hathor Montes. In Themis Regio, a total of seven volcanic centers (considering the 13 coronae and several large volcanoes nearby) have higher heat flows, including Shiwanokia and Shulamite Coronae as well as Mielikki Mons (Stofan et al., 2009; Smrekar et al., 2010).

Chapter 5

Methodology

The calculations were based on two basic features of hotspots, namely the heat flow as well as the topographic uplift. The first step in order to calculate the heat flow of a mantle plume was to estimate its buoyancy flux. This can be done by using the following formula:

$$B_{pt} = (\rho_m - \rho_s)vA_s \ . \tag{5.1}$$

This equation is based on the assumption that the topographic swell is the excess mass that arises as the mantle plume impinges on the lithosphere. This excess mass is thought to be compensated by the lighter rock material making up the plume (Turcotte and Schubert, 2002). Therefore, ρ_m denotes the density of the mantle, ρ_s the density of the surface, and A_s the cross-sectional area of the hotspot swell. The v in this formula stands for the velocity with which the plate moves over the hotspot. Since there is no evidence of plate tectonics on Venus, this formula is just seen as a first approximation.

The mantle density of Venus is assumed to resemble the terrestrial one. Furthermore, the density of the Venusian crust was taken as the surface density. For the velocity of the plate, the smallest value as found on Earth was used. Morgan and Morgan (2007) mention a velocity of 3 mm yr^{-1} of the plate at the Kerguelen hotspot. For comparison, the Hawaiian hotspot is located on the fast-moving Pacific Plate with a velocity of about 90 mm yr^{-1}. The parameters and their values can be looked up in *table 5.1*.

To obtain the cross-sectional area of the Venusian volcanic rises, topographic maps were used. One difficulty in this task was to determine the edges of the volcanic rises. Atla Regio, for example, is part of the Aphrodite highland zone. Hence, the volcanic rise gradually merges with the highland region. After the edges had been

Table 5.1: The parameters used

	Parameter	Unit	Value
Mantle density	ρ_m	[g m^{-3}]	3.33 x 10^6
Surface density	ρ_s	[g m^{-3}]	2.8 x 10^6
Density of volcanic material	ρ_v	[g m^{-3}]	2.8 x 10^6
Plate velocity	v	[mm yr^{-1}]	3
Plume material velocity	u	[mm yr^{-1}]	50
Thermal expansion coefficient	α	$[K^{-1}]$	3 x 10^{-5}
Specific heat	c_p	[J $g^{-1}K^{-1}$]	1.25
Temperature difference between plume and surrounding mantle	ΔT_{pm}	[K]	250
Temperature difference between erupting magma and ambient surface	ΔT_{es}	[K]	1,300
Heat of fusion of the magma	ΔH_f	[J g^{-1}]	400

determined, several straight parallel lines were laid through each rise. Care was taken that these lines did not cross any major volcanoes since those are a consequence of volcanic construction. However, for equation 5.1 only the topography which is a result of pure uplift is of interest.

I wrote a small Fortran 90 program (look at appendix A) that calculates orthodromes in order to obtain the length of each elevation along the lines. When the coordinates of two points (A and B) on a sphere are known, the angle Θ of the vertex at the center of the sphere is given by

$$\Theta = \arccos[\sin\phi_A \sin\phi_B + \cos\phi_A \cos\phi_B * \cos(\lambda_B - \lambda_A)] \ . \qquad (5.2)$$

The degrees of latitude are denoted by ϕ, the degrees of longitude by λ. They are used in radians. The distance between the points is then obtained by multiplying Θ with the radius of the sphere.

Cubic spline interpolation was applied in order to smoothen the topographic profiles and to calculate the cross-sectional area A_s indicated by each line (*figure 5.3*). Since the whole mantle plume was considered, several lines were drawn, taking the minimum and maximum elevations (disregarding volcanoes) into account.

There are n points and k $=$ n $-$ 1 intervals. Each point consists of an x- and a y-coordinate. The x-coordinate gives the distance to the previous point and the y-coordinate is the altitude of the point. A cubic spline is applied to each interval between two contiguous points:

$$f_k(x) = A_k(x - x_k)^3 + B_k(x - x_k)^2 + C_k(x - x_k) + D_k \ . \qquad (5.3)$$

If equation 5.3 is differentiated twice, the coefficients A_k, B_k, C_k, and D_k can be written as:

$$A_k = \frac{1}{6\Delta x_k}(y''_{k+1} - y''_k) \tag{5.4}$$

$$B_k = \frac{1}{2}y''_k \tag{5.5}$$

$$C_k = \frac{\Delta y_k}{\Delta x_k} - \frac{1}{6}\Delta x_k(y''_{k+1} + 2y''_k) \tag{5.6}$$

$$D_k = y_k \tag{5.7}$$

where $k = (1, ..., n-1)$, $\Delta x_k = x_{k+1} - x_k$ and $\Delta y_k = y_{k+1} - y_k$ (Spaeth, 1986).

To avoid bends at the transition from one interval to another, the following condition is set:

$$f'_{k-1}(x_k) = f'_k(x_k) \ . \tag{5.8}$$

Following this condition, the system of equations

$$M * y'' = d \tag{5.9}$$

can be formed using the unknown variables y''_n (Spaeth, 1986). The n-2 x n-2 matrix M is constructed by using the variables Δx_k:

$$M = \begin{pmatrix} 2(\Delta x_1 + \Delta x_2) & \Delta x_2 & & \\ \Delta x_2 & 2(\Delta x_2 + \Delta x_3) & \Delta x_3 & \\ & \ddots & \ddots & \\ & & \Delta x_{n-2} & 2(\Delta x_{n-2} + \Delta x_{n-1}) \end{pmatrix} \tag{5.10}$$

The array d on the right side of equation 5.9 is formed by using both, Δx_k and Δy_k. Therefore,

$$d = \begin{pmatrix} 6(\frac{\Delta y_2}{\Delta x_2} - \frac{\Delta y_1}{\Delta x_1}) - \Delta x_1 y''_1 \\ 6(\frac{\Delta y_3}{\Delta x_3} - \frac{\Delta y_2}{\Delta x_2}) \\ \vdots \\ 6(\frac{\Delta y_{n-1}}{\Delta x_{n-1}} - \frac{\Delta y_{n-2}}{\Delta x_{n-2}}) - \Delta x_{n-1} y''_n \end{pmatrix} \tag{5.11}$$

The program that I wrote for the cubic spline interpolation is straightforward (appendix B). First, the points of one topographic profile are read into the program and two arrays are constructed. The program then calculates the differences

between all contiguous points, forming two further arrays. In the next step, the differences are used to construct the matrix M and the array d of equation 5.9 with the boundary conditions $y_1'' = 0$ and $y_n'' = 0$.

In order to obtain the values of the variables y_n'', the program splits the matrix M up by using LU decomposition. Due to the fact that M = L*U, the lower triangular matrix L has the following appearance:

$$
L = \begin{pmatrix}
M_{11} & & & \\
M_{21} & M_{22} - L_{21}U_{12} & & \\
& \ddots & \ddots & \\
& & M_{n-2,n-3} & M_{n-2,n-2} - L_{n-2,n-3}U_{n-3,n-2}
\end{pmatrix}
\tag{5.12}
$$

The upper triangular matrix U looks as follows:

$$
U = \begin{pmatrix}
1 & \frac{M_{12}}{L_{11}} & & & \\
& 1 & \frac{M_{23}}{L_{22}} & & \\
& & \ddots & \ddots & \\
& & & 1 & \frac{M_{n-3,n-2}}{L_{n-3,n-3}} \\
& & & & 1
\end{pmatrix}
\tag{5.13}
$$

In the next step, the program solves a system of equations that consists of the lower matrix L and the array d from equation 5.9. The new array z is introduced here:

$$
L * z = d
\tag{5.14}
$$

Since it applies to the array z that

$$
z = U * y'' \;,
\tag{5.15}
$$

the variables y_n'' can be obtained now. Afterwards, the coefficients are determined with equations 5.4 - 5.7 and the cubic spline for each interval is formed. *Figure 5.1* shows the result of the application of cubic spline interpolation to the topography of Atla Regio. The chosen profile is indicated with a red line in *figure 5.3*.

In the last step, all cubic splines of one profile are integrated and summed up, giving the cross-sectional area of the rise:

$$
A_s = \sum_{k=1}^{n-1} \int_{x_k}^{x_{k+1}} [A_k \Delta x_k^3 + B_k \Delta x_k^2 + C_k \Delta x_k + D_k]\mathrm{d}x \;.
\tag{5.16}
$$

The values obtained are listed in *table 5.2.*
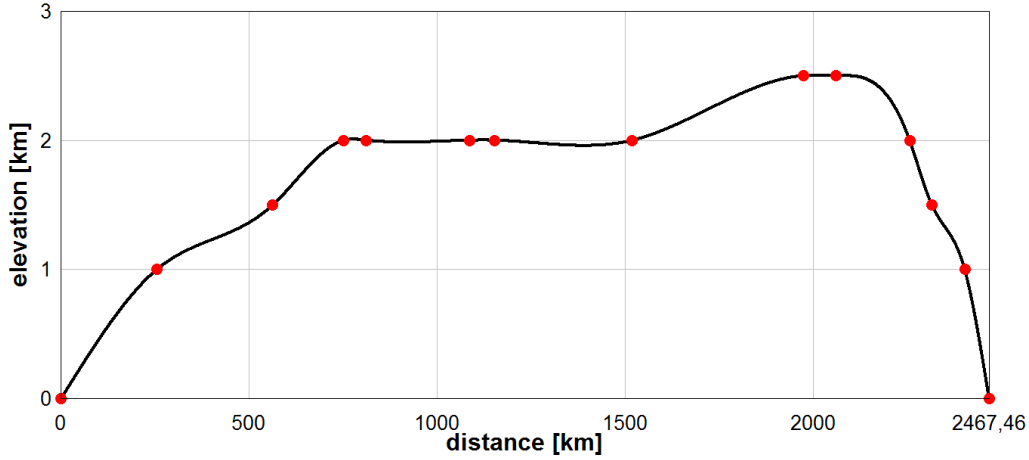
Figure 5.1: The topographic profile of Atla Regio as obtained by applying cubic spline interpolation. The red dots are the points that have been read into the program.

For comparison, the buoyancy flux of each mantle plume was also calculated in another way in which several assumptions about the plume itself had to be made. The formula looks as follows:

$$B_{mp} = \Delta\rho * \pi r^2 u \; . \tag{5.17}$$

Here, the mantle plume is envisioned as a vertical cylinder with radius r. The material of the plume ascends through this cylinder with velocity u, driven by the density difference $\Delta\rho$ between the mantle plume and the surrounding mantle. In order to be able to distinguish between the two differently calculated buoyancy fluxes, they are denoted with pt for "plate tectonics" on the one hand and mp for "mantle plume" on the other hand.

According to Duncan and Richards (1991) the velocities inside mantle plumes have values between 10 and 100 mm yr^{-1}. Therefore, a velocity of 50 mm yr^{-1} was applied. The radius of the hotspot conduit was chosen individually for each hotspot. Farnetani and Hofmann (2011) mention radii of plume tails in the range of 50 and 150 km. Applying a 1:10 ratio to the diameters of the volcanic rises and the plume tails yields radii that fall neatly into this range. Hence, Central Eistla Regio has the smallest plume tail radius with a value of 69 km, whereas for Beta Regio a conduit radius of 152 km was found. All the values are listed in *table 5.2.*

The density difference $\Delta\rho$ in equation 5.17 is calculated by

$$\Delta\rho = \rho_m \alpha \Delta T_{pm} \; .\tag{5.18}$$

Here, $\Delta\mathrm{T}_{pm}$ denotes the temperature difference between the mantle plume and the surrounding mantle. This excess temperature usually is assumed to lie in the range between 200 and 300 K. For my calculations I adopted a value of 250 K.

Table 5.2: Parameters of the volcanic rises on Venus

	Cross-sectional area [km^2]	Surface area [x 10^5 km^2]	Diameter [km]	Plume radius [km]
Beta	4,427	46	3,048	152
Atla	3,067	37.5	2,915	146
Bell	568	8.9	1,412	71
Western Eistla	880	24.1	2,202	110
Central Eistla	830	7.9	1,377	69
Eastern Eistla	835	23.6	1,831	92
Themis	975	16	2,092	105
Dione	829	19.5	2,600	130
Imdr	815	11.3	1,504	75

With the following formula the obtained buoyancy fluxes can be converted into the heat flux of the mantle plume at the base of the lithosphere:

$$Q = \frac{c_p B}{\alpha} \; .\tag{5.19}$$

In this equation, c_p is the specific heat (taken to be 1.25 J g^{-1} K^{-1}) and α is the coefficient of thermal expansion with a value of 3 x 10^{-5} K^{-1}.
Taking the equation from Solomon and Head (1982) that describes the rate of heat loss which is attributable solely to hotspot volcanism and rearranging it yields the volumetric flux of magma with time:

$$\frac{dV}{dt} = \frac{Q}{\rho_v(c_p\,\Delta T_{es} + \Delta H_f)} \; ,\tag{5.20}$$

where ρ_v is the density of the volcanic material, $\Delta\mathrm{T}_{es}$ describes the difference in temperature between the erupting magma and the ambient surface, and $\Delta\mathrm{H}_f$ denotes the heat of fusion of the magma. The values that were applied in Solomon and Head (1982) are adopted here: ρ_v has a value of 2.8 x 10^6 g m^{-3}, $\Delta\mathrm{T}_{es}$ is taken to be 1,300 K, and $\Delta\mathrm{H}_f$ resumes a value of 400 K. The parameters and their values are summarized in *table 5.2*.

The properties of the major volcanoes that are located on the nine volcanic rises are listed in *table 6.1*. In order to obtain the growth duration of the volcanoes, their volumes had to be estimated. The basal diameters of the edifices are known. The heights of the volcanoes were estimated by using the information that is given in literature. However, depending on the size of the summit region, the volume can cover a large range. The descriptions of the summit regions of most volcanoes regarding their sizes are rather vague. Therefore, whenever necessary, I roughly measured the dimensions using radar maps.

For the calculation of the volumes, I used the following formula:

$$f(r) = \frac{H}{(R-a)^2} (r-R)^2 \ . \tag{5.21}$$

H describes the height of the volcano, R the radius at the base of the edifice, and a is the radius of the summit region. In the case of a well-developed summit caldera, the above formula was combined with the following one:

$$f(r) = \frac{H-h}{a^2} r^2 + h \ . \tag{5.22}$$

Here, h denotes the height of the volcano minus the depth of the caldera.

Figure 5.2 shows that the combination of the two functions creates the outline of a volcano.
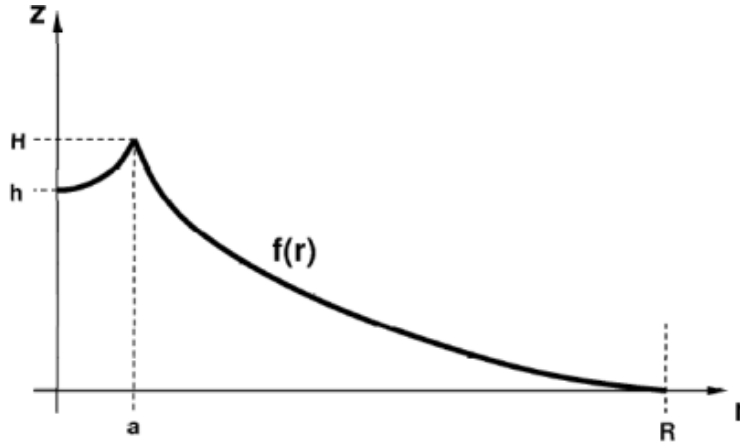
Figure 5.2: The cross section of a volcano that is obtained by combining the equations 5.21 and 5.22.

I calculated the volume of a volcano without a summit caldera by rotating the function of equation 5.21 around the y-axis and subtracting from that the volume

of the cone at the top with a basal radius of H. The volume is thus given by

$$V = \pi[\frac{1}{2}(R-a)^2H - \frac{4}{3}RH(R-a) + R^2H] \; . \tag{5.23}$$

In case of a summit caldera, the volume which is obtained by rotating equation 5.22 around the y-axis is additionally subtracted from the volume of equation 5.23. Therefore, the final calculation can be written as:

$$V = \pi[\frac{1}{2}(R-a)^2H - \frac{4}{3}RH(R-a) + R^2H - \frac{1}{2}a^2H + \frac{3}{2}a^2h] \; . \tag{5.24}$$
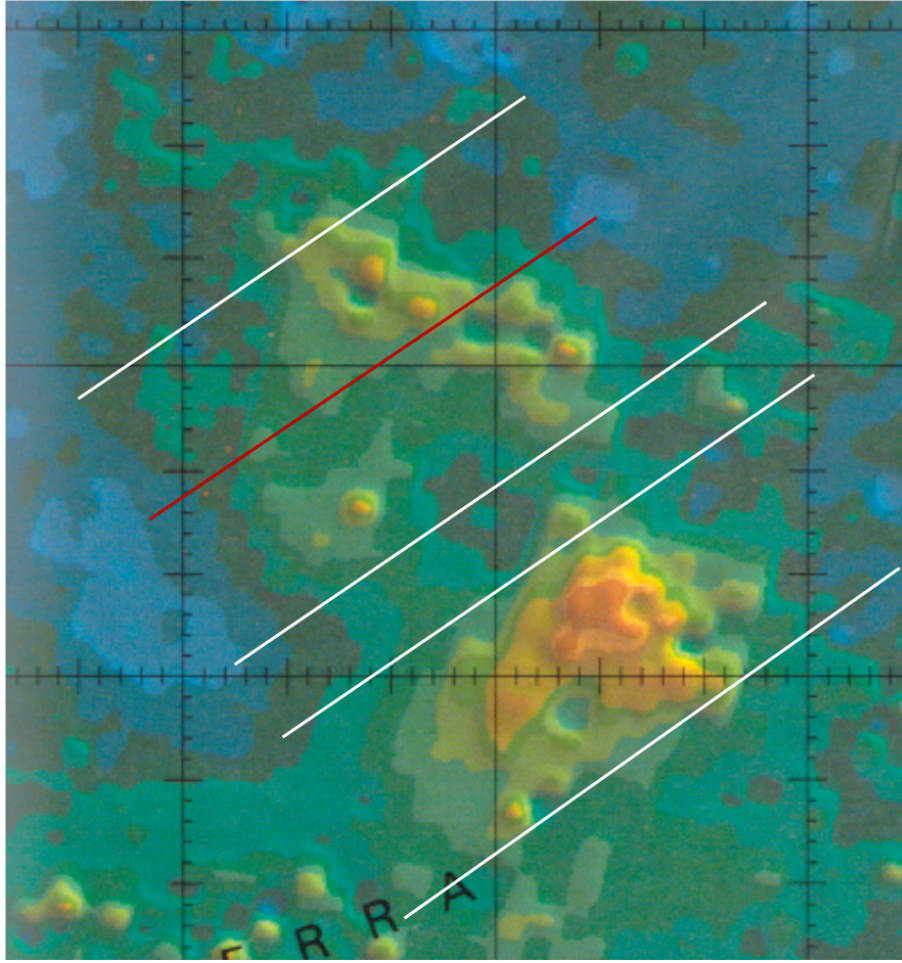
Figure 5.3: This is a detail of a topographic map of Venus showing Atla Regio. Blue represents low areas, yellow and brown high regions. Cubic spline interpolation was applied along the white lines. The resulting topography marked by the red line is shown in *figure 5.1*. (`http://www.lpi.usra.edu/resources/venus_maps/1324/index.html`, retrieved: 2013-11-20)

Chapter 6

Results

As mentioned in the methodology section, calculating the volumes of the volcanoes was a rather challenging task considering the lack of reliable data. However, with all the information gathered from various papers as well as with the help of the radar maps, the volumes could be estimated. Comparing the results to volumes that are given in literature shows the uncertainty.

Table 6.1: Volcano parameters

	Basal diameter [km]	Height [km]	Volume [x 10^3 km^3]	Basal area [km^2]
Theia	226	2.9	35	40,115
Ozza	500	3.85	287	196,350
Maat	395	5.9	206	122,542
Sapas	217	2.4	38	36,984
Tepev	300	4	89	70,686
Nyx	875	1	127	601,320
Gula	400 x 250	3.2	125	78,540
Sif	300	1.7	27	70,686
Anala	550	1.25	62	237,583
Irnini	400	0.75	42	125,664
Ushas	413	1.4	146	133,965
Hathor	400	2.2	213	125,664
Innini	339	2.2	69	90,259
Nepthys	350	1.1	84	96,211
Idunn	200	0.9	8	31,416

Theia Mons in Beta Regio, for example, is considered as a large volcano that sits atop the Devana Chasma rift system. Its flanks are heavily cut by fractures and it has a deep caldera whose floor even lies below the base of the volcano.

My calculations yield a volume of about 35,000 km^3 for this volcano. Compared to the other major volcanoes, this makes Theia Mons one of the smaller ones. However, Stofan et al. (1995) obtain a volume of 160,000 km^3, more than four times than my calculation yields.

Table 6.2: Results that are based on buoyancy fluxes which are dependent on the plate velocity. B$_{pt}$ = buoyancy flux, Q = heat flux, q = heat flux per unit area, dV/dt = volumetric flux of magma

	B$_{pt}$ [kg s^{-1}]	Q [x 10^{10} W]	q [mW m^{-2}]	dV/dt [x 10^{-3} km^3 yr^{-1}]
Beta	223	0.93	2	51.7
Atla	155	0.64	1.72	35.8
Bell	29	0.12	1.34	6.6
W. Eistla	44	0.19	0.77	10.3
C. Eistla	42	0.17	2.2	9.7
E. Eistla	42	0.18	0.74	9.76
Themis	49	0.21	1.27	11.4
Dione	42	0.17	0.89	9.68
Imdr	41	0.17	1.52	9.5

Table 6.3: Results from calculations based on assumptions about the mantle plumes. B$_{mp}$ = buoyancy flux, Q = heat flux, q = heat flux per unit area, dV/dt = volumetric flux of magma

	B$_{mp}$ [kg s^{-1}]	Q [x 10^{10} W]	q [mW m^{-2}]	dV/dt [km^3 yr^{-1}]
Beta	2,889	12	26	0.67
Atla	2,643	11	29	0.61
Bell	620	2.6	29	0.14
Western Eistla	1,508	6.3	26	0.35
Central Eistla	589	2.5	31	0.14
Eastern Eistla	1,042	4.3	18	0.24
Themis	1,361	5.7	35	0.32
Dione	2,101	8.8	45	0.49
Imdr	703	2.9	26	0.16

For Idunn Mons in Imdr Regio I get a volume of about 8,000 km^3. It appears, hence, as the smallest volcano in this selection. Stofan et al. (1995) give a volume of 48,000 km^3, even six times more than my estimation. This would make Idunn

Mons larger than several other volcanoes such as Sif and Gula Montes. For these two volcanic edifices they list volumes of 16,400 km^3 and 22,700 km^3, respectively. My calculations, however, yield values of 27,000 km^3 for Sif and 125,000 km^3 for Gula.

The properties of the volcanoes, their basal diameters and areas as well as their heights and volumes are summarized in *table 6.1*.

Table 6.2 shows the results that have been obtained with the calculations based on the buoyancy flux that considers the plate velocity. Beta and Atla Regiones clearly stand out here with buoyancy fluxes of 223 kg s^{-1} and 155 kg s^{-1}, respectively. Bell Regio represents the lower limit with only 29 kg s^{-1}. The other volcanic rises all have values between 40 and 50 kg s^{-1}. However, compared to Hawaii which has an estimated buoyancy flux of about 8,000 kg s^{-1}, or Iceland with a buoyancy flux of about 1,400 kg s^{-1} (Farnetani and Hofmann, 2011) the Venusian buoyancy fluxes are particularly low.

Table 6.4: Duration of growth of the volcanoes: The second column lists the durations that result from buoyancy fluxes based on plate velocity. The third column comprises the results based on the properties of the mantle plumes.

	t_{pt} [x 10^6 yr]	t_{mp} [x 10^4 yr]
Theia	0.68	5.3
Ozza	8	64.1
Maat	5.7	51.9
Sapas	0.11	9.2
Tepev	13.5	62.2
Nyx	19.15	88.5
Gula	12	35.7
Sif	2.67	7.8
Anala	6.36	45.1
Irnini	4.37	31
Ushas	15.1	30
Hathor	22	43.7
Innini	7.1	14.2
Nepthys	8.69	17.3
Idunn	0.85	5

Column 4 of *table 6.2* lists the heat flow per unit area. It was obtained by dividing the heat flux by the total area of the volcanic rise as given in *table 5.2*.

Low buoyancy fluxes lead to low heat fluxes, which result in low volumetric fluxes

of magma with time. This means that the growth duration of the volcanoes is prolonged. Column 2 of *table 6.4* shows that it took the majority of the volcanoes several million years to reach their current size. According to these calculations, Hathor Mons in Dione Regio needed about 22 million years for its volume of 213,000 km^3.

Table 6.3 resembles *table 6.2*. However, the results are based on assumptions about the mantle plume. The buoyancy and heat fluxes are clearly higher than in *table 6.2* and resemble terrestrial values. The durations of growth of the volcanoes are listed in column 3 of *table 6.4*. The higher buoyancy and heat fluxes result in larger volumetric fluxes of magma. Therefore, the durations of growth of the volcanoes are greatly shortened. They all formed in less than a million years.

Chapter 7

Discussion and Conclusion

The buoyancy fluxes for the Venusian features calculated by assuming plate tectonics (*table 6.2*) are one to two orders of magnitude smaller than the terrestrial ones. Most of them lie in the range of 40 and 50 kg s^{-1}. Only Beta and Atla Regiones have buoyancy fluxes larger than 100 kg s^{-1}. However, these values appear too small. Similar values as on Earth in the range of Mg s^{-1} would be expected.

The same scenario is given by the heat fluxes. Hawaii is associated with a heat flux of about 3 x 10^{11} W (Turcotte and Schubert, 2002; Farnetani and Hofmann, 2011). The ones obtained for the Venusian volcanic rises from B$_{pt}$ have values of 10^9 W, two orders of magnitude smaller than the terrestrial ones. However, it is difficult to make a statement about the heat flux, when only the entire heat flux per volcanic rise is regarded. Therefore, the heat fluxes per unit area were calculated.

The total surface heat flow of Earth lies in the range of (4.2-4.4) x 10^{13} W with an average heat flow of about 82-86 mW m^{-2} (Fowler, 2005). About 80% of the heat flow originates from radiogenic decay, the rest is primordial heat. For Venus, no measurements of the surface heat flow exist yet. It can only be estimated. The mass of Earth is about M$_E$ = 5.974 x 10^{24} kg, the mass of Venus M$_V$ = 4.869 x 10^{24} kg. Scaling Earth's heat loss to Venus by using their masses yields a Venusian heat loss of 2.91 x 10^{13} W with an average surface heat flux of 63 mW m^{-2} (Schubert et al., 2001; Turcotte and Schubert, 2002). Another estimation by Phillips et al. (1997) sets 35 mW m^{-2} as a lower limit.

Based on a total heat flow of 10^9 W, heat fluxes in the range of 0.7 and 2.2 mW m^{-2} for the volcanic rises on Venus were obtained. Such low values would indicate that the planet is a dead body. Another consideration can be made. Hence, it can be expected that the heat flow is more concentrated to the volcanic centers rather

than being uniformly distributed across the entire topographic rise. Since this work is focused on volcanoes, coronae are not included, and therefore Themis and Eastern Eistla Regiones will not be mentioned either.

However, even if the heat flux is considered as being concentrated to the volcanoes, the values at Bell, Dione, Western and Central Eistla Regiones do not exceed 5 mW m^{-2}.

From such low buoyancy and heat fluxes, weak volumetric fluxes result. They lie in the range of 10^{-3} and 10^{-2} km^3 yr^{-1}. As a consequence, the durations of growth of the volcanoes are particularly long (see *table 6.4*). Theia, Sapas, and Idunn Montes are the only three volcanoes that formed in less than a million years. It took Tepev, Gula, and Ushas Montes more than 10 million years to grow. Nyx and Hathor Montes are even associated with durations of growth around 20 million years.

Resurfacing is associated with vigorous volcanism. Volcanic constructs are expected to have formed within geologically short periods of time. In Dione Regio, four major volcanoes formed. Since one mantle plume was assumed for each volcanic rise and, therefore, only a single volumetric flux of magma was obtained, the durations of growth have to be combined. For Dione Regio, this yields a collective duration of growth of about 53 million years. Strom et al. (1994) estimated a length of tens of millions of years for the resurfacing event. The formation of the major volcanoes can be set towards the end of it, after regional plains had been emplaced (Basilevsky et al., 1997). Therefore, in the framework of resurfacing, these durations of growth are unrealistic.

However, approximating the buoyancy fluxes based on the underlying mantle plumes yields values that seem more appropriate (see *table 6.3*). Sleep (1990) lists about 40 hotspots on Earth with their buoyancy fluxes. The values lie in the range of 300 and 3,300 kg s^{-1} (excluding Hawaii which stands out with a buoyancy flux exceeding 8,000 kg s^{-1}). **The buoyancy fluxes that I found for the Venusian hotspots fit perfectly into that range.** Central Eistla Regio is characterized by the weakest buoyancy flux with a value of 589 kg s^{-1}, whereas Beta Regio has the largest one (2,889 kg s^{-1}).

The consequent heat fluxes fall into the range of 10^{10} and 10^{11} W (Atla and Beta Regiones). These values resemble the terrestrial hotspot heat fluxes as well. Calculating the heat fluxes per unit area, values result that are very similar for all nine volcanic rises. While Eastern Eistla is characterized by the lowest heat flux with a value of 18 mW m^{-2}, Dione Regio represents the volcanic rise with the highest heat flow of 45 mW m^{-2}. However, comparing them to the heat fluxes that were obtained based on B$_{pt}$, the present values based on B$_{mp}$ are more real-

istic.

I used the argument before that even if the heat flux of each volcanic rise is concentrated at its volcanic centers, it is still too low. This argument does not hold true in the second scenario as the spatially limited heat flow here yields exaggerated high values. However, the heat flows per unit area averaged over the entire rise have all very similar values.

The volumetric fluxes of magma range between 0.14 and 0.67 km^{-3} yr^{-1}. They yield durations of growth that are altogether shorter than a million years (*table 6.4*). According to these calculations, Nyx Mons had the most prolonged formation with about 880 thousand years. Theia and Idunn Montes were the fastest and developed within about 50 thousand years.

Compared to terrestrial values, the Venusian ones appear rather short. The Hawaiian volcano Mauna Loa is estimated to have a volume of about $70,000$ km^3 comparable to Innini Mons in Dione Regio. However, whereas Mauna Loa is estimated to have started growth about a million years ago (Farnetani and Hofmann, 2011), Innini Mons formed within only 142,000 years. Taking all the major volcanoes of Dione Regio together results in a building-duration of a million years. Such a value is consistent with the resurfacing theory. Considering the vigorous volcanism and the lower gravitational acceleration, a significantly faster formation of volcanoes can be expected.

The results of this study show that the calculation which yields the buoyancy flux of a mantle plume based on the relative motion between the hotspot and the overlying lithospheric plate is not applicable to a planet that has no plate tectonics. Choosing the velocity of a slow-moving plate (3 mm yr^{-1}) yields unrealistic values. In order to obtain similar values as in the second scenario, a plate velocity of almost 40 mm yr^{-1} would have to be used. In this second scenario, assumptions about the hidden mantle plumes were made based on the observable topography. The obtained buoyancy and heat fluxes are similar to those that are associated with hotspots on Earth. Moreover, the duration of growth of the large volcanoes, even though a lot shorter than for their terrestrial counterparts, is realistic. First of all, the lower gravitational acceleration supports the fast formation of volcanoes that are larger than on Earth. Secondly, catastrophic resurfacing forms a fitting framework. It is believed that during the last resurfacing event the widespread regional plains were emplaced within a rather short period of time (tens of millions of years as estimated by Strom et al. (1994)). The construction of the large volcanoes is thought to have occurred towards the end of the resurfacing event as the activity of Venus was already declining. Despite a reduced activity, it was still strong enough to form the volcanoes within tens or hundreds of thousand years.

Bibliography

A. Aitta. Venus' internal structure, temperature and core composition. *Icarus*, 218:967–974, 2012.

D.L. Anderson. Scoring hotspots: The plume and plate paradigms. In G.R. Foulger, J.J. Natland, D.C. Presnall, and D.L. Anderson, editors, *Plates, Plumes, and Paradigms*, pages 31–54. Geological Society of America, 2005.

F. Anguita and A.F. Chicarro. Ovoid structures in the solar system: the coronae of Venus and Miranda, and the domes on the Earth. *Earth, Moon and Planets*, 53:109–116, 1991.

J.C. Aubele. Venus Small Volcano Classification and Description. *Lunar Planet Sci. Conf.*, 24:47–48, 1993.

H. Bahlburg and C. Breitkreuz. *Grundlagen der Geologie*. Elsevier Spektrum Akademischer Verlag, 2004.

A. Basilevsky. Geologic Map of the Beta Regio Quadrangle (V-17), Venus, 2008. U.S. Geological Survey Geologic Investigations Series Map I-3023, scale 1:5,000,000.

A.T. Basilevsky. Age of rifting and associated volcanism in Atla Regio, Venus. *Geophys. Res. Lett.*, 20(10):883–886, 1993.

A.T. Basilevsky. Concentric wrinkle ridge pattern around Sif and Gula. *Lunar Planet Sci. Conf.*, 25:63–64, 1994.

A.T. Basilevsky and J.W. Head. Geologic units on Venus: evidence for their global correlation. *Planetary and Space Science*, 48:75–111, 2000.

A.T. Basilevsky and J.W. Head. Venus: Analysis of the degree of impact crater deposit degradation and assessment of its use for dating geological units and features. *J. Geophys. Res.*, 107:5–1 – 5–38, 2002a. doi: 10.1029/2001JE001484.

A.T. Basilevsky and J.W. Head. On rates and styles of late volcanism and rifting on Venus. *J. Geophys. Res.*, 107:8–1 – 8–17, 2002b. doi: 10:1029/2000JE001471.

A.T. Basilevsky and J.W. Head. Impact craters on regional plains on Venus: Age relations with wrinkle ridges and implications for the geological evolution of Venus. *J. Geophys. Res.*, 111:1–23, 2006. doi: 10.1029/2005JE002473.

A.T. Basilevsky and J.W. Head. Beta Regio, Venus: Evidence for uplift, rifting, and volcanism due to a mantle plume. *Icarus*, 192:167–186, 2007.

A.T. Basilevsky, O.V. Nikolayeva, and V.P. Volkov. Introduction. In V.L. Barsukov, A.T. Basilevsky, V.P. Volkov, and V.N. Zharkov, editors, *Venus Geology, Geochemistry, and Geophysics: Research Results from the USSR*, pages 1–7. University of Arizona Press, 1992.

A.T. Basilevsky, J.W. Head, G.G. Schaber, and R.G. Strom. The Resurfacing History of Venus. In S.W. Bougher, D.M. Hunten, and R.J. Phillips, editors, *Venus II: Geology, Geophysics, Atmosphere, and Solar Wind Environment*, pages 1047–1084. University of Arizona Press, 1997.

F. Bilotti and J. Suppe. The Global Distribution of Wrinkle Ridges on Venus. *Icarus*, 139:137–157, 1999.

D.L. Bindschadler, G. Schubert, and W.M. Kaula. Coldspots and Hotspots: Global Tectonics and Mantle Dynamics of Venus. *J. Geophys. Res.*, 97:13495–13532, 1992.

N.T. Bridges. Stratigraphy and Observations of Nephtys Mons Quadrangle (V54), Venus. *Lunar Planet Sci. Conf.*, 32:abstr. 1376, 2001.

D.L. Buczkowski. Kinematic analysis of radial structures around Irnini Mons, Venus. *Journal of Structural Geology*, 28:2156–2168, 2006.

K. Burke and T.H. Torsvik. Derivation of Large Igneous Provinces of the past 200 million years from long-term heterogeneities in the deep mantle. *Earth Planet. Sci. Lett.*, 227:531–538, 2004.

K. Burke, W.S. Kidd, and J.T. Wilson. Relative and Latitudinal Motion of Atlantic Hot Spots. *Nature*, 245:133–137, 1973.

K.C. Burke and J.T. Wilson. Hot Spots on the Earth's Surface. *Scientific American*, 235:46–57, 1976.

C. Cadio, M.D. Ballmer, I. Panet, M. Diament, and N. Ribe. New constraints on the origin of the Hawaiian swell from wavelet analysis of the geoid to topography ratio. *Earth Planet. Sci. Lett.*, 359:40–54, 2012.

B.A. Campbell and P.G. Campbell. Geologic Map of the Bell Regio Quadrangle (V-9), Venus, 2002. U.S. Geological Survey Geologic Investigations Series Map I-2743, scale 1:5,000,000.

B.A. Campbell and D.A. Clark. Geologic Map of the Mead Quadrangle (V-21), Venus, 2006. U.S. Geological Survey Geologic Investigations Series Map I-2897, scale 1:5,000,000.

B.A. Campbell, L. Glaze, and P.G. Rogers. Pyroclastic deposits on Venus: remote-sensing evidence and modes of formation. *Lunar Planet Sci. Conf.*, 29:abstr. 1810, 1998.

P. Cattermole. *Venus - The geological story.* UCL Press, 1994.

U.R. Christensen and A.W. Hofmann. Segregation of subducted oceanic crust in the convecting mantle. *J. Geophys. Res.*, 99:19867–19884, 1994.

R.L. Christiansen, G.R. Foulger, and J.R. Evans. Upper-mantle origin of the Yellowstone hotspot. *GSA Bulletin*, 114:1245–1256, 2002.

M.F. Coffin and O. Eldholm. Large igneous provinces: crustal structure, dimensions, and external consequences. *Rev. Geophys.*, 32:1–36, 1994.

K.C. Condie. *Mantle Plumes and their Record in Earth History.* Cambridge University Press, 2001.

K.C. Condie. *Earth as an evolving planetary system.* Elsevier Acad. Press, 2005.

D.L. Copp and J.E. Guest. Geologic Map of the Sif Mons Quadrangle (V-31), Venus, 2007. U.S. Geological Survey Geologic Investigations Series Map I-2898, scale 1:5,000,000.

V. Courtillot, A. Davaille, J. Besse, and J. Stock. Three distinct types of hotspots in the Earth's mantle. *Earth Planet. Sci. Lett.*, 205:295–308, 2003.

S.T. Crough. Hotspot Swells. *Annu. Rev. Earth Planet. Sci.*, 11:165–193, 1983.

S.T. Crough and D.M. Jurdy. Subducted lithosphere, hotspots, and the geoid. *Earth Planet. Sci. Lett.*, 48:15–22, 1980.

L.S. Crumpler, J.W. Head, and J.C. Aubele. Venus volcanism: global distribution and classification from Magellan data. *Lunar Planet Sci. Conf.*, 23:277–278, 1992.

L.S. Crumpler, J.W. Head, and J.C. Aubele. Large volcanoes on Venus: Examples of geologic and structural characteristics from different classes. *Lunar Planet Sci. Conf.*, 24:365–366, 1993.

L.S. Crumpler, J.C. Aubele, D.A. Senske, S.T. Keddie, K.P. Magee, and J.W. Head. Volcanoes and Centers of Volcanism on Venus. In S.W. Bougher, D.M. Hunten, and R.J. Phillips, editors, *Venus II: Geology, Geophysics, Atmosphere, and Solar Wind Environment*, pages 697–756. University of Arizona Press, 1997.

A. Davaille. Simultaneous generation of hotpots and superswells by convection in a heterogeneous planetary mantle. *Nature*, 402:756–760, 1999.

G.F. Davies. *Dynamic Earth. Plates, Plumes and Mantle Convection.* Cambridge University Press, 2nd edition, 2001.

D.J. DePaolo and M. Manga. Deep Origin of Hotspots - the Mantle Plume Model. *Science*, 300:920–921, 2003.

R.D. Van der Hilst, S. Widiyantoro, and E.R. Engdahl. Evidence for deep mantle circulation from global tomography. *Nature*, 386:578–584, 1997.

R.A. Duncan and M.A. Richards. Hotspots, Mantle Plumes, Flood Basalts, and True Polar Wander. *Reviews of Geophysics*, 29(1):31–50, 1991.

P.B. Esposito, W.L. Sjogren, N.A. Mottinger, B.G. Bills, and E. Abbott. Venus Gravity: Analysis of Beta Regio. *Icarus*, 51:448–459, 1982.

K.A. Farley and E. Neroda. Noble gases in the Earth's mantle. *Annu. Rev. Earth Planet. Sci.*, 26:189–218, 1998.

C.G. Farnetani and A.W. Hofmann. Mantle Plumes. In H.K. Gupta, editor, *Encyclopedia of solid earth geophysics*, volume 2, pages 857–869. Springer, 2011.

C.G. Farnetani and M.A. Richards. Numerical investigations of the mantle plume initiation model for flood basalt events. *J. Geophys. Res.*, 99:13813–13833, 1994.

G. Faure and T.M. Mensing. *Introduction to Planetary Science: The Geological Perspective.* Springer Verlag, 2007.

T.R. Fleming and E.R. Stofan. Eastern Eistla Regio and Implications for Coronae Modeling. *Lunar Planet Sci. Conf.*, 29:abstr. 1566, 1998.

C.P. Florensky, L.B. Ronca, A.T. Basilevsky, G.A. Burba, O.V. Nikolayeva, A.A. Pronin, A.M. Trakhtman, V.P. Volkov, and V.V. Zazetsky. The surface of Venus as revealed by Soviet Venera 9 and 10. *Geological Society of America Bulletin*, 88:1537–1545, 1977.

C.M.R. Fowler. *The Solid Earth. An Introduction to Global Geophysics.* Cambridge University Press, 2nd edition, 2005.

P. Francis and C. Oppenheimer. *Volcanoes.* Oxford University Press, 2004.

C. Frankel. *Worlds on Fire: Volcanoes on the Earth, the Moon, Mars, Venus and Io.* Cambridge University Press, 2005.

J.B. Garvin, J.W. Head, and A.T. Basilevsky. Venera Lander Site Geologic Characteristics from Pioneer-Venus Radar Measurements. *Lunar Planet Sci. Conf.*, 15:292–293, 1984.

D.H. Green. Composition of basaltic magmas as indicators of conditions of origin: application to oceanic volcanism. *Phil. Trans. R. Soc. Lond. A.*, 268:707–725, 1971.

R.W. Griffiths and I.H. Campbell. Stirring and structure in mantle starting plumes. *Earth Planet. Sci. Lett.*, 99:66–78, 1990.

R.E. Grimm. The Deep Structure of Venusian Plateau Highlands. *Icarus*, 112: 89–103, 1994.

R.E. Grimm and R.J. Phillips. Hot-spot tectonics of Eistla Regio, Venus: Results from Magellan images and Pioneer Venus gravity. *Lunar Planet Sci. Conf.*, 22: 497–498, 1991.

R.E. Grimm and R.J. Phillips. Anatomy of a Venusian Hot Spot: Geology, Gravity, and Mantle Dynamics of Eistla Regio. *J. Geophys. Res.*, 97:16035–16054, 1992.

J.E. Guest, M.H. Bulmer, J. Aubele, K. Beratan, R. Greeley, J.W. Head, G. Michaels, C. Weitz, and C. Wiles. Small Volcanic Edifices and Volcanism in the Plains of Venus. *J. Geophys. Res.*, 97:15949–15966, 1992.

V.L. Hansen, J.J. Willis, and W.B. Banerdt. Tectonic Overview and Synthesis. In S.W. Bougher, D.M. Hunten, and R.J. Phillips, editors, *Venus II: Geology, Geophysics, Atmosphere, and Solar Wind Environment*, pages 797–844. University of Arizona Press, 1997.

J.W. Head and L. Wilson. Volcanic Processes and Landforms on Venus: Theory, Predictions, and Observations. *J. Geophys. Res.*, 91:9407–9446, 1986.

J.W. Head, L.S. Crumpler, and J.C. Aubele. Large shield volcanoes on Venus: distribution and classification. *Lunar Planet Sci. Conf.*, 23:513–514, 1992a.

J.W. Head, L.S. Crumpler, J.C. Aubele, J.E. Guest, and R.S. Saunders. Venus Volcanism: Classification of Volcanic Features and Structures, Associations, and Global Distribution from Magellan Data. *J. Geophys. Res.*, 97:13153–13197, 1992b.

R.R. Herrick and R.J. Phillips. Implications of a Global Survey of Venus Impact Craters. *Icarus*, 111:387–416, 1994.

R.R. Herrick, B.G. Bills, and S.A. Hall. Variations in effective compensation depth across Aphrodite Terra, Venus. *Geophys. Res. Lett.*, 16:543–546, 1989.

R.P. Von Herzen, R.S. Detrick, S.T. Crough, D. Epp, and U. Fehn. Thermal Origin of the Hawaiian Swell: Heat Flow Evidence and Thermal Models. *J. Geophys. Res.*, 87:6711–6723, 1982.

P.C. Hess and J.W. Head. Derivation of primary magmas and melting of crustal material on Venus: some preliminary petrogenetic considerations. *Earth, Moon and Planets*, 50/51:57–80, 1990.

R.I. Hill, I.H. Campbell, G.F. Davies, and R.W. Griffiths. Mantle Plumes and Continental Tectonics. *Science*, 256:186–193, 1992.

A.W. Hofmann. Mantle geochemistry: the message from oceanic volcanism. *Nature*, 385:219–229, 1997.

M. Ishii and J. Tromp. Normal-Mode and Free-Air Gravity Constraints on Lateral Variations in Velocity and Density of Earth's Mantle. *Science*, 285:1231–1236, 1999.

D.M. Jurdy. Early Tertiary Subduction Zones and Hot Spots. *J. Geophys. Res.*, 88:6395–6402, 1983.

P. Kearey and F.J. Vine. *Global Tectonics*. Blackwell Science, 2nd edition, 1996.

S.T. Keddie. Preliminary Analysis of Dione Regio, Venus: The final Magellan regional Imaging Gap. *Lunar Planet Sci. Conf.*, 24:771–772, 1993.

S.T. Keddie and J.W. Head. Sapas Mons Venus: Sequence of Events in a large Shield Volcano. *Lunar Planet Sci. Conf.*, 23:669–670, 1992.

S.T. Keddie and J.W. Head. Dione Regio Venus: A Comparison to other Regional Highlands. *Lunar Planet Sci. Conf.*, 25:675–676, 1994a.

S.T. Keddie and J.W. Head. The Geology and Stratigraphy of Dione Regio, Venus. *Lunar Planet Sci. Conf.*, 25:677–678, 1994b.

S.T. Keddie and J.W. Head. Sapas Mons: Evolution of a type-shield Volcano on Venus. *Lunar Planet Sci. Conf.*, 25:679–680, 1994c.

S.T. Keddie and J.W. Head. Sapas Mons, Venus: Evolution of a large shield Volcano. *Earth, Moon and Planets*, 65:129–190, 1994d.

S.T. Keddie and J.W. Head. Height and altitude distribution of large volcanoes on Venus. *Planet. Space Sci.*, 42:455–462, 1994e.

S.T. Keddie and J.W. Head. Formation and evolution of volcanic edifices on the Dione Regio rise, Venus. *J. Geophys. Res.*, 100:11729–11754, 1995.

W.S. Kiefer and B.H. Hager. A Mantle Plume Model for the Equatorial Highlands of Venus. *J. Geophys. Res.*, 96:20947–20966, 1991.

W.S. Kiefer and L.C. Swafford. Rift system architecture on Venus. *Lunar Planet Sci. Conf.*, 35:abs. 1607, 2004.

W.S. Kiefer and L.C. Swafford. Topographic analysis of Devana Chasma, Venus: implications for rift system segmentation and propagation. *Journal of Structural Geology*, 28:2144–2155, 2006.

D.M. Koch and M. Manga. Neutrally buoyant diapirs: A model for Venus coronae. *Geophys. Res. Lett.*, 23:225–228, 1996.

A.B. Kucinskas and D.L. Turcotte. Isostatic Compensation of Equatorial Highlands on Venus. *Icarus*, 112:104–116, 1994.

X. Li, R. Kind, X. Yuan, I. Wöblern, and W. Hanka. Rejuvenation of the lithosphere by the Hawaiian plume. *Nature*, 427:827–829, 2004.

D.E. Loper and F.D Stacey. The dynamical and thermal structure of deep mantle plumes. *Phys. Earth Planet. Inter.*, 33:304–317, 1983.

B.D. Malamud and D.L. Turcotte. How many plumes are there? *Earth Planet. Sci. Lett.*, 174:113–24, 1999.

P. Martin, E.R. Stofan, L.S. Glasze, and S. Smrekar. Coronae of Parga Chasma, Venus. *J. Geophys. Res.*, 112, 2007. doi: 10.1029/2006JE002758.

G. Masters, G. Laske, H. Bolton, and A. Dziewonski. The Relative Behavior of Shear Velocity, Bulk Sound Speed, and Compressional Velocity in the Mantle: Implications for Chemical and Thermal Structure. In S. Karato, A. Forte, R. Liebermann, G. Masters, and L. Stixrude, editors, *Earth's Deep Interior: Mineral Physics and Tomography From the Atomic to the Global Scale*, pages 63–87. American Geophysical Union, 2000.

A. Matias and D.M. Jurdy. Impact craters as indicators of tectonic and volcanic activity in the Beta-Atla-Themis region, Venus. In G.R. Foulger, J.H. Natland, D.C. Presnall, and D.L. Anderson, editors, *Plates, Plumes, and Paradigms*, pages 825–839. Geological Society of America Special Paper 388, 2005. doi: 10.1130/2005.2388(46).

G.E. McGill. Wrinkle Ridges, Stress Domains, and Kinematics of Venusian Plains. *Geophys. Res. Lett.*, 20:2407–2410, 1993.

G.E. McGill. Hotspot evolution and Venusian tectonic style. *J. Geophys. Res.*, 99:23149–23161, 1994.

G.E. McGill. Central Eistla Regio: Origin and relative age of topographic rise. *J. Geophys. Res.*, 103:5889–5896, 1998.

G.E. McGill. Geologic Map of the Sappho Patera Quadrangle (V-20), Venus, 2000. U.S. Geological Survey Geologic Investigations Series Map I-2637, scale 1:5,000,000.

P.J. McGovern and S.C. Solomon. Factors affecting the Growth, Development, and Structure of Large Volcanoes on Venus. *Lunar Planet Sci. Conf.*, 26:939–940, 1995.

P.J. McGovern and S.C. Solomon. Growth of large volcanoes on Venus: Mechanical models and implications for structural evolution. *J. Geophys. Res.*, 103:11071–11101, 1998.

D. McKenzie. The Relationship between Topography and Gravity on Earth and Venus. *Icarus*, 112:55–88, 1994.

D. McKenzie, J.M. McKenzie, and R.S. Saunders. Dike Emplacement on Venus and on Earth. *J. Geophys. Res.*, 97:15977–15990, 1992.

W.B. McKinnon, K.J. Zahnle, B.A. Ivanov, and H.J. Melosh. Cratering on Venus: Models and Observations. In S.W. Bougher, D.M. Hunten, and R.J. Phillips, editors, *Venus II: Geology, Geophysics, Atmosphere, and Solar Wind Environment*, pages 969–1014. University of Arizona Press, 1997.

M.K. McNutt, D.W. Caress, J. Reynolds, K.A. Jordahl, and R.A. Duncan. Failure of plume theory to explain midplate volcanism in the southern Austral islands. *Nature*, 389:479–482, 1997.

P. Molnar and J. Francheteau. The Relative Motion of 'Hot Spots' in the Atlantic and Indian Oceans During the Cenozoic. *Geophys. J. R. astr. Soc.*, 43:763–774, 1975.

R. Montelli, G. Nolet, F.A. Dahlen, G. Masters., E.R. Engdahl, and S.-H. Hung. Finite-Frequency Tomography Reveals a Variety of Plumes in the Mantle. *Science*, 303:338–343, 2004.

W.B. Moore and G. Schubert. Lithospheric thickness and mantle/lithosphere density contrast beneath Beta Regio, Venus. *Geophys. Res. Lett.*, 22:429–432, 1995.

W.J. Morgan. Convection Plumes in the Lower Mantle. *Nature*, 230:42–43, 1971.

W.J. Morgan. Deep Mantle Convection Plumes and Plate Motions. *Amer. Assoc. Petrol. Geol. Bull.*, 56:203–213, 1972a.

W.J. Morgan. Plate motions and Deep Mantle Convection. In R. Shagam, R.B. Hargraves, W.J. Morgan, F.B. Van Houten, C.A. Burk, H.D. Holland, and L.C. Hollister, editors, *Studies in Earth and Space Sciences: A memoir in honor of Harry Hammond Hess*, volume 132, pages 7–22. Geol. Soc. Am. Mem., 1972b.

W.J. Morgan. Rodriguez, Darwin, Amsterdam, ..., A second type of hotspot island. *J. Geophys. Res.*, 83:5355–5360, 1978.

W.J. Morgan and J.P. Morgan. Plate velocities in the hotspot reference frame. In G.R. Foulger and D.M. Jurdy, editors, *Plates, Plumes, and Planetary Processes*, volume 430, pages 65–78. Geological Society of America Special Paper, 2007.

F. Nimmo. Why does Venus lack a magnetic field? *Geology*, 30:987–990, 2002. URL `http://www2.ess.ucla.edu/~nimmo/website/paper25.pdf`. retrieved: 2013-09-15.

P. Olson and I.S. Nam. Formation of Seafloor Swells by Mantle Plumes. *J. Geophys. Res.*, 91:7181–91, 1986.

R.J. Phillips. Estimating Lithospheric Properties at Atla Regio, Venus. *Icarus*, 112:147–170, 1994.

R.J. Phillips, R.E. Arvidson, J.M. Boyce, D.B. Campbell, J.E. Guest, G.G. Schaber, and L.A. Soderblom. Impact Craters on Venus: Initial Analysis from Magellan. *Science*, 252:288–297, 1991a.

R.J. Phillips, R.E. Grimm, and M.C. Malin. Hot-Spot Evolution and the Global Tectonics of Venus. *Science*, 252:651–658, 1991b.

R.J. Phillips, R.F. Raubertas, R.E. Arvidson, I.C. Sarkar, R.R. Herrick, N. Izenberg, and R.E. Grimm. Impact Craters and Venus Resurfacing History. *J. Geophys. Res.*, 97:15923–15948, 1992.

R.J. Phillips, C.L. Johnson, S.J. Mackwell, P. Morgan, D.T. Sandwell, and M.T. Zuber. Lithospheric Mechanics and Dynamics of Venus. In S.W. Bougher, D.M. Hunten, and R.J. Phillips, editors, *Venus II: Geology, Geophysics, Atmosphere, and Solar Wind Environment*, pages 1163–1204. University of Arizona Press, 1997.

M.A. Richards, B.H. Hager, and N.H. Sleep. Dynamically Supported Geoid Highs over Hotspots: Observation and Theory. *J. Geophys. Res.*, 93:7690–7708, 1988.

M.A. Richards, R.A. Duncan, and V.E. Courtillot. Flood Basalts and Hot-Spot Tracks: Plume Heads and Tails. *Science*, 246:103–107, 1989.

P.G. Rogers and M.T. Zuber. Tectonic evolution of Bell Regio, Venus: Regional stress, lithospheric flexure, and edifice stresses. *J. Geophys. Res.*, 103:16841–16853, 1998.

B. Romanovicz and Y. Gung. Superplumes from the Core-Mantle Boundary to the Lithosphere: Implications for Heat Flux. *Science*, 296:513–516, 2002.

F.L. Scarf. Lightning on Venus. *Adv. Space Res.*, 5:31–36, 1985.

G.G. Schaber, H.J. Moore, R.G. Strom, and J.M. Boyce. The uniform distribution but nonuniform modification of impact craters on Venus. *Lunar Planet Sci. Conf.*, 23:1213–1214, 1992a.

G.G. Schaber, R.G. Strom, H.J. Moore, L.A. Soderblom, R.L. Kirk, D.J. Chadwick, D.D. Dawson, L.R. Gaddis, J.M. Boyce, and J. Russell. Geology and

distribution of impact craters on Venus: What are they telling us? *J. Geophys. Res.*, 97:13257–13301, 1992b.

E. Schinella, C. O'Neill, and J.C. Alfonso. Processes forming volcanic topography at Atla Regio, Venus. In I. Cairns and W. Short, editors, *Proceedings of the 10th Australian Space Science Conference*, pages 105–118, 2011.

H.-U. Schmincke. *Volcanism.* Springer, 2004.

G. Schubert, W.B. Moore, and D.T. Sandwell. Gravity over Coronae and Chasmata on Venus. *Icarus*, 112:130–146, 1994.

G. Schubert, D.L. Turcotte, and P. Olson. *Mantle Convection in the Earth and Planets.* Cambridge University Press, 2001.

G. Schubert, G. Masters, P. Olson, and P. Tackley. Superplumes or plume clusters? *Phys. Earth Planet. Inter.*, 146:147–162, 2004.

D.A. Senske. Regional Topographic Rises on Venus: Geology of Western Eistla Regio, Beta Regio, and Atla Regio. *Lunar Planet Sci. Conf.*, 23:1267–1268, 1992.

D.A. Senske and J.W. Head. Atla Regio, Venus: Geology and Origin of a major equatorial volcanic Rise. *Lunar and Planetary Institute*, 789:107–109, 1992.

D.A. Senske, D.B. Campbell, J.W. Head, P.C. Fisher, A.A. Hine, A. deCharon, S.L. Frank, S.T. Keddie, K.M. Roberts, E.R. Stofan, J.C. Aubele, L.S. Crumpler, and N. Stacy. Geology and Tectonics of the Themis Regio-Lavinia Planitia-Alpha Regio-Lada Terra Area, Venus: Results from Arecibo Image Data. *Earth, Moon and Planets*, 55:97–161, 1991a.

D.A. Senske, J.W. Head, E.R. Stofan, and D.B. Campbell. Geology and Structure of Beta Regio, Venus: Results from Arecibo Radar Imaging. *Geophys. Res. Lett.*, 18:1159–1162, 1991b.

D.A. Senske, G.G. Schaber, and E.R. Stofan. Regional Topographic Rises on Venus: Geology of Western Eistla Regio and Comparison to Beta Regio and Atla Regio. *J. Geophys. Res.*, 97:13395–13420, 1992.

H.R. Shaw. Mantle Convection and Volcanic Periodicity in the Pacific; Evidence from Hawaii. *Geol. Soc. Am. Bull.*, 84:1505–1526, 1973.

N.H. Sleep. Hotspots and Mantle Plumes: Some Phenomenology. *J. Geophys. Res.*, 95:6715–6736, 1990.

E.N. Slyuta and O.V. Nikolayeva. Volcanism. In V.L. Barsukov, A.T. Basilevsky, V.P. Volkov, and V.N. Zharkov, editors, *Venus Geology, Geochemistry, and Geophysics: Research Results from the USSR*, pages 13–30. University of Arizona Press, 1992.

S.E. Smrekar. Evidence for Active Hotspots on Venus from Analysis of Magellan Gravity Data. *Icarus*, 112:2–26, 1994.

S.E. Smrekar and E.M. Parmentier. The interaction of mantle plumes with surface thermal and chemical boundary layers: Applications to hotspots on Venus. *J. Geophys. Res.*, 101:5397–5410, 1996.

S.E. Smrekar and R.J. Phillips. Venusian highlands: geoid to topography ratios and their implications. *Earth Planet. Sci. Lett.*, 107:582–597, 1991.

S.E. Smrekar and E.R. Stofan. Corona Formation and Heat Loss on Venus by Coupled Upwelling and Delamination. *Science*, 277:1289–1294, 1997.

S.E. Smrekar and E.R. Stofan. Origin of Corona-Dominated Topographic Rises on Venus. *Icarus*, 139:100–115, 1999.

S.E. Smrekar and E.R. Stofan. Venus: Surface and Interior. In L.-A. McFadden, P.R. Weissman, and T.V. Jonson, editors, *Encyclopedia of the solar system*, pages 149–168. Academic Press/Elsevier, 2nd edition, 2006.

S.E. Smrekar, W.S. Kiefer, and E.R. Stofan. Large Volcanic Rises on Venus. In S.W. Bougher, D.M. Hunten, and R.J. Phillips, editors, *Venus II: Geology, Geophysics, Atmosphere, and Solar Wind Environment*, pages 845–878. University of Arizona Press, 1997.

S.E. Smrekar, E.R. Stofan, N. Mueller, A. Treiman, L. Elkins-Tanton, J. Helbert, G. Pissioni, and P. Drossart. Recent Hotspot Volcanism on Venus from VIRTIS Emissivity Data. *Science*, 328:605–608, 2010.

S.C. Solomon and J.W. Head. Mechanisms for Lithospheric Heat Transport on Venus: Implications for Tectonic Style and Volcanism. *Journal of Geophysical Research*, 87:9236–9246, 1982.

S.C. Solomon, P.J. McGovern, M. Simons, and J.W. Head. Gravity anomalies over volcanoes on Venus: Implications for lithospheric thickness and volcano history. *Lunar Planet Sci. Conf.*, 25:1317–1318, 1994.

Helmuth Spaeth. *Spline-Algorithmen zur Konstruktion glatter Kurven und Flaechen*. Oldenbourg, 4th edition, 1986.

M. Stefanick and D.M. Jurdy. The Distribution of Hot Spots. *J. Geophys. Res.*, 89:9919–9925, 1984.

D.J. Stevenson, T. Spohn, and G. Schubert. Magnetism and thermal Evolution of the terrestrial Planets. *Icarus*, 54:466–489, 1983.

E.R. Stofan. Coronae on Venus: Topographic Variations and Correlations between Morphology and Regional Setting. *Lunar Planet Sci. Conf.*, 26:1361–1362, 1995.

E.R. Stofan and A.W. Brian. Geologic Map of the Themis Regio Quadrangle (V-53), Venus, 2012. U.S. Geological Survey Geologic Investigations Series Map I-3165, scale 1:5,000,000.

E.R. Stofan, J.W. Head, D.B. Campbell, S.H. Zisk, A.F. Bogomolov, O.N. Rzhiga, A.T. Basilevsky, and N. Armand. Geology of a rift zone on Venus: Beta Regio and Devana Chasma. *Geological Society of America Bulletin*, 101:143–156, 1989.

E.R. Stofan, V.L. Sharpton, G. Schubert, G. Baer, D.L. Bindschadler, D.M. Janes, and S.W. Squyres. Global Distribution and Characteristics of Coronae and Related Features on Venus: Implications for Origin and Relation to Mantle Processes. *J. Geophys. Res.*, 97:13347–13378, 1992.

E.R. Stofan, S.E. Smrekar, D.L. Bindschadler, and D.A. Senske. Large Topographic Rises on Venus: Implications for Mantle Upwelling. *J. Geophys. Res.*, 100:23317–23327, 1995.

E.R. Stofan, V.E. Hamilton, D.M. Janes, and S.E. Smrekar. Coronae on Venus: Morphology and Origin. In S.W. Bougher, D.M. Hunten, and R.J. Phillips, editors, *Venus II: Geology, Geophysics, Atmosphere, and Solar Wind Environment*, pages 931–965. University of Arizona Press, 1997.

E.R. Stofan, J.E. Guest, and D.L. Copp. Development of Large Volcanoes on Venus: Constraints from Sif, Gula, and Kunapipi Montes. *Icarus*, 152:75–95, 2001.

E.R. Stofan, S.E. Smrekar, J. Helbert, P. Martin, and N. Mueller. Coronae and Large Volcanoes on Venus with Unusual Emissivity Signatures in VIRTIS-Venus Express Data. *Lunar Planet Sci. Conf.*, 40:abstr. 1033, 2009.

R.G. Strom, G.G. Schaber, and D.D. Dawson. The global resurfacing of Venus. *J. Geophys. Res.*, 99:10899–10926, 1994.

D.L. Turcotte. An Episodic Hypothesis for Venusian Tectonics. *J. Geophys. Res.*, 98:17061–17068, 1993.

D.L. Turcotte. How does Venus lose heat? *J. Geophys. Res.*, 100:16931–16940, 1995.

D.L. Turcotte and E.R. Oxburgh. Intra-Plate Volcanism. *Phil. Trans. R. Soc. Lond. A.*, 288:561–579, 1978.

D.L. Turcotte and G. Schubert. *Geodynamics - Second Edition.* Cambridge University Press, 2002.

P.R. Vogt and W.Y. Jung. Origin of the Bermuda volcanoes and the Bermuda Rise: History, observations, models and puzzles. In G.R. Foulger and D.M. Jurdy, editors, *Plates, Plumes, and Planetary Processes*, volume 430, pages 553–591. Geological Society of America Special Paper, 2007.

W.R. Ward, J.A. Burns, and O.B. Toon. Past Obliquity Oscillations of Mars: The Role of the Tharsis Uplift. *J. Geophys. Res.*, 84:243–259, 1979.

A.B. Watts. *Isostasy and Flexure of the Lithosphere.* Cambridge University Press, 2001.

D. Waugh. *Geography: An Integrated Approach.* Nelson Thornes, 3rd edition, 2002.

D.A. Williams, L.P. Keszthelyi, D.A. Crown, J.A. Yff, W.L. Jaeger, P.M. Schenk, P.E. Geissler, and T.L. Becker. Volcanism on Io: New insights from global geologic mapping. *Icarus*, 214:91–112, 2011.

J.T. Wilson. A possible Origin of the Hawaiian Islands. *Can. J. Phys.*, 41:863–870, 1963.

K.J. Zahnle. Airburst Origin of Dark Shadows on Venus. *J. Geophys. Res.*, 97: 10243–10255, 1992.

Appendix A

Source Code - Orthodrome Calculation

```fortran
1  !************************************************************
2  ! Calculation of distances on the Venusian surface
3  !************************************************************
4  MODULE constants
5
6  REAL*8 :: pi = 3.141592653589793238d0
7  REAL*8 :: r = 6051.84d0
8
9  END MODULE constants
10 !************************************************************
11 PROGRAM coordinates
12 USE constants
13 IMPLICIT NONE
14
15 ! declaration of variables
16
17 REAL*8 :: phiA, phiB           ! latitudes of point A and B
18 REAL*8 :: lambdaA, lambdaB        ! longitudes of point A and B
19 REAL*8 :: ceta, d            ! central angle and the great-circle-
       distance between the two points
20 REAL*8 :: phiArad, phiBrad        ! latitudes of point A and B in
       radian
21 REAL*8 :: lambdaArad, lambdaBrad  ! longitude of point A in radian
22
23   WRITE(*,*) 'This is a program for the calculation of distances on
        the surface of a sphere'
24   WRITE(*,*)
25
26   phiA = 0.d0
```

```fortran
27    lambdaA = 0.d0
28    phiB = 0.d0
29    lambdaB = 0.d0
30    ceta = 0.d0
31    d = 0.d0
32    phiArad = 0.d0
33    lambdaArad = 0.d0
34    phiBrad = 0.d0
35    lambdaBrad = 0.d0
36
37    ! input of coordinates
38
39    WRITE(*,*) 'Please enter the latitude of the first point with -90 <
          phi < +90'
40    READ(*,*) phiA
41    WRITE(*,*) 'Please enter the longitude of the first point with 0 <
          lambda < +360'
42    READ(*,*) lambdaA
43    WRITE(*,*) 'Please enter the latitude of the second point with -90
          < phi < +90'
44    READ(*,*) phiB
45    WRITE(*,*) 'Please enter the longitude of the second point with 0 <
          lambda < +360'
46    READ(*,*) lambdaB
47
48    ! conversion of coordinates from degrees to radians
49
50    phiArad = phiA*pi/180.d0
51    lambdaArad = lambdaA*pi/180.d0
52    phiBrad = phiB*pi/180.d0
53    lambdaBrad = lambdaB*pi/180.d0
54
55    ! calculation of the central angle
56
57    ceta = acos(sin(phiArad)*sin(phiBrad) + cos(phiArad)*cos(phiBrad) &
58      * cos(lambdaBrad-lambdaArad))
59
60    ! calculation of the distance between the two points
61
62    d = ceta * r
63
64    WRITE(*,*) 'The distance between the two points is d =', d, 'km'
65
66 END PROGRAM
```

Appendix B

Source Code - Cubic Spline Interpolation

```fortran
1  !****************************************************************************
2  ! Cubic Spline Interpolation
3  ! f_k(x) = A_k(x-x_k)^3 + B_k(x-x_k)^2 + C_k(x-x_k) + D_k
4  !****************************************************************************
5
6  PROGRAM main              ! beginning of the main program
7  IMPLICIT NONE
8
9     REAL(8), DIMENSION(:), ALLOCATABLE :: x, y
10    REAL(8), DIMENSION(:), ALLOCATABLE :: deltax, deltay
11    REAL(8), DIMENSION(:,:), ALLOCATABLE :: M, L, U
12    REAL(8), DIMENSION(:), ALLOCATABLE :: d, z, ddy
13    REAL(8), DIMENSION(:), ALLOCATABLE :: A, B, C, f
14    INTEGER(8) :: n, i, j
15    REAL(8) :: area
16
17 WRITE(*,*) 'How many points are there?'
18 READ(*,*) n
19
20    ALLOCATE( x(1:n), y(1:n) )
21
22 WRITE(*,*) 'enter the x-coordinates in strict ascending order'
23 READ(*,*) x(1:n)
24 WRITE(*,*)
25 WRITE(*,*) 'enter the y-coordinates in accord with the x-coordinates'
26 READ(*,*) y(1:n)
27
28 !*****************************************************
29    ALLOCATE( deltax(1:n-1), deltay(1:n-1) )
```

```fortran
30
31      DO i = 1, n-1
32         deltax(i) = x(i+1) - x(i)
33         deltay(i) = y(i+1) - y(i)
34      END DO
35 !**********************************************************
36 ! Construction of the matrix of the system of equations M*y'' = d
37
38   ALLOCATE( M(1:n-2,1:n-2) )
39   M = 0.d0
40      DO i = 1, n-2
41         j = i
42           M(i,j-1) = deltax(i)
43           M(i,j) = 2.d0 * (deltax(i)+deltax(i+1))
44           M(i,j+1) = deltax(i+1)
45      END DO
46 !**********************************************************
47 ! LU decomposition of the matrix M
48
49   ALLOCATE( L(1:n-2,1:n-2), U(1:n-2,1:n-2) )
50   L = 0.d0
51   U = 0.d0
52   L(1,1) = M(1,1)
53
54      DO i = 1, n-2
55         j = i
56           U(i,j) = 1.d0
57           U(i,j+1) = M(i,j+1)/L(i,j)
58           L(i+1,j) = M(i+1,j)
59           L(i+1,j+1) = M(i+1,j+1) - L(i+1,j)*U(i,j+1)
60      END DO
61 !**********************************************************
62 ! the vector of the right side in the system of equations
63
64      DO i = 1, n-1
65         deltax(i) = x(i+1) - x(i)
66         deltay(i) = y(i+1) - y(i)
67      END DO
68
69   ALLOCATE( d(1:n-2) )
70      DO i = 1, n-2
71         d(i) = 6.d0 * (deltay(i+1)/deltax(i+1) - deltay(i)/deltax(i))
72      END DO
73 !**********************************************************
74 ! solution of the equation system L*z = d
75
```

```fortran
76     ALLOCATE( z(1:n-2) )
77        DO i = 1, n-2
78           j = i
79              z(i) = (d(i) - L(i,j-1)*z(i-1))/L(i,j)
80        END DO
81  !***********************************************************
82  ! solution of the equation system U*y" = z
83
84     ALLOCATE( ddy(1:n) )
85     ddy(n) = 0.d0
86     ddy(n-1) = z(n-2)
87     ddy(1) = 0.d0
88        DO i = n-2, 2, -1
89           j = i
90              ddy(i) = z(i-1) - U(i-1,j)*ddy(i+1)
91        END DO
92  !***********************************************************
93  ! The coefficents Ak, Bk, Ck of the cubic spline
94  ! fk(x) = Ak*deltax^3 + Bk*deltax^2 + Ck*deltax + yk
95  ! are now determined
96
97     ALLOCATE( A(1:n-1), B(1:n-1), C(1:n-1) )
98        DO i = 1, n-1
99           A(i) = 1.d0/(6.d0*deltax(i)) * (ddy(i+1)-ddy(i))
100          B(i) = 1.d0/2.d0 * ddy(i)
101          C(i) = deltay(i)/deltax(i) - 1.d0/6.d0*deltax(i)*(ddy(i+1)+2.d0
                  *ddy(i))
102       END DO
103 !***********************************************************
104 ! Output
105
106    OPEN(unit=27,file='plot.txt',status='unknown')
107    OPEN(unit=28,file='points.txt',status='unknown')
108    DO i = 1, n-1
109       xx = x(i)
110       yy = 0.d0
111       DO WHILE ( xx <= x(i+1) )
112          yy = A(i)*(xx-x(i))**3 + B(i)*(xx-x(i))**2 + C(i)*(xx-x(i)) + y
                 (i)
113          WRITE(27,*) xx, yy
114          xx = xx + 0.1d0
115       END DO
116       WRITE(28,*) x(i), y(i)
117    END DO
118 WRITE(28,*) x(i), y(i)
119 !***********************************************************
```

```fortran
120 ! Now the cross-sectional area is calculated by
121 ! integrating each spline
122
123    area = 0.d0
124
125    ALLOCATE( f(1:n-1) )
126       DO i = 1, n-1
127          f(i) = A(i)/4.d0*deltax(i)**4.d0 + B(i)/3.d0*deltax(i)**3.d0 &
128            + C(i)/2.d0*deltax(i)**2.d0 + y(i)*deltax(i)
129          area = area + f(i)
130       END DO
131
132    WRITE(*,*) area
133
134 DEALLOCATE(x,y,deltax,deltay)
135 DEALLOCATE(M,L,U)
136
137 END PROGRAM main                    ! end of the program
```

Curriculum Vitae

Elisabeth Fahrngruber, Bakk.rer.nat.

School education:

09/1997 – 06/2005	Secondary Academic School, Seitenstetten

Academic studies:

Since 10/2011	M.Sc. studies in Astronomy, University of Vienna M.Sc. thesis: Physical constraints on the evolution of Hotspot Swells on Earth and Venus Supervisor: Univ.-Prof. Dr. Maria G. Firneis
10/2007 –06/2011	B.Sc. studies in Astronomy, University of Vienna B.Sc. thesis: The Kennicutt-Schmidt-law Supervisor: Univ.-Prof. Dipl.-Phys. Dr. Gerhard Hensler
09 – 12/2008	Exchange semester: University of Jyväskylä, Finland
10/2006 – 06/2010	B.Phil. studies in Fennistic, University of Vienna Passed with distinction

Activities:

03/2006 – 07/2006	
08/2008	
09/2010	Participation in the WWOOF program, Finland

Scientific experience:

05/2012	Participation in the LOC (local organizing committee) at the Workshop: "Extraterrestrial Life – Beyond our Expectations" 21.-22.05.2012, Zaunergasse 1-3, 1010 Vienna
09/2013	Conference Poster at the 63rd Annual Convention of ÖPG, Linz: E. Fahrngruber, J.J. Leitner, M.G. Firneis, 2013, Mantle Plumes on Earth and Venus
09/2014	Conference Poster at the 64th Annual Convention of ÖPG, Pöllau: E. Fahrngruber, J.J. Leitner, M.G. Firneis, 2014, Hotspots and the Heat Budget of Venus